Department of Experimental and Health Sciences
Pompeu Fabra University
Barcelona

# Snail1- the architect behind the matrix

Novel roles in desmoplastic microenvironments

**Jelena Stanisavljević**

TESI DOCTORAL UPF/2014

Director de la Tesi: Dr. Josep Baulida Estadella

Epithelial-mesenchymal transition in tumor development
Cancer Research Program
Hospital del Mar Medical Research Institute

Mami, tati i Maji

“Niko nije tako dobar kako bi mogao da bude ako se još potrudi.”

Dr Zoran Đinđić

# Table of contents

.

# Acknowledgements

My deepest gratitude is to my thesis supervisor, Dr. Josep Baulida, for immense patience and support he provided during all these years, for being remarkable teacher and, most of all, for being my friend.

My respect and appreciation I owe to Dr. Antionio Garcia de Herreros for his time, his expertise and for material and financial support.
I owe gratefulness to every person I have met here in Catalunya, for teaching me each what I had needed to learn.
Thank you, Clara, Sandra, and Victor, for the lesson that one can be in a mentoring position without losing the common touch.
Thank you, Raul, Jordina, Jessica, and Ali, for the support and help beyond the bench.
Thank you, Niko and Manolo, for being my chicos malos.
Thank you, Alex, for all the music we had shared (and will share!).
Thank you, mammospheres, for Erika I admire and adore.
Thank you, Ane, Joan Pau, and Laura, for turning me into epigenetics fan. Thank you, Joan Pau, for la farola.
Thank you, Montse, Raquel, Rosa, Maria, Belen, Natalia, Susana, Ariadna, Patri, Alba, Estel, Fani, Nuria, Lorena, and Silvia for sharing the hardships of being a woman in science.
Thank you, Steffen, David, Rocco, Guillem, and Pere for sharing the hardships of being a scientist in Spain.

Thank you, Josu, Alba, and Cristina, for teaching me the hardest virtue of all: how to teach.

Thank you, all the people from the PRBB's second floor, for the smiles you had had for me in the hall, for the advice given, for the reagents shared, for the unconditional help.

IMIM (Hospital del Mar Medical research Institute) financially aided the printing of this manuscript.

Хвала вам, мама и тата, што сте подржали сваки мој избор, што сте били строги кад је било неопходно и што сте увек били ту. Хвала вам што савладавате сматрфоне, интернете и скајпове да бисте били Мајина и моја подршка где год да смо.

Хвала, кумо, за оне две недеље коришћења Барселоне као пречице до ваших студентских дана, хвала на помоћи, на подршци и што знам да пазите на маму за мене.

Хвала вам, сви моји драги људи расејани по свету; хвала вам, Јасмина и Миро, за љубав из студентских дана која опстаје упркос раздвојености, хвала ти, Владо, за више од двадесет година искреног и правог пријатељства, за савете, за разговоре и за Тању. Хвала, Тања, за тренутке откривања Барселоне, за кафе и разговоре, за Лазу, Ивану и Биљу. Биљо и Ђуане, хвала што сте ми пружили дом. Хвала, Оља, што си ми пружила дом и ти, што си била ту кад ми је било најпотребније. Хвала ти, Драгане, што си пазио на Мају уместо мене. Хвала, Марко, што је пазиш уместо мене сад.

Хвала вам, моја компаса два, што и на даљину без милиметра одступања умете да ми покажете где је смисао. Мајо, хвала ти што си мој универзални мелем, што ме развеселиш у милисекунди и заборавим да на различитим континентима живимо.  Душане, хвала ти на подршци, на правим саветима и за бескрајне сличне светове што под нашим капама од станиола налазимо. Хвала ти што си ту.

The author thanks all the collaborators.

Special thanks to Dr. Raúl Peña for the design of the covers.

# Abstract

Carcinomas initiate their invasion hijacking the innate plasticity of both epithelial cells and mesenchymal stromal cells in a reciprocal way. Chemical and mechanical dialogue between stromal fibroblasts and carcinoma cells causes on one hand fibroblast-to-myofibroblast transdifferentiation, and on the other, epithelial-mesenchymal transition (EMT) as a response to myofibroblast-generated desmoplasia. First part of this thesis addresses the description of a protein complex including Snail1, p65 subunit of NF-κB, and PARP1 involved in poorly understood issue of mesenchymal gene activation (especially extracellular matrix, ECM, coding genes) in epithelial cells undergoing EMT and in fibroblasts. In the second part of this work, we describe Snail1 transcription factor to be the molecular power-source of the stroma-remodeling myofibroblasts. We demonstrate that even few Snail-expressing fibroblasts among the majority of non-expressing ones define through a RhoA/αSMA pathway the mechanical properties of the stroma needed for proper wound healing and tumor invasion. Our work shows that the presence of Snail1-positive fibroblasts and oriented ECM fiber organization in the stroma of breast infiltrating carcinomas are robust prognostic factors for malignant breast cancers with lymph node involvement.

# Resum

Els carcinomes inicien la seva invasió segrestant la plasticitat innata de les cèl·lules afectades, tant les epitelials del tumor com les mesenquimals de l'estroma tumoral. El diàleg químic i mecànic recíproc entre els fibroblasts de l'estroma i les cèl·lules de carcinoma promou d'una banda la transdiferenciació de fibroblasts a miofibroblasts, i de l'altra, la transició epiteli-mesenquima (EMT). La primera part d'aquesta tesi aborda la descripció d'un complex de proteïnes, que inclou Snail1, la subunitat p65 de NF-κB i PARP1, que regula la transcripció de gens mesenquimals (especialment els gens que codifiquen els proteïnes de matriu extracel·lular, ECM) en fibroblasts i en cèl·lules epitelials durant l'EMT. En la segona part d'aquest treball, descrivim que el factor de transcripció Snail1 actua com a font d'alimentació molecular dels miofibroblasts que remodelen l'estroma. Demostrem que uns quants fibroblasts expressant Snail1 entre una majoria que no n'expressen defineixen, a través de l'activació de RhoA/αSMA, les propietats mecàniques de l'estroma necessaries pel tancament de ferides i la promoció de la invasió tumoral. El nostre treball revela que la presència de fibroblasts positius per Snail1 i d'una organització orientada de les fibres de l'ECM en l'estroma de carcinomes infiltrants de mama són factors pronòstics robustos per als càncers malignes de mama amb afectació ganglionar.

# Introduction

# Introduction

Cancer is even more ancient than its Greek name (karkinos-crab and -oma, growth). There are mentions of noted cases in the oldest medical textbooks known to mankind[1] and documented remains of humans suffering metastasis 3200 years ago[2]. The term itself, although widely used, is obsolete, since the concept nowadays includes a broad spectrum of diseases that rise in different organs, have different progression exhibiting great heterogeneity and require different approach and most likely personalized treatment. A word tumor (tumere-to swell) refers simply to a mass or abnormal growth and it may be benign (localized, does not spread, and responds well to treatment) or, unfortunately, malignant, when it is referred to as cancer. Frightening as it may sound, every other man and every third woman will develop some form of tumor during life. Not all of those will progress into malignancies and very little is known about how this decision is reached within the growing tumor and about the factors going in favour of its growth and eventual spread to distant sites within the body.

## 1. A hallmark of cancer

The most obvious question is: is there anything that sets tumor cells apart from the rest of the body? A feature that makes them unique and vulnerable target for a therapy? Addressing this issue in 2000, Douglas Hanahan and Robert A. Weinberg first defined "six essential alterations in cell physiology that collectively dictate malignant growth"[3]. However, all of these features but one are shared between cancers and benign tumors. Benign tumors can weight few kilograms and in order to reach this proportions require most certainly *de novo* angiogenesis, cell death evasion, insensitivity to growth arrest signals, unlimited replication potential, apoptosis evasion and self-provided growth signals. The sole unique property of malignant tumors is their ability to escape the primary site and establish colonies in distant organs, in a word- to metastasize. In order to do so, cancers cells must establish communication with their surrounding and this fact was stressed out by Hanahan and Weinberg in 2011, when they revisited their original concept, expanding the list with two more hallmarks and two emerging characteristics[4]. Most importantly, they recognized that tumors should not be studied any longer without taking into account the microenvironment they reshape during the course of tumorigenesis trough reciprocal heterotypical signaling (Figure I 1). Instructive and permissive interactions between stroma and the epithelium ensure proper organ development, function, and maintenance of the epithelial structure and function, and malignancies disrupt such homeostatic dialogue.

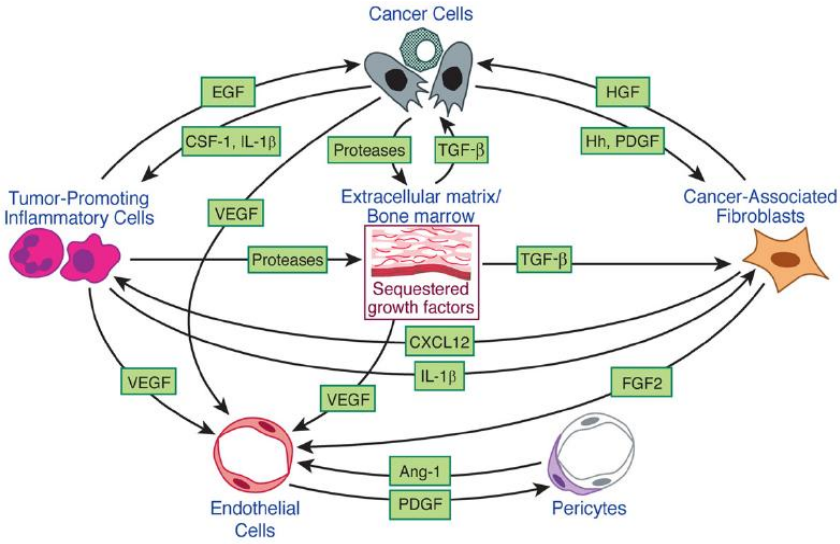


**Figure I 1: Signaling interactions in the tumor microenvironment.**[4] Simplistic illustration of the signaling interactions between assorted cell types constituting the tumor microenvironment. Detailed discussion is further in the text.

## 2. A need for stromal plasticity in cancer

Cancers resemble organs in most of their aspects, not only in deep interconnection with their microenvironment. They have multiple cell types and use processes that are aberrant copies of those occurring during development. Like organs, cancers are also composed of the parenchymal cells and the supporting scaffold, stroma. Within the stromal compartment, non-malignant cells reside- cells of the immune and vascular system and mesenchymal cells such as adipocytes and fibroblasts. The later are the main source of the second component of the stroma, the extracellular matrix; an intricate mesh composed fibrous proteins and ground substance of glycoproteins, proteoglycans and hyaluronans. ECM is embedded with metabolites, chemokines, cytokines, growth factors and other signaling molecules that both tumor and stromal cells produce. Although initially stroma inhibits tumor growth, morphological changes that tumor undergoes as it evolves also include stroma, making it more supportive of tumor progression. Stromagenesis

is initiated by cancer cells and orchestrated mainly by fibroblasts.

## 2.1. Fibroblasts and signals mediating their activation

Fibroblasts are easier to define as what they are not: non-epithelial, non-vascular and non-inflammatory main cellular type of the stroma, highly heterogeneous, easy to grow in culture and rather lacking markers of other lineages than having specific markers themselves. Under normal physiologic conditions, factors that fibroblasts produce restrict epithelial cells proliferation and suppress transformation[5]. They are principal contributors in the ECM production, but also ECM remodelling and homeostasis, synthesizing both fibrillar proteins and ECM-degrading matrix metalloproteinases. For this reason, fibroblasts play crucial role in physiological processes like wound healing and scarring, and their pathological counterpart, fibrosis. In such situations, these cells have higher secretory activity and large endoplasmatic reticulum[6], they proliferate more and express α-smooth muscle actin (αSMA)[7]. The appearance of the mentioned features is referred to as fibroblast activation and fibroblasts positive for αSMA are called myofibroblasts, to stress out the contractile resemblance with smooth muscle cells. In fact, myofibroblasts were first described in murine models of wound healing[7,8,9].

Wound healing is a response elicited in all types of organs after an injury and involves an immediate appearance of immune cells and formation of the platelet-embedded fibrin plug that prevents further blood loss. The second stage starts with the formation of the granulation tissue. As a response to inflammatory cues, resident fibroblasts (or fibrocytes, their precursors) through local stroma remodelling and ECM deposition cause gradual increase in ECM stiffness that exerts a force on cell-substrate focal adhesions (FA) (Figure I 2). FAs containing actin stress fibers that generate small traction forces are formed and if the stimuli from the environment persist, these protomyofibroblasts will start to form larger focal

adhesions that would permit the incorporation of newly synthesized αSMA into the stress fibers[10], thus allowing the myofibroblasts to generate even more counterforce, leading to further focal adhesion maturation and ECM remodelling. In the context of the injury, the traction is needed to bring the wound edges closer together. Myofibroblasts in granulation tissue persist only while the recruiter signals are present.

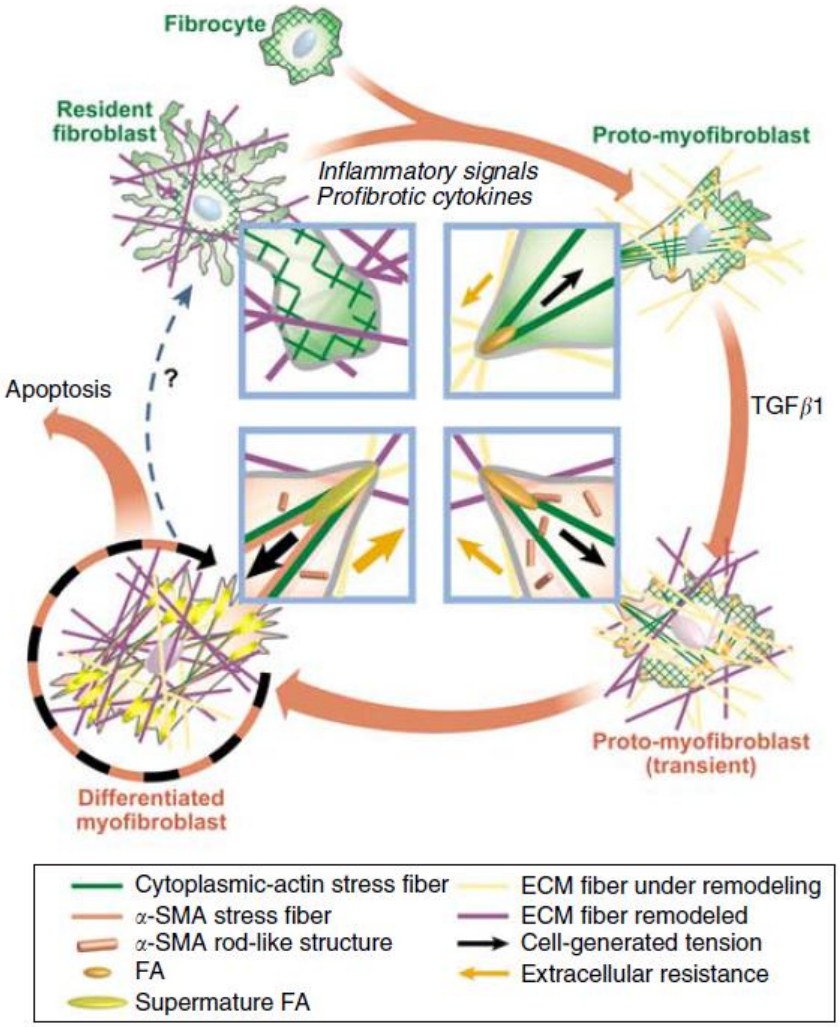


**Figure I 2: The mechanical feedback loop in myofibroblast development.**[11]

A proposed scenario is that, no longer needed, myofibroblasts either undergo apoptosis, allowing the repopulation of the zone by resident not-activated fibroblasts, or the transdifferentiation is reversible and myofibroblasts have the capacity to recuperate resting phenotype.

However, in pathological contexts, like in fibrotic processes of all the organs and in the reactive stroma of progressing primary cancer, myofibroblasts are kept active via chronic inflammation. Inflammation is a normal physiological response to aberrant proliferation and tissue remodeling caused by growing tumor, but the inflammation itself, *de facto*, can also be a primary event in cancer progression, providing it with microenvironment that promotes genetic instability via the production of reactive oxygen species[12], microenvironment rich in factors that promote angiogenesis, proliferation, survival and metastasis. Chronic inflammation is one essential element of the detrimental feed-forward loop leading to persistent myofibroblast activation in cancer stroma. In this context, they are often called cancer-associated fibroblasts (CAFs), though CAFs are most likely composed of heterogeneous population that includes myofibroblasts as well as cells in all the stages of fibroblast activation. The acronym itself was first used in 1999[13], although there were prior mentions of altered fibroblasts present in the stroma. Microarray analysis of CAFs isolated from different samples show significant differences in genes encoding ECM proteins, cytokines and growth factors, suggesting that the phenotype of each CAF cohort is tuned by the specific signaling from the adjacent carcinoma cells.

One driver of the chronic inflammation is nuclear factor (NF)-κB[14]. NF- κB is surely one of the most investigated transcription factors since it is constitutively active in cancer cells and involved in virtually all cellular processes in cancer. Its functions in the microenvironment affect cancer progression both positively and negatively. Inhibiting NF-κB in tumor-associated macrophages converts their phenotype from tumor-promoting to cytotoxic[15]. In CAFs, NF-κB promotes proinflammatory gene signature in the earliest phases of multistep carcinogenesis (Figure I 3), suggesting its crucial role

in the generation of inflammatory niche that sustains cancer progression[16]. Both the induction and the maintenance of CAFs gene signature in this system was shown to be NF-κB dependent.

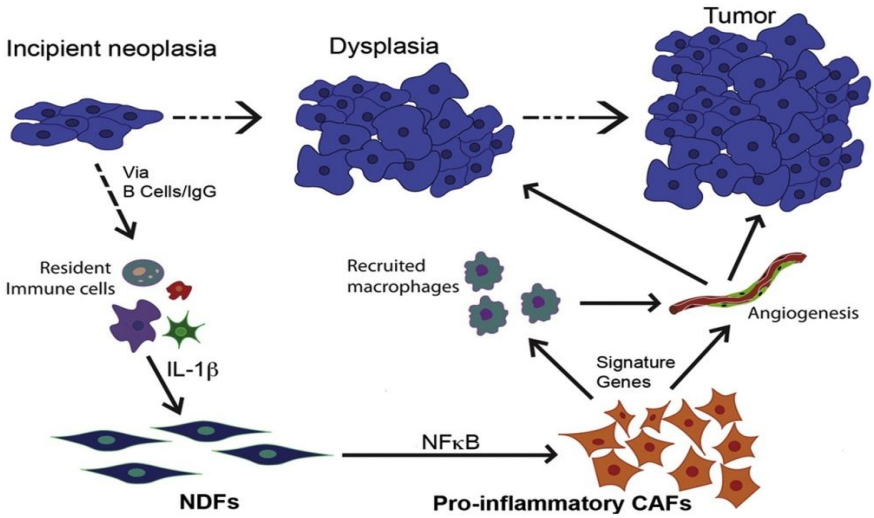


**Figure I 3: A model for NF-κB driven inflammation-promoting role of CAFs.**[16]
Tumor cells induce innate immune cells to produce IL1-β that activates normal dermal fibroblasts (NDF). In CAFs, NF- κB promote angiogenesis and inflammatory response recruiting macrophages.

Through inflammatory response, sarcomas develop at sites of wounding in Rous sarcoma virus infected chickens[17]. This seminal work on the subject identified transforming growth factor beta, TGFβ, as the factor responsible for the cancer development. Upon injury, in fact, most tissues will release TGFβ. TGFβs are matrix-associated growth factors with important roles in all the situations where fibroblast activation takes place- in embryogenesis, during wound healing, in fibrosis and in malignancies. TGFβ induces excessive deposition of connective tissue initially required for organ repair, as well as myofibroblastic differentiation[18] (Figure I 2) and forces ECM remodeling[19] in cultured fibroblasts. Fully activated CAFs secrete TGFβ in autocrine fashion, sustaining themselves in perpetually active state. However, secreted TGFβ is trapped in latent complex that adheres to ECM proteins like fibronectin

and fibrillin[20] and to cells via integrins, and the release of active TGFβ form requires that cells exert force through integrins[21] and that the ECM is stiff enough to resist this stretch, allowing the release. Feed-forward loop sustains the active state of CAFs and ECM stiffness and provokes other TGFβ driven processes, such as epithelial-mesenchymal transition.

Active TGFβ levels were reported to be increased only in colorectal carcinomas, not in premalignant adenomas, and its levels correlated significantly with the levels of αSMA, which was increased significantly only in colorectal carcinomas as well[22]. In a model of pancreatic cancer TGFβ was shown to induce in mice the same desmoplastic reaction observed in human adenocarcinomas.[23] In breast cancer, ECM signature analysis revealed upregulation of TGFβ pathway in highly metastatic mammary carcinomas[24]. Low stromal TGFβ levels are good prognostic factor in colorectal cancer patients and metastasis greatly depends on TGFβ-induced stromal program[25]. Moreover, the interaction with colon cancers cells is sufficient to promote TGFβ signaling in CAFs *in vitro*[26]. The interaction is not unilateral and several studies used fibroblasts from different origins to demonstrate that those coming from cancer stroma have highly increased tumor-promoting potential as compared to normal, non-activated fibroblasts[13,16]. CAFs exert their effect on other stromal components, promoting neoangiogenesis, inflammation, immunosuppression, but also provide cancer cells with metastatic and mesenchymal features, the later through the induction of epithelial-mesenchymal transition.

CAFs sustain and promote cancer progression at various levels. Neoangiogenesis[27], inflammation and proliferation, growth and survival of the cancer cells are promoted largely through secretion of growth factors and cytokines by CAFs. Surprisingly, in pancreatic ductal adenocarcinoma, CAFs are responsible for poorly vascularized architecture and excessive rock-hard enveloping stroma that represents a drug delivery barrier[28]. CAFs metabolically support cancer cells, supplying them with energy-rich metabolites such as lactate and pyruvate (so-called reverse Warburg effect)[29,30]. But most importantly, both in the

context of wound healing and reactive tumor stroma, myofibroblasts act as a contractile cohort, forming strong direct contacts with surrounding ECM called fibronexus[31,32,33,34] that promotes profound changes in physical and mechanical traits of the ECM.

## 2.2. Extracellular matrix- an active component in cancer evolution

ECM surrounds, supports, and organizes cells, serving as anchorage site and determining cell polarity (Figure I 4, stage 1). Its physical properties like rigidity, 3D architecture and porosity allow it to act as both physical barrier when ECM forms disorganized meshwork around the cells, and a movement track, whenever the ECM fibers are organized, determining how likely cells are to migrate or to stay put (stages 2 and 3). ECM's biochemical features determined by its molecular composition allow it to bind various growth factors, acting as a limiting factor of their diffusion and their accessibility to the receptors, creating concentration gradient and as a co-receptor (stages 4 and 5). ECM can initiate signaling indirectly as signal presenter (stage 6) or directly, providing signaling fragments upon matrix metalloproteinase action (stage 7).

Its biomechanical properties like elasticity (stage 8) provoke conformational changes in the focal adhesion complexes of interacting cells (both epithelial and mesenchymal) perceiving the stiffness, causing changes in the cytoskeleton, nuclear shape and various cell behaviors.

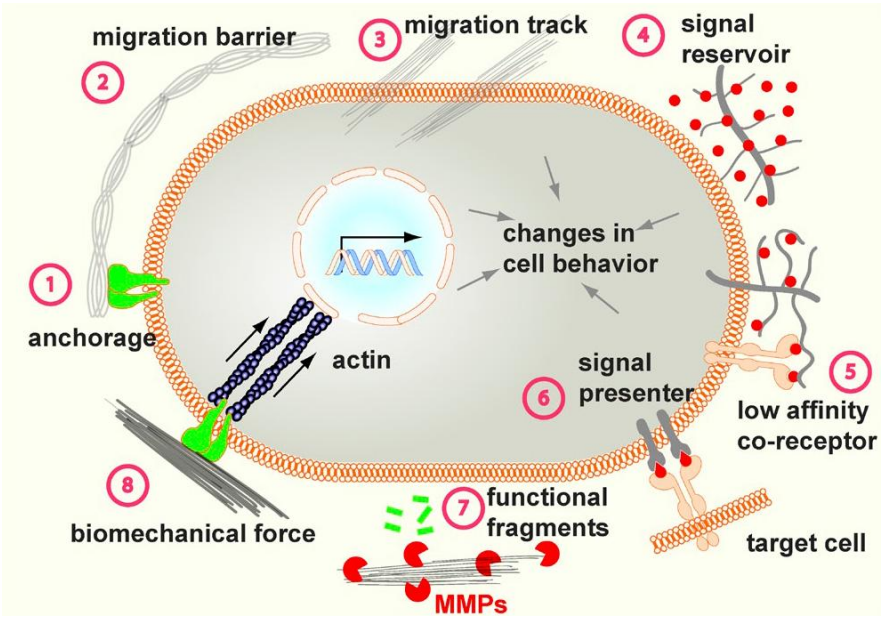


**Figure I 4: Mechanisms of ECM function.**[35]

This mechanical-to-biochemical conversion of the stimuli is called mechanotransduction. Perception of any alterations in mechanical features of the 3D microenvironment[36] and continual feedback response is a constant process (Figure I 5). Mechanotransduction happens not only in sensory cells such are cells of the inner ear; all cells are mechanosensitive and the responsiveness to the changes in their environment is crucial in tissue development and maintenance. Cells respond intracellularly via fast structural reorganization of the cytoskeleton (as described for the fibroblast activation); the chemical propagation of the signal reaches the nucleus, causing the changes in protein expression (e.g. αSMA synthesis).

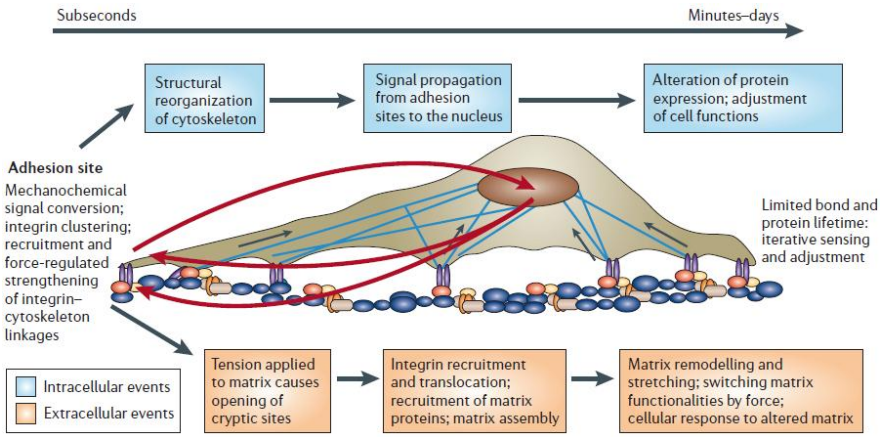


**Figure I 5:Processes of mechanosensing.**[37]

### 2.2.1. Fibronectin- the prime organizer of the ECM topography

Fibronectin (FN) is a very abundant extracellular glycoprotein in all the tissues and all developmental stages. FN initiates ECM assembly and aids the assembly of other fibrous proteins[38]. In solutions (interstitial fluid and plasma), FN is a dimer of a compact conformation and does not form fibrils[39]. FN fibrilogenesis requires conformational changes promoted by selective binding of FN dimer to either αV-class integrins or integrin α5β1[40,41] within the focal contacts. Through the binding, FN converts itself to active linear form in which binding domains for other proteins of the ECM and FN itself[42] are exposed, promoting the formation of dense and detergent-insoluble fibrillar network (Figure I 6). Direct interaction with integrins links FN to the actin cytoskeleton, regulated by the Rho GTPases signaling[43]. Rho-mediated contractility promotes assembly of FN into a fibrillar matrix[42].

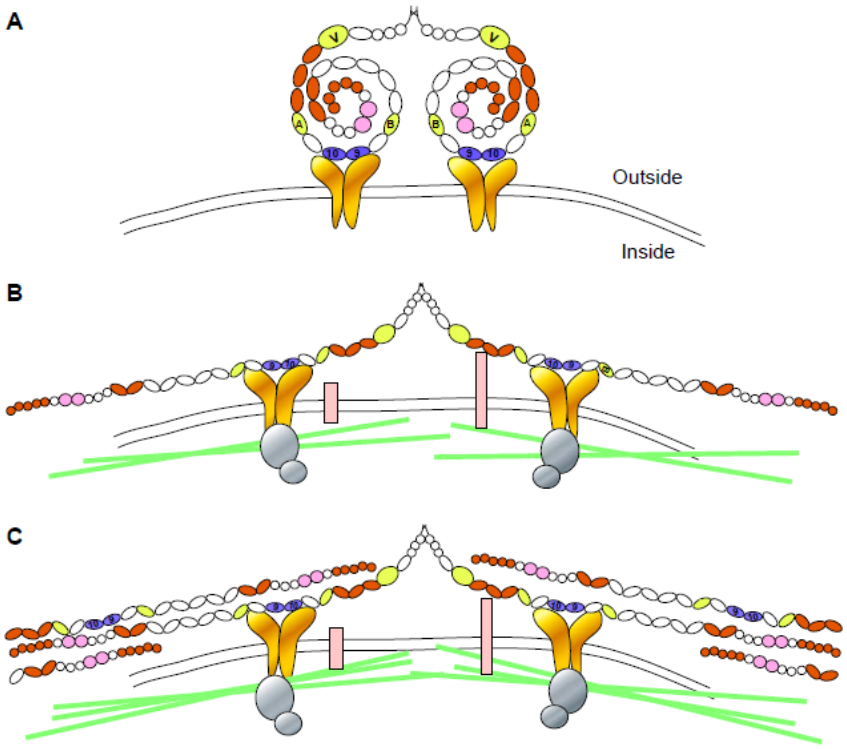


**Figure I 6: Fibronectin matrix assembly.**[44]
Soluble FN dimers in compact form bind integrin α5β1 (A, in orange)) and other receptors (B, in pink) inducing actin cytoskeleton reorganization (green) and activating intracellular signaling (grey) such as RhoA GTPase. Cell contractility causes conformational changes exposing FN binding domains and allowing thorough FN-FN interactions (C).

Several cellular FN variants exist as a product of alternative mRNA splicing. Two spliced exons (EDA and EDB) are present in FN forms produced during embryonic development. Out of these two, EDA-FN is found upregulated in adult tissues in response to increased ECM tension and in response to TGFβ[45] during wound healing and fibrosis progression. EDA-FN promotes tumor growth, epithelial-mesenchymal transition and tumor angiogenesis.

### 2.2.2. Collagen- a key component of mechanoresponse

The physical response to mechanical forces is dominated by collagen, the most abundant protein of the connective tissue and in mammals[46]. Collagens provide structural support, tensile strength and elasticity[47], especially in tendons, bones and dermis. Collagen is secreted as a soluble precursor, procollagen, typically containing Gly-X-Y (where X and Y are commonly proline and hydroxiproline) motifs crucial for the formation of triple helical heterotrimer known as tropocollagen, the extracellular monomer unit of collagens. Although it has been shown possible *in vitro* parallel packaging of tropocollagen into fibrils and then fibers through self-assembly[48], *in vivo* the process is sensitive to cell-mediated regulation. In fact, the presence of collagen-binding integrins and already formed FN fibers is needed *in vivo* for collagen fibers assembly[49]. The inhibition of FN assembly and the disruption of αSMA positive stress fibers both inhibit collagen assembly[49]. Also, blocking collagen-binding sites on FN inhibits collagen fibrilogenesis[50].

The most important covalent change in collagen molecule is its cross-linking. LOX (lysil oxidase) is a copper-dependent amine oxidase that cross-links collagen[51] and elastin[52,53] at peptidyl lysine residues, thereby regulating the tensile strength essential for normal connective tissue function and remodeling. LOX is crucial for proper development and morphogenesis, since knock-out mice exhibit perinatal lethality[54]. Several factors such as TGFβ increase LOX expression and activity in cultured cells[55].

LOX can bind FN, but the protein is not its substrate. The mentioned interaction enhances the enzymatic activity of LOX and in FN-null mice LOX enzyme activity is decreased[56]. LOX is also a downstream target of HIF-1α and promote epithelial-mesenchymal transition in hypoxic conditions by repressing E-cadherin[57]. It is expressed aberrantly in many fibrotic diseases and its overexpression has been associated with poor prognosis in patients with head and neck cancers[58,59], oral cancers[60], colorectal cancer[61] and breast cancer[59]. Targeting LOX reduces

efficiently both injury-caused fibrosis and associated fibrosis-enhanced metastasis[62].

Direct consequence of LOX mediated collagen cross-linking is the increase in tissue stiffness. Each organ and niche can be defined among other criteria by the mechanical stress that its parenchymal cells are subjected to (Figure I 7). The elastic modulus E quantifies the force needed to strain a tissue and has the same units as pressure.

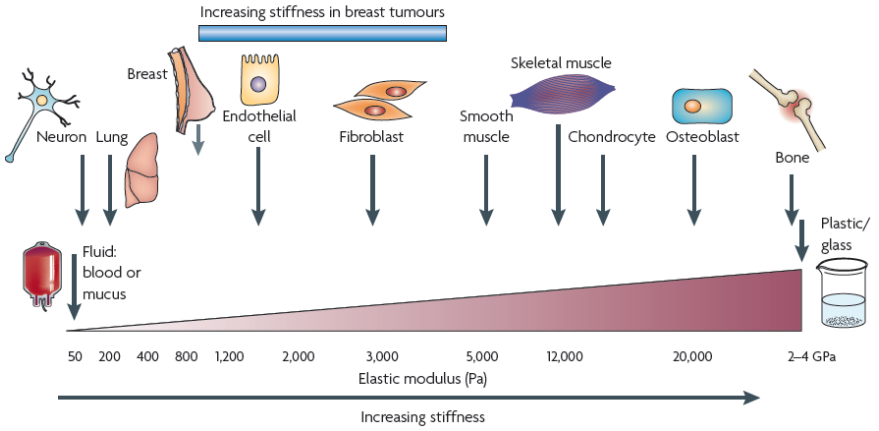


**Figure I 7: Cells are tuned to the materials properties of their matrix.**[63] Differentiation, growth and survival of the resident cells of the soft tissues is favored by a highly compliant matrix, while cells residing in rigid tissues optimally grow on stiffer matrices. During breast cancer progression, tissue becomes progressively stiffer, causing hyper-responsive phenotype in tumor cells.

Cancer cells promote tissue stiffness inducing desmoplastic reactions in their surrounding connective tissue that involve intricate biochemical and biophysical cross-signaling between tumor and the reactive stromal cells. Desmoplasia (desmos- to restrain, and plasis- formation), an accumulation of rich fibrous stroma, takes place in many solid tumors (breast, prostate, colon, or lung) and has long been considered to be a defense barrier mechanism of the host organism (thus the phrase desmoplastic reaction). However, many clinical studies have demonstrated that dense desmoplastic zones happen to be the strongest known risk factor for breast cancer[64], suggesting that desmoplastic reaction is not merely a reaction of the host, but

the maturation of a cancer-supportive niche stimulated by cancer cells.

## 3. A need for epithelial plasticity in cancer

An elegant way to model the mechanical reciprocity of biological systems was developed by Donald E. Ingber[65]. Tensional integrity, or tensegrity (term coined by the engineer Buckminster Fuller) is an architectural principle by which a tridimensional structure is stabilized by continuous tension (attraction) with discontinuous compression (repulsion), not by gravitational compressive forces. The principle explains the cell's capacity to retain its structural integrity with minimum of energy expenditure. Cells function as prestressed tensegrity structures, poised to receive and convert mechanical signals into biochemical changes through already mentioned non-linear process of mechanotransduction. At the tissue level, cells (their actin cytoskeleton) representing tension element, and ECM representing compression element, are connected via mechanosensitive multipoint molecular bridges of integrins within focal adhesions. The composition of these adhesions is modulated in a tension-dependent manner and determines their capacity to trigger chemical signals across the cell membrane in response to mechanical ECM cues. Secondary responses are provoked later on by mechanosensitive sites present along the cytoskeleton fibers, causing further focal adhesion assembly[66,67], cytoskeleton redistribution[68], cell movement[69], and ECM remodeling[70].

Cancer is classically viewed as abnormal cellular proliferation, but what makes it malignant (as already pointed out) is the ability to oppose the tissue architecture, disrupt tissue boundaries and colonize distant organs. Therefore, cancer can be considered as disease of epithelial-mesenchymal interactions that govern how cells organize into tissues and tissues into organs[71]. When multiple simultaneous signaling changes cause a collapse of structural organization of the tissue and a disturbance in the dynamic homeostasis maintained by mechanosensors, cytoskeleton, molecular biomechanical intra-

cellular pathways of the tumor cells and their ECM (Figure I 8)[72], cancer cells switch the entire gene regulatory networks, undergoing profound phenotypic and behavioral transformations.

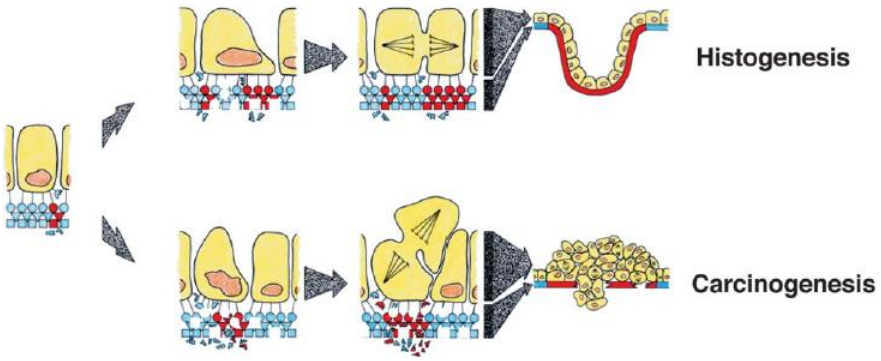


**Figure I 8: Mechanical model of normal and malignant tissue differentiation.**[71] In normal development, basement membrane thinning and increase in compliance promotes local growth. Increased cell division is accompanied by basement membrane expansion and tissue can branch. During carcinogenesis, however, basement membrane expansion after the initial thinning does not occur, having as a result tissue disorganization. Additional signals promoting cell proliferation and adhesion-free growth are needed for the irreversibility of the tumor formation.

## 3.1. Epithelial to mesenchymal transition

A change in phenotype of epithelial cancer cells has been reported first in the context of breast cancer metastasis by Santiago Ramón y Cajal in his "*Manual of Anatomopathology*". In breast carcinomas, he drew and described both the apparent loss of the basement membrane around the epithelial islands, and star-shaped cells not attached to each other, the feature allowing, in his opinion, invasion through the connective tissue (Figure I 9).

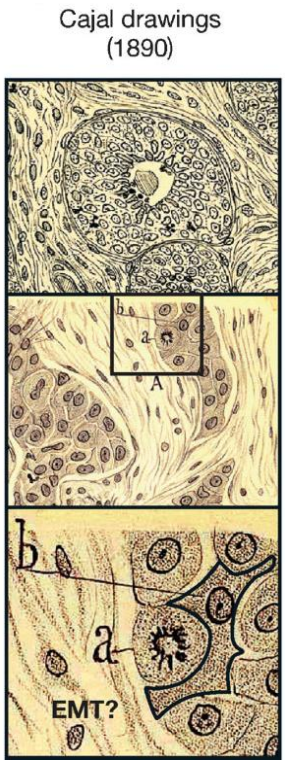


**Figure I 9: Drawings by Santiago Ramón y Cajal.**
Morphological appearance of breast carcinoma[73].

What Ramón y Cajal had described without knowing was naturally occurring step in development and physiological processes where motility of the epithelium is needed called epithelial-mesenchymal transition (EMT)[74]. EMT most likely captures the best the plasticity of epithelial tissue; not only that the process is reversible, but in certain stages of development epithelial cells have the capacity to undergo consecutive rounds of EMT and its counterpart, mesenchymal-epithelial transition (MET), in order to give rise to secondary epithelia. In other cases, EMT may produce fully functional mesenchymal cells and it is thought that some of the fibroblasts and myofibroblasts present during fibrosis and wound healing have epithelial origin[75]. EMT, however, is not all or nothing event; for instance, some epithelial cells during wound healing convert to fibroblasts and participate in wound contraction and other keratinocytes undergo only a partial transition that allows movement in sheets to close the epithelial breach[76]. In human

ovarian surface epithelium, partial EMT takes place after each menstrual cycle[77].

Long abandoned after the initial observation, the idea that EMT occurs during cancer progression was revived during the last decades of the past century, when it was shown that several EMT-TFs enhance tumor formation and metastasis[78]. It is still quite debated[79], since up to date there are no solid pathological proofs that EMT actually takes place in patients, although a significant amount of data in cell lines and xenografts demonstrate that it happens *in vitro*. The final product of cancer-related EMT may not necessarily be a lineage switch, but a change in motility and behavior, just like during partial EMT taking place during wound healing. Pierre Savagner first suggested the existence of intermediate, metastable phenotype that would allow the cells at the tumor-host interface to take profit of the both states. It is assumed that cancer cells over time accumulate genetic alterations causing aberrant expression of many of the factors that facilitate the EMT, but the genetic alterations may affect the adhesive proteins themselves, facilitating the movement without the need for EMT. Loss of E-cadherin function is an indicator of poor prognosis and metastasis in many carcinomas[80,81].

## 3.2. The consequences of E-cadherin loss

The architectural organization of epithelial cell-cell contacts follows highly conserved pattern (Figure I 10, upper left) and the first steps of EMT include the loss of cobblestone morphology, and deconstruction of tight junctions, adherens junctions, desmosomes, and gap junctions through the repression of the epithelial genes[74]. E-cadherin is cleaved and degraded, and, as a consequence, cortical actin cytoskeleton reorganization takes place, allowing the release of transcription factors such as β-catenin, or p65 subunit of NF- κB that translocate to the nucleus and participate in transcription regulation[82]. Actin cytoskeleton is rearranged into structures called stress fibers, facilitating the acquisition of front-rear polarity and directional motility[83]. As in fibroblasts, members of

the Rho GTPase family are the main regulators of the actin cytoskeleton remodeling during EMT[84]. The family includes 23 members and almost 200 proteins involved in GTP-GDP exchange (guanine nucleotide exchange factors (GEFs), GTPase activating proteins (GAPs), and guanine nucleotide dissociation inhibitors (GDIs))[85,86]. RhoA induces actin stress fibers formation and regulates signals from cell-substrate and cell-cell adhesions[87], while other family members (such as Rac and Cdc42) govern lamellipodia and filopodia formation, structures crucial for invasive phenotype. The formation of the actin stress fibers in direct contact with integrin receptors makes the cells more responsive to the mechanical cues in their environment.

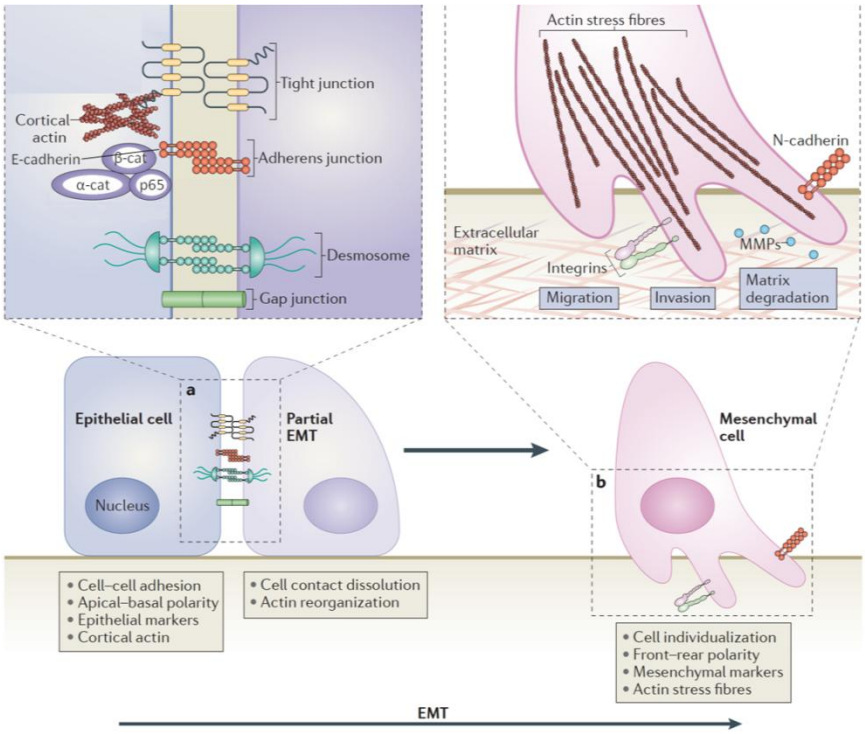


**Figure I 10: Cellular events during EMT.**[88]

## 3.3. The induction of Snail1 during EMT

Among all the cues from tumor microenvironment that trigger EMT, such as growth factors[89,90,91,92], components of the ECM[93,94], hypoxia and ROS, TGFβ has a predominant role. TGFβ family includes several ligands that all exert their action through binding to heteromeric protein kinase receptor complex[95]. TGFβ1 is a potent inducer of EMT combining both Smad and non-Smad signaling[96]. Three families of transcription factors (referred to by some authors as EMT-TFs) regulate the switch in gene expression needed for the transition: Snail, ZEB and Twist (Figure I 11), and TGFβ1 directly activates their expression. Moreover, TGFβ1 is involved in the translational and posttranslational regulation of these factors.

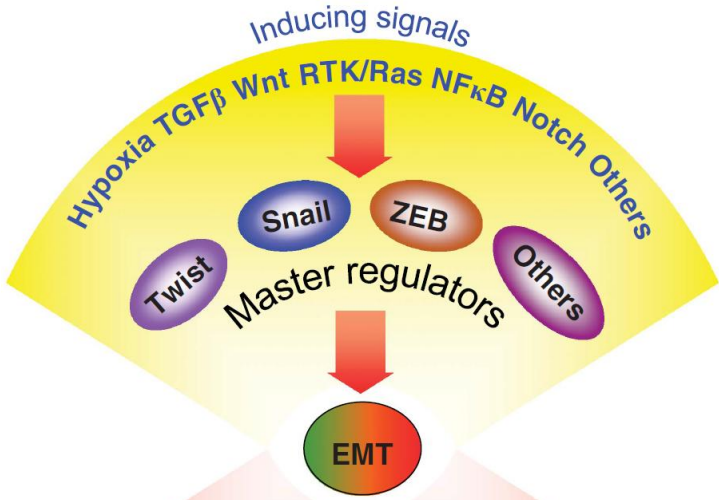


**Figure I 11: Inducing signals in EMT.**[97]

Snail1 transcription factor was first described having crucial role in *Drosophila*'s development[98]. In the following years, it was shown that its homologues in vertebrates[99] play important part in mesoderm[100] and neural crest formation[101], and that Snail1 is a potent repressor of E-cadherin in epithelial cells during EMT[102,103]. As a direct consequence, Snail KO mice are not viable because of uncompleted gastrulation[104]. In cultured tumor cells lines, ectopic expression of Snail1 inhibits E-cadherin[102,105],

reinforces the deconstruction of cell-cell contacts and further promotes EMT[106].

Snail1 (Figure I 12) belongs to zinc-finger type family of transcription factors, sharing with other family members (Snail2 and Snail3) highly conserved C-terminus containing four to six zinc fingers which mediate interactions with promoters containing E-box sequence (5'-CAACTG-3'). Mid-part of the protein is rich in serine and proline residues, important for its stability and sub-cellular localization, adjacent to nuclear export sequence (NES) and destruction box (DB). At N-terminus, regulatory region is situated, comprised of SNAG domain important for the interaction with the co-repressors.

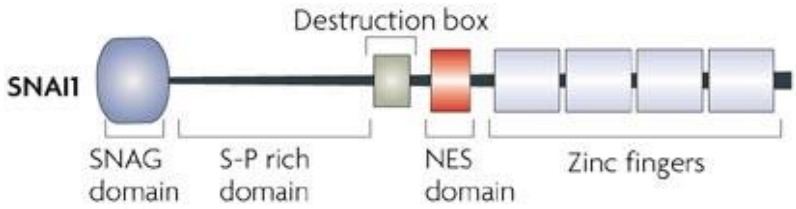


**Figure I 12: Snail1 protein structure.**[107]

Multiple extracellular signaling factors that induce EMT result in Snail1 activation (the choice of the factor *in vivo* largely depends on the context), including indicators of stress, such as hypoxia. Intratumoral hypoxia promotes EMT directly, through transcription regulation of Twist via hypoxia-inducible factor-1 alpfa (HIF1α)[108], and indirectly, through the downregulation of FBXl14 ubiquitin ligase that targets Snail1[109]. Several transduction pathways have been involved in the Snail1 transcription, including extracellular signal regulated kinase (ERK), integrin-linked kinase (ILK), AKT and NF-κB. Receptor tyrosine kinase signaling induces Snail1 through glycogen synthase kinase 3 beta (GSK3β) suppression. Pharmacological inhibition of GSK3β stimulates Snail1 transcription[110]. Snail1 has a short half-life and a well-defined posttranslational regulation, so mRNA and protein levels do not necessarily coincide. GSK3β shows direct dual regulation of Snail1 protein function: it phosphorilates Snail1 at two consensus motifs, the first causes its nuclear export, and the second ubiquitination in the cytoplasm through the interaction with β-TrCP1 ubiquitin

ligase[111]. Another ubiquitin ligase, Fbxl14, promotes Snail1 ubiquitination precluding the phosphorylations introduced by GSK3β[109]. Exportins like CRM1 export phosphorylated Snail1 to the cytosol[112].

The expression of EMT-TFs has temporal hierarchy and Snail1 is the factor induced the earliest. Upon TGFβ treatment, Snail1 transcription is activated via mechanism that involves the interaction of Smads and high mobility group A2 (HMGA2) with its promoter[113]. In addition, TGFβ promotes Snail1 protein stabilization through Lats2 kinase dependent phosphorylation and nuclear retention[114]. This phosphorylation also prevents Snail1 downregulation by FBLX5, ubiquitin ligase that targets nuclear Snail1[115]. p21-activated kinase-1 (PAK1) phosphorylation of Snail1 supports its nuclear localization[116].

Through binding to the E-boxes present close to the transcription start site, Snail1 represses other epithelial genes important for cell-cell contacts, like occludin and claudin3[117], as well as vitamin D receptor[118]. Through the SNAG domain, Snail1 interacts directly or indirectly with several co-repressors, such as SIN3A[119], HDAC1 and HDAC2[119], PRC2[120], LSD1[121], LOXL2[122], and a member of protein arginine N-methyltransferase family, PRMT5[123]. Snail1 is also involved in the repression of heterochromatin transcription through LOXL2 during EMT[124]. Ectopic expression of Snail1 in epithelial cells was shown to upregulate mesenchymal markers FN and LEF1 via unknown mechanism[106], suggesting that Snail1 may not be acting solely as a transcription repressor.

Snail1-triggered EMT and E-cadherin levels regulate NF-κB. Reciprocally, NF-κB can promote EMT and chemoresistance through the induction of Twist[125] and Snail1[126,127]. While other groups reported an inverse correlation between E-cadherin levels and p65NF-κB[128] without providing the mechanism, our group have described the existence of a p65NF-κB membrane-bound pool dependent of the functional E-cadherin that transits to the nucleus upon EMT[82]. This E-cadherin dependent regulation differs from the classical canonical and alternative pathways involving regulation by degradation and protein truncation.

As mentioned before, NF-κB is one of the prime movers involved in cancer-related inflammation. NF-κB family includes five members, p65 (RelA), RelB, c-Rel, p50 and p52, primarily regulated through the interaction with IκB proteins. NF-κB is ubiquitously expressed, but in most cell types remains sequestered in the cytoplasm. High levels of nuclear NF-κB are found in primary breast cancers. Ectopic expression of p65NF-κB induces breast tumor in transgenic murine models. In cancer cells, NF-κB activation is often a result of genetic alterations. NF-κB is key regulator of EMT in murine model of breast cancer progression[129].

p65NF-κB does not act alone promoting transcription and there is a substantial amount of work dedicated to identification of its co-factors. Two members of protein arginine N-methyltransferase family, PRMT1 and PRMT4 (CARM1) form part of the p65NF-κB activator complex[130]. Another such co-factor is PARP1[131,132,133,134,135] (Figure I 13), highly conserved enzyme that catalyses poly(ADP-ribosy)lation. PARP1 is the most abundant non-histone nuclear protein and plays important role in base excision repair and single strand break repair. In this context, therapeutic targeting of its enzymatic activity has been the object of various studies[136]. It is suggested, however, that PARP1 enzymatic role may not be required for the protein to act as p65NF-κB co-factor[137]. Although PARP1 KO mice are viable, they exhibit increased mitochondrial metabolism[138] and exhibit reduced pulmonary fibrosis in response to bleomycin-induced lung injury[139]. PARP1 has been shown to promote EMT upon ILK overexpression through binding to integrin-linked kinase responsive element in the Snail1 promoter, maintaining its transcription[140]. PARP1 interacts with Snail1 directly and enhances its stability[141].

### 3.3.1. Other functions of Snail1

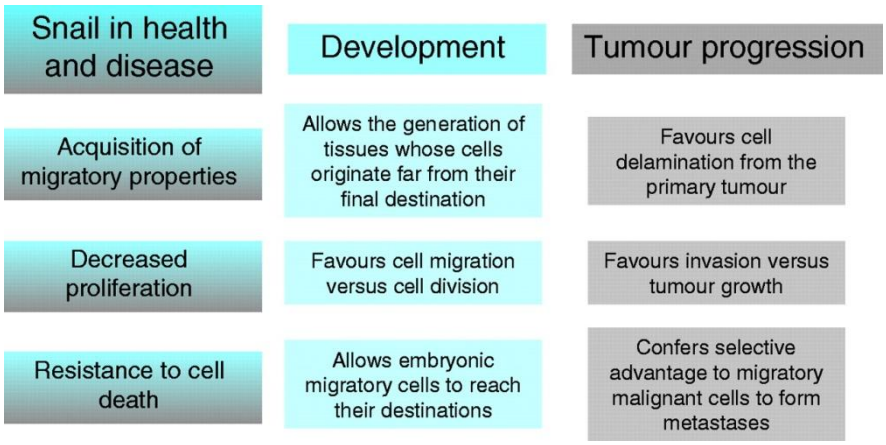


**Figure I 13: Snail functions in development and disease.**[142]

Snail1 plays important cellular functions that are independent of the induction of EMT (although still related; Figure I 13). For instance, Snail1 plays important role in the acquisition of resistance to several types of programmed cell death. Via direct repression of PTEN, Snail1 promotes resistance to gamma radiation induced apoptosis[143]. Ectopic expression of either Snail1, or Snail2 in breast cancer cells alters the response to DNA-damaging agents via downregulation of multiple genes related to cell death[144]. Snail confers resistance to death caused by serum depletion and TNFα administration[145] in EMT-independent way, and suppresses TGFβ-induced apoptosis through the induction of EMT[146,147]. Although proliferation is an important part of cancer progression, Snail1 expression impairs cell cycle progression[145], suggesting that profound morphological changes caused by EMT and high proliferation are incompatible. Accordingly, cells of the invasive front of colorectal carcinomas have been shown to proliferate less[148].

In oral keratinocytes, Snail1 and Slug have been shown to cause impaired terminal differentiation, a common feature of head and neck squamous cell carcinoma[149]. In agreement with these findings, our group has reported that Snail1 depletion promotes premature differentiation, and that Snail1 controls the differentiation of mesenchymal cell lines[150]. Similarly, Snail1

controls bone homeostasis, repressing Runx2 and vitamin D receptor, and it must be downregulated for the final differentiation of osteoblasts[151]. All these data suggest a role for Snail1 in stem cell maintenance. In fact, it has been shown that Snail1 overexpression disturbs the asymmetric division homeostasis of the stem cells in colorectal cancer, causing asymmetric to symmetric division switch[152], thus, increasing the stem cell population.

Weinberg's group showed that an induction of EMT in mammary epithelial cells not only caused mesenchymal phenotype, but the expression of stemness markers[153] and increased mammosphere forming ability (*in vitro* assay for testing stem cell properties[154]). Ectopic expression of Snail1 also increased the mammosphere formation. Other groups related TGFβ-stimulated EMT with the selection and expansion of the cancer stem cells[155]. The only piece of work that captured EMT *in vivo*, a paper on pancreatic tumor formation from Ben Z. Stanger's lab[156], demonstrated using lineage tracing method[157] that tagged epithelial cells underwent EMT, invaded the stroma, entered bloodstream where they maintained mesenchymal (Zeb1 expression, loss of E-cadherin) and markers of stemness ($CD24^{low}/CD44^{high}$).

The existence of cancer stem cells in unperturbed tumor, however, was unconfirmed until three independent works (employing again lineage tracing strategy) reported cellular subsets in intact brain[158], skin[159], and intestinal tumors[160] that act as cancer stem cells while tumor develops from non-tumoral cells in mice. Cédric Blanpain's group (paper on skin tumor) found that there is a neutral competition between cancer stem cells present in the tumor and that the likeness of one winning over the other relies on the mutations that provide advantages *ad hoc*, in the given moment and given microenvironment.

Regardless of its undeniable importance, Snail1 expression in adult tissues is quite limited to situations where not only EMT, but also fibroblast activation takes place. Snail1 is involved in kidney fibrosis, and its expression has been observed in desmoplastic fibrotic areas of human kidneys[161]. Its expression has been reported in spindle-shaped cells adjacent to healing

skin wounds in mice[162]. More importantly, its expression has been reported in the stroma of colorectal tumors, showing correlation with lower specific survival of the patients[163]. The role of Snail1 in fibroblasts remained an open question.

A great volume of work generated by this lab and by others describes how Snail1 initiates the repression of E-cadherin[102] and how the repression is maintained through either direct binding of transcription factors or via epigenetic modifications. However, this is only the first step of the transition: while a set of epithelial genes is being shut down, a whole spectrum of mesenchymal genes involved in motility, invasiveness and stemness is being turned on. Some aspects of the molecular mechanisms behind this activation have already been a subject of a thesis finished in our lab; however, a molecular role of Snail1 and a meaning of Snail1 expression in fibroblasts remained to be elucidated.

Based on the data we obtained analyzing the transcription role of Snail1 and all the information on the importance of the mechanical aspect of the stroma summed up in the introduction, we studied how Snail1 expression in fibroblasts modulates wound healing and cancer progression determining the mechanical properties of the ECM.

# Objectives

# Objectives

To study the role of Snail1 in transcription regulation of mesenchymal genes in epithelial cells undergoing EMT, in invasive cancer cells and in fibroblasts.

To study the role of Snail1 in desmoplasia in the context of cancer progression and wound healing.

# Results

# Results

## 1. Characterization of Snail1-dependent transcription complex involved in mesenchymal genes activation

### 1.1. Interaction of Snail1, p65NF-κB and PARP1 with *FN1* promoter

The initial objective of this thesis was to study the transcription regulation of mesenchymal genes by Snail1. We focused our work on fibronectin (FN1), mesenchymal gene previously studied in the lab and a hallmark of EMT. Using various epithelial cancer cell lines that acquire a mesenchymal phenotype when forced to express Snail1, a former student (Montserrat Porta-de-la Riva) demonstrated that Snail1 was binding proximal *FN1* promoter activating FN1 transcription[82]. Using reporter assays, she defined a proximal nucleotide fragment from -341 to +72 (relative to the transcription start site, TSS) of the *FN1* promoter sensitive to Snail1. This region contains p65NF-κB binding box just after the TSS, crucial for promoter activity, since mutating the box prevented promoter activation[82]. Previous data obtained in the lab demonstrated that E-cadherin present in the adherens junctions of epithelial cells retains a small pool of p65NF-κB, inhibiting its activity as transcription factor. In Snail1 overexpressing cells, this pool was released and nuclear accumulation of p65NF-κB was observed[82].

To study further the relationship between p65NF-κB and Snail1, we performed ChIP assay using SW620 cells, a colon cancer cell line that expresses detectable endogenous Snail1 levels [102] (see inputs in Figure 4B). Within *FN1* promoter sequence there are no E-boxes that Snail1 could bind directly, but significant levels of endogenous Snail1, p65NF-κB and its known cofactor, PARP1, bound to the proximal region of the *FN1* promoter (Figure 1).

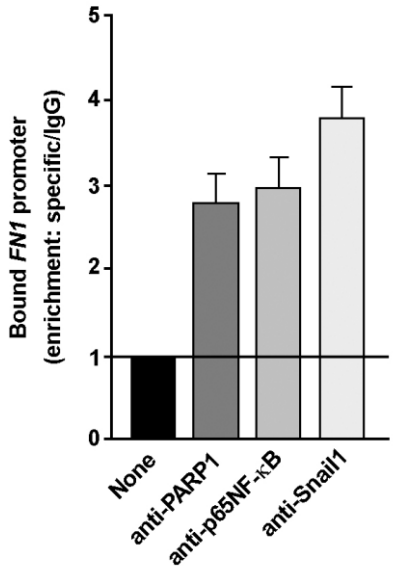


**Figure 1: In vivo binding of Snail1, p65NF-κBp65NF-κB and PARP1 to Fibronectin promoter.**
ChIP in SW620 cells. The *FN1* (+116/+265) promoter from the immunoprecipitates of the indicated antibodies and assay inputs were analyzed by qPCR. Bars show *FN1* promoter enrichment for each specific antibody relative to an unspecific mouse or rabbit IgG, whereby the percentage of input in these IgGs was 0.021 ± 0.002% or 0.09 ± 0.02%, respectively.

Pull-down and reporter assays performed previously in the lab pinpointed the exact region of the FN1 promoter which Snail1 binds. Since this region contained p65NF-κB binding sequence (+33/+50) already described to be crucial for Snail1-mediated FN1 activation[82], we performed the EMSA experiment with +24/+53 *FN1* promoter sequence as a probe (Figure 2A). When the probe was incubated with the nuclear extracts from SW480 Snail1-HA, we observed the retarded bands that were not formed when we used the nuclear extracts from SW480 Snail1-HA/E-cadherin cells, demonstrating the formation of a protein complex binding to this sequence in E-cadherin dependent manner. Moreover, using the antibodies specific for Snail1 and PARP1, we could observe the mobility shift of the same band as the one our lab reported before using the antibody against p65NF-κB. This result indicated that all three proteins are

present in the complex formed between them and *FN1* promoter sequence containing NF-κB binding site.

By ChIPs performed in HT29 M6 epithelial colon cancer cell line and in SW480 Snail-HA/E-cadherin, we could detect that PARP1 was already bound to proximal *FN1* promoter (Figure 2B) and that this union was upregulated in the presence of ectopic Snail1 in the case of HT29-M6 cell line, or in the absence of exogenous E-cadherin in the case of SW480 cells overexpressing Snail1-HA, in agreement with reported omnipresence of PARP1 as chromatin remodeler and insulator[164].

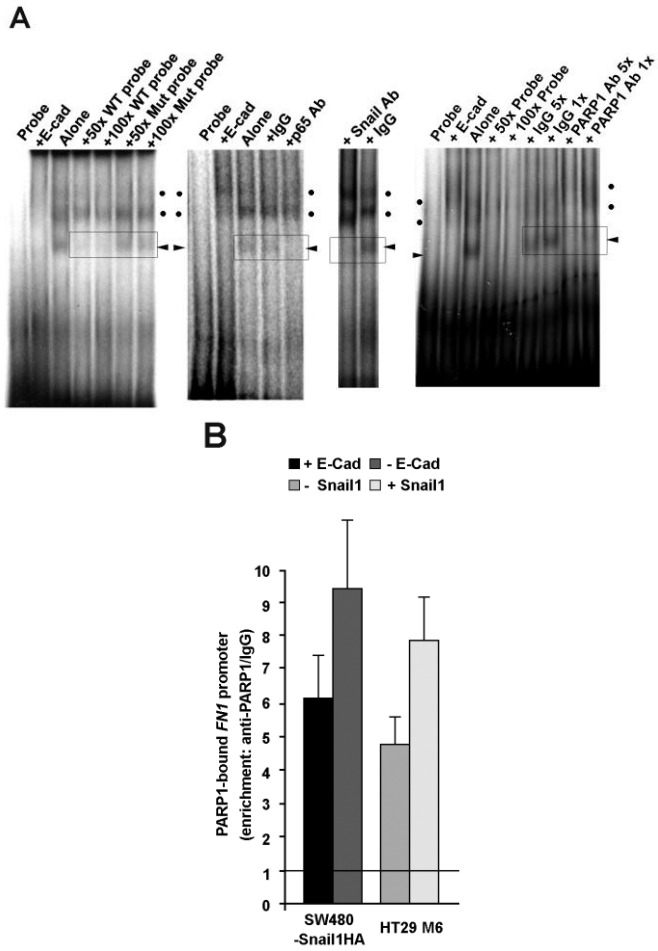


**Figure 2: PARP1 binding to the *FN1* promoter.**

(A) Comparison of the effect of PARP1, p65NF-kB, and Snail1 antibodies on EMSA bands obtained with a +24/+53 *FN1* promoter probe and nuclear extracts from Snail1-HA SW480 cells. The panel on the right corresponds to an EMSA with anti-PARP1 added to the indicated lanes. The two most left panels were extracted from the paper previously published in the lab[82] and middle experiment was kindly performed by Montserrat Porta-de-la-Riva. Arrowheads point to the specific band that: i) was competed out by the wild type but not by the NF-KB-binding site-mutated probe; and ii) disappeared when the EMSA reaction was incubated with the p65NF-κB antibody[82], Snail1 antibody, or PARP1 antibody (right panel). Reference bands are indicated with a dot. (B) ChIP from subconfluent E-cadherin SW480 and HT29 M6 cell populations. The *FN1* promoter (+116/+265) from anti-PARP1 and unspecific IgG immunoprecipitates and inputs were analyzed by qPCR. Bars show *FN1* promoter enrichment in anti-PARP1 relative to IgG, whereby the percentage of input in the IgG in E-cadherin SW480 cells and HT29 M6 clones was 0.023 ± 0.005% and 0.074 ± 0.009%, respectively.

## 1.2. PARP1, p65NF-κB and Snail1 form nuclear complex

To confirm that the three proteins coincide in the nuclear compartment upon Snail1 expression, we performed immunofluorescence in HT29 M6 cells expressing HA tagged murine Snail1 (Snail1-HA).

We could detect both Snail1 (Figure 3A) and p65NF-κB (Figure 3B) co-localizing with PARP1 when Snail1-HA was overexpressed. While PARP1 expression was strictly nuclear regardless of the presence of Snail1, detection of nuclear p65NF-κB signal and co-localization with PARP1 (Figure 3C) was possible only when, as reported before[82], the overexpression of Snail1-HA caused its re-localization.

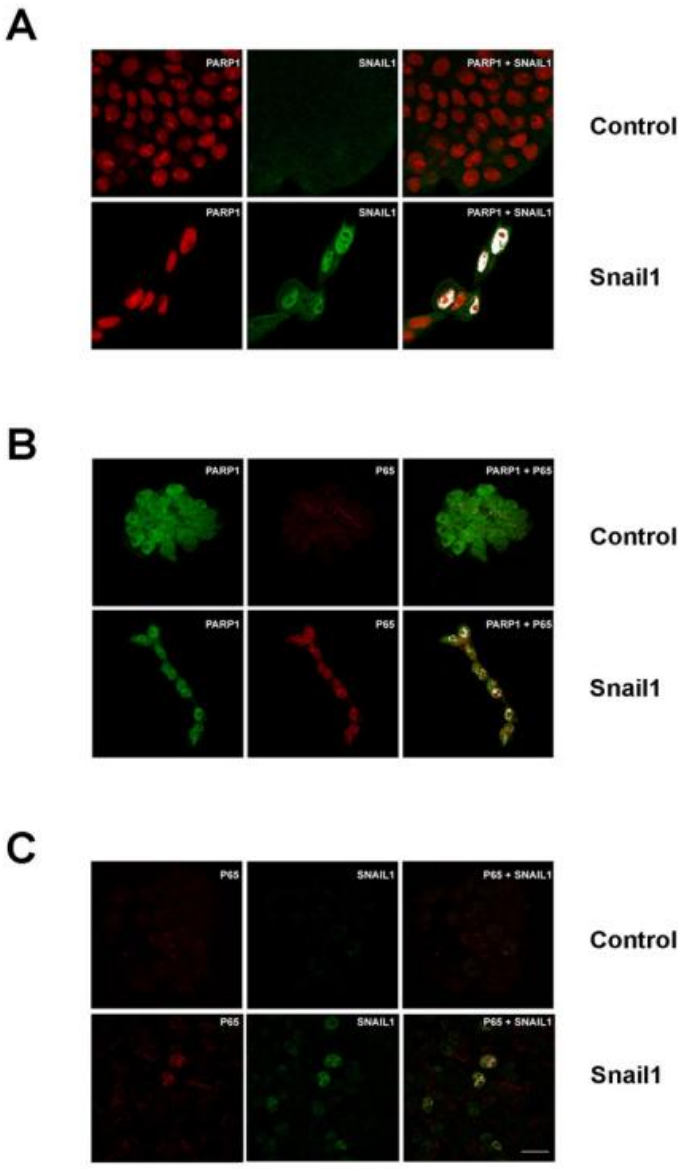


**Figure 3: Snail1-HA, p65NF-κB and PARP1 co-localize in the nucleus of HT29 M6 cells**.
Control and Snail1 HT29 M6 cells were analyzed by immunofluorescence with antibodies against HA (in the case of Snail1-HA), p65NF-κB and PARP1. A) Co-localization of PARP1 and Snail1; B) Co-localization of PARP1 and p65NF-κB; C) Co-localization of Snail1 and p65NF-κB. The secondary antibody for PARP1 was always anti-mouse Alexa647, and for p65NF-κB anti-rabbit Alexa 555. Snail1 was detected with rabbit anti-HA/anti-rabbit

Alexa 488 (green) when co-analyzed with PARP1, or with mouse anti-Snail1/anti-mouse Alexa 488 when co-analyzed with p65NF-κB. Co-localizing pixels are shown in white (see materials and methods).

Next, we analyzed by co-immunoprecipitation if the three proteins were forming part of the same protein complex. Both p65NF-κB and PARP1 were detected in the immunoprecipitates obtained with anti-HA using nuclear extracts of HEK293T cells transiently transfected with Snail1-HA. Co-immunoprecipitation of p65NF-κB and PARP1 was also achieved using the antibody against Snail1 protein and nuclear extracts from SW620 cell line that has high endogenous Snail1 levels[165] (Figure 4).

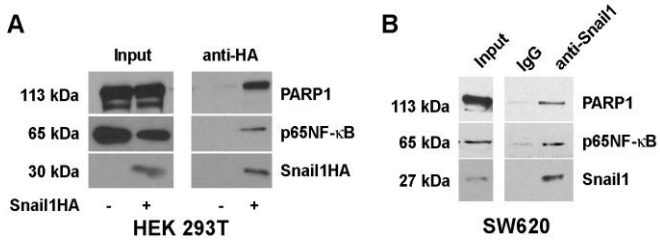


**Figure 4: Snail1, p65NF-κB and PARP1 co-immunoprecipitate.**
Co-immunoprecipitation was performed from HEK293T (A) and SW620 (B). Snail1-HA was immunoprecipitated with anti-HA from nuclear extracts of HEK293T transiently transfected with either pcDNA or a pcDNA Snail1-HA vector. Endogenous Snail1 was immunoprecipitated with a Snail1 antibody from nuclear extracts of SW620 cells treated for 2 hours with 20 μM MG132.

## 1.3. PRMT family members interact with Snail1 and *FN1* promoter in E-cadherin dependent manner

Apart from PARP1, there are several other proteins described to form part of co-activation complex with p65NF-κB[130]. Two such transcription co-activators, CARM1 and PRMT1, are members of the protein arginine methyl transferase (PRMT) family of proteins and are responsible for the histone methylation (H3R17[166] and H4R3[167] dimethylation, respectively). It has been demonstrated that a member of the protein arginine methyl transferase family of proteins, namely, PRMT5, forms part of the co-repressor complex responsible for Snail1-dependent transcription repression[123], we thought that the two family

members shown to have a role in transcription activation could interact with Snail1.

By co-immunoprecipitation we were able to detect CARM1 and PRMT1 present in immunoprecipitates obtained using nuclear extracts from HT29 M6 cells expressing ectopic Snail1-HA (Figure 5). Both proteins were upregulated in the presence of Snail1 (see protein levels in the inputs).

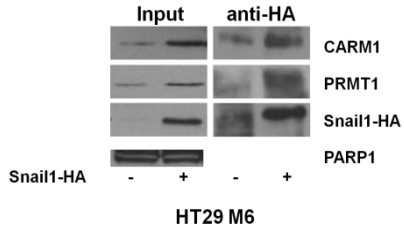


**Figure 5: CARM1 and PRMT1 co-immunoprecipitate with Snail1.**
Snail1-HA was immunoprecipitated using anti-HA from nuclear extracts of HT29 M6 cells expressing or not ectopic Snail1-HA (HT29 M6 C9). PARP1 was used as nuclear loading control.

Next we performed ChIP assay to check if we could detect the binding of PRMT1 and CARM1 to the proximal *FN1* promoter, as we described for Snail1, PARP1 and p65NF-κB (Figure 6). Significant levels of both proteins were found bound to proximal *FN1* promoter in SW620 cell line.

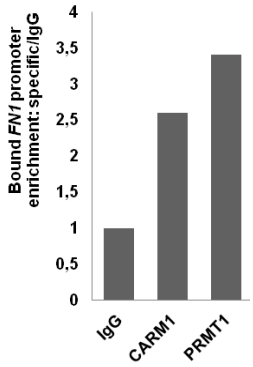


**Figure 6: In vivo binding of CARM1 and PRMT1 to Fibronectin promoter.**
ChIP in SW620 cells. The *FN1* (+116/+265) promoter from the immunoprecipitates of the indicated antibodies and assay inputs were analyzed by qPCR. Bars show *FN1* promoter enrichment for each specific antibody relative to an unspecific mouse or rabbit IgG.

Since the formation of the ternary PARP1- p65NF-κB-Snail1 complex was E-cadherin dependent, we checked if E-cadherin protein levels were indeed responsible for the exchange of Snail1 PRMT cofactors. Using SW480 cells stably expressing Snail1-HA and expressing or not ectopic E-cadherin, we performed immunoprecipitation of Snail1-HA from nuclear extracts (Figure 7). E-cadherin presence had the same effect like in the case of PARP1 and p65NF-κB interaction with Snail1**,** disturbing the complex between PRMT1 and Snail1. Instead, ectopic E-cadherin presence favored the interaction between Snail1 and PRMT5, already described as repression cofactor of Snail1[123].

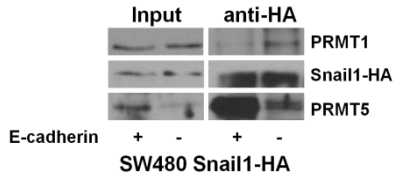


**Figure 7: E-cadherin controls the interaction of Snail1 with its cofactors.**
Snail1-HA was immunoprecipitated using nuclear extracts from SW480 Snail1-HA cells expressing or not ectopic E-cadherin.

Altogether, our findings suggest that Snail1 can form part of two distinct transcription complexes (Figure 8). Well-described complex including proteins like PRMT5, PRC2 and Ajuba is formed when Snail1 acts as transcription repressor of epithelial genes. However, we show that under certain conditions, Snail1can exchange its nuclear co-repressor partners for co-activators.

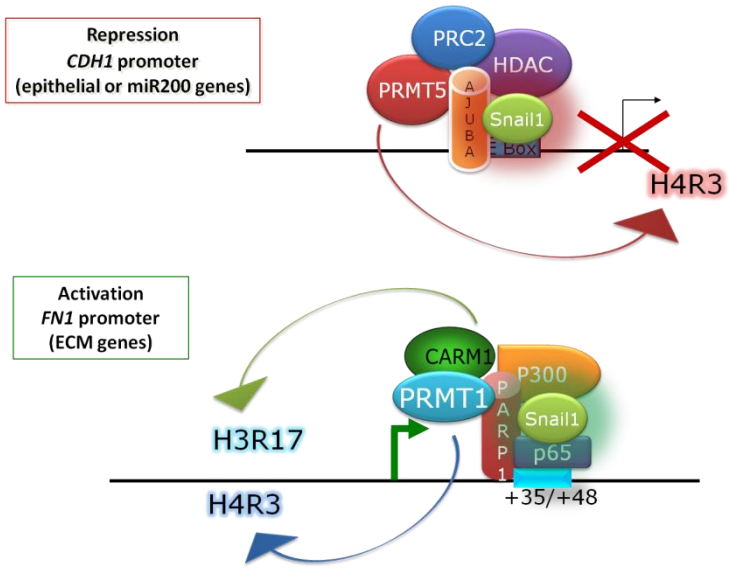


**Figure 8: Different roles, different partners.**

## 1.4. EMT induces a formation of PARP1-p65NF-κB-Snail1 complex that promotes *FN1* transcription

In order to study in more detail how this co-factor switch is orchestrated and its consequences, we decided to use a model of normal epithelial cells undergoing EMT.

Normal murine mammary gland (NMuMG) cells are routinely used physiological model of EMT. Upon TGFβ1 stimulation, these cells undergo full transition program[168], changing their phenotype and gene expression profile. Nuclear accumulation of Snail1 protein was detected as early as 1hr after the stimulation, (final concentration of TGFβ1 that we used throughout this work was 5ng/ml) and it was accompanied by increase in fibronectin levels 8hrs after the treatment (Figure 9).

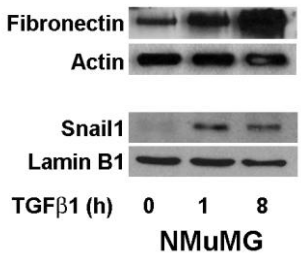


**Figure 9: Western blot from NMuMG cells treated for 0, 1, or 8 hours with 5 ng/ml of TGFβ1.**
The expression levels of the indicated proteins were analyzed using 5 μg of cytosolic (for fibronectin and actin) or 50 μg nuclear (for Snail1 and lamin B1) extracts.

We checked by ChIP if Snail1 binding kinetics to FN1 promoter coincided with this later accumulation of fibronectin protein (Figure 10). Upon TGFβ1 treatment, Snail1 was detected, as expected, bound to *CDH1* promoter, but after 8hrs of the treatment binding changed in favor of *FN1* promoter, suggesting that Snail1 may be playing a dual role in the induction of EMT program.

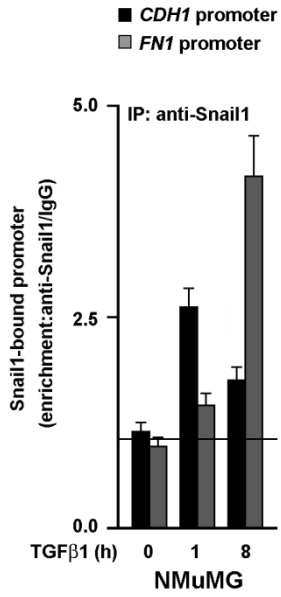


**Figure 10: ChIP from NMuMG cells treated for 0, 1, or 8 hours with 5 ng/ml of TGFβ1.**
The levels of FN1 (+116/+265) and CDH1 (-178/+72) proximal promoters in anti-Snail1 or unspecific IgG immunoprecipitates and assay inputs were

analyzed by qPCR. Bars show promoter enrichment in anti-Snail1 relative to IgG. The percentage of input in the IgG samples in all the conditions for the FN1 and CDH1 promoter was 0.061 ± 0.005% and 0.069 ± 0.008%, respectively.

Nuclear accumulation of p65NF-κB was detected after 8hrs of treatment, in agreement with our observations that the activation of mesenchymal genes requires prior translocation of p65NF-κB to the nucleus. PARP1 nuclear levels remained unchanged regardless of the treatment, in agreement with our results in Snail1 and E-cadherin overexpressing epithelial cells (Figure 11).

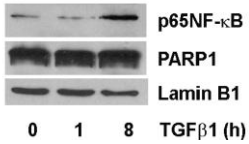


**Figure 11: Western blot from NMuMG cells treated for 0, 1, or 8 hours with 5 ng/ml of TGFβ1.**
Expression of the indicated proteins was analyzed using 50 μg of nuclear extracts.

This result was confirmed by immunofluorescence: PARP1 was strictly nuclear in all conditions, Snail1 nuclear accumulation was observed after 1hr of TGFβ1 treatment, while it took longer to detect nuclear p65NF-κB (Figure 12). We also observed the same later appearance of fibronectin concomitant with p65NF-κB nuclear accumulation.

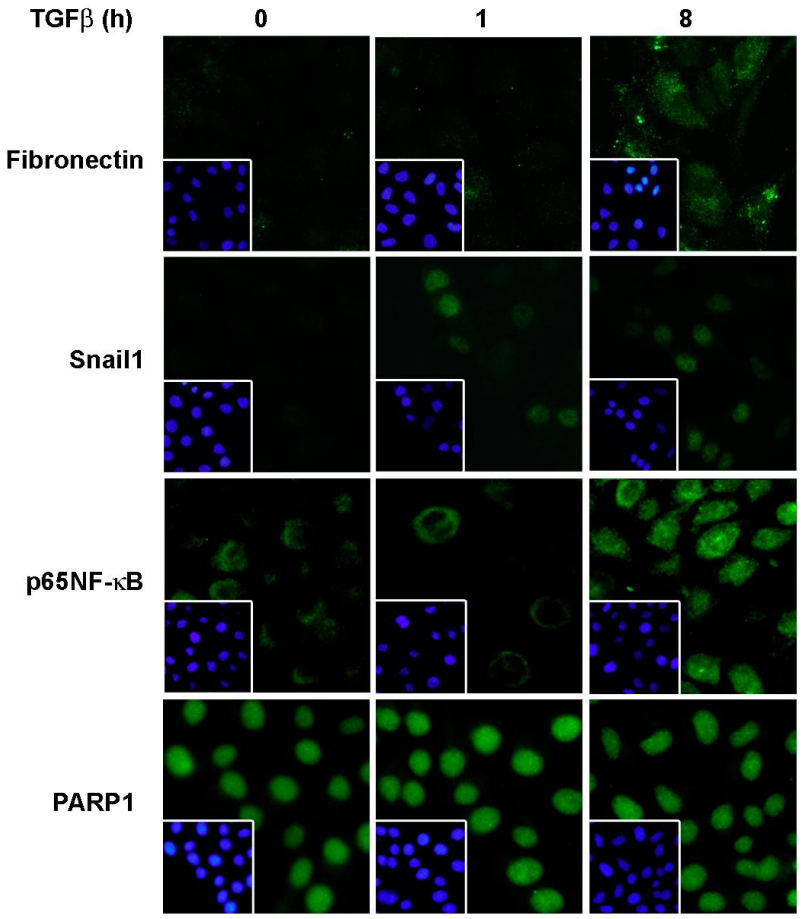


**Figure 12: Immunofluorescence of NMuMG cells treated for 0, 1, or 8 hours with 5ng/ml of TGFβ1**
Immunofluorescence of NMuMG cells treated for 0, 1, or 8 hours with 5ng/ml of TGFβ1. Fibronectin expression and nuclear p65NF-κB were first observed after 8 hours of TGFβ1 treatment. NMuMG cells grown on glass coverslips and treated for 0, 1, or 8 hours with 5ng/ml of TGFβ1 were analyzed by immunofluorescence with antibodies against fibronectin, Snail1, p65NF-κB, and PARP1. All secondary antibodies were conjugated to Alexa 488. Nuclei were counterstained with DAPI.

Based on these observations, we expected that nuclear accumulation of p65NF-κB is the principal recruiter of Snail1 to the promoters of mesenchymal genes. For this reason, we checked by ReChIP assay if we could detect simultaneous presence of both proteins at the proximal *FN1* promoter region. By semi-quantitative PCR, we were able to detect the

enrichment in double immunoprecipitates of the cells treated for 8hrs with TGFβ1, regardless of the order in which the antibodies were used (Figure 13).

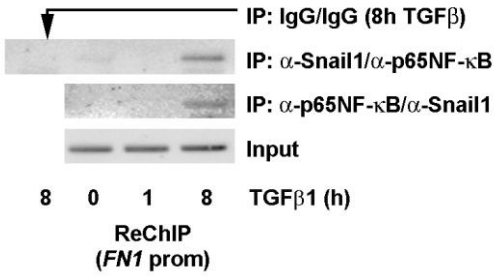


**Figure 13: ReChIP from NMuMG cells treated for 0, 1, or 8 hours with 5ng/ml of TGFβ1**
sqPCR was used to analyze the *FN1* (+116/+265) proximal promoter from double immunoprecipitates with anti-Snail1 and anti-p65NF-κB, or unspecific IgG, immunoprecipitates, as well as inputs, taken at the indicated time points.

## 1.5. PARP1, p65NF-κB and Snail1 form nuclear complex upon TGFβ1 induction and are required for *FN1* activation

This prompted us to validate that the ternary PARP1-p65NF-κB-Snail1 complex was forming upon the induction of EMT. By Western blot, we confirmed the presence of both Snail1 and PARP1 in the immunoprecipitate obtained using the antibody against p65NF-κB only in nuclear extracts of the cells treated for 8hrs with TGFβ1 (Figure 14).

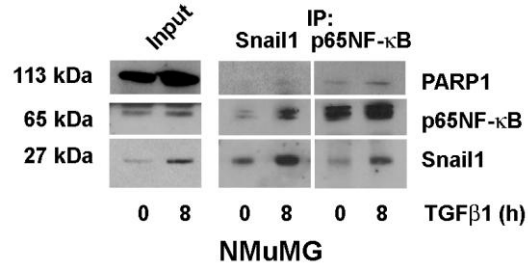


**Figure 14: Snail1, p65NF-κB, and PARP1 co-immunoprecipitate.**
Co-immunoprecipitation was performed from NMuMG cells. Endogenous Snail1 was immunoprecipitated with a Snail1 antibody from nuclear extracts of NMuMG cells not treated or treated for 8 hours with 5 ng/ml of TGFβ1.

p65NF-κB was also immunoprecipitated from nuclear extracts of NMuMG cells (right panel). The indicated proteins were detected by Western blot.

We further confirmed the presence of the protein complex by immunofluorescence (Figure 15). Nuclear accumulation of p65NF-κB and its co-localization with Snail1 and PARP1 was mainly detected in the nuclei of NMuMG cells that have been treated with TGFβ1 for 8hrs.

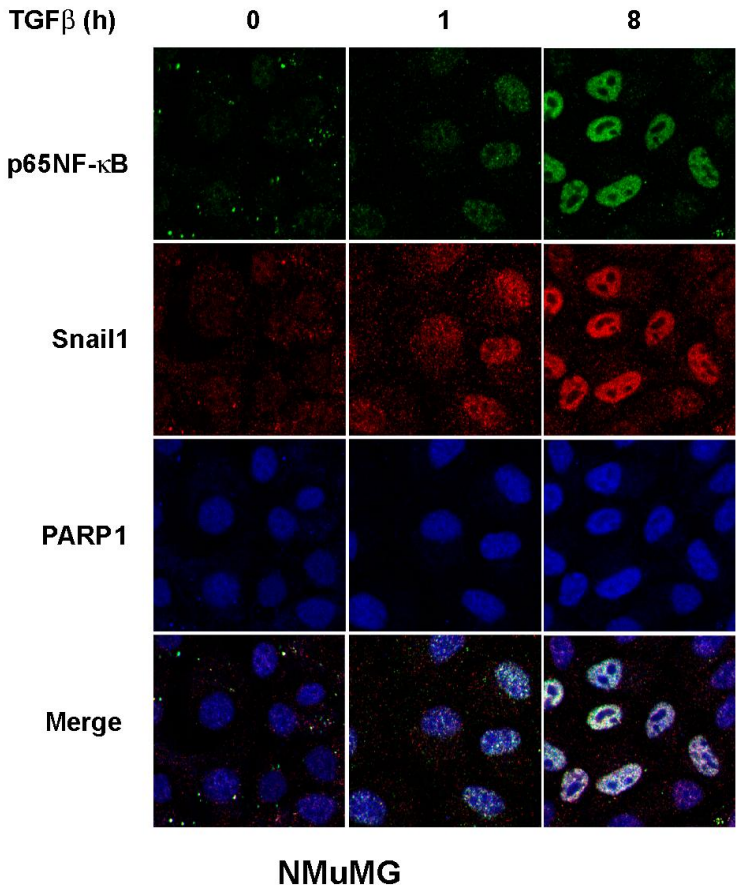


**Figure 15: Nuclear colocalization of p65NF-kB, Snail1, and PARP1 in NMuMG cells.**
Cells grown on glass coverslips and treated for 0, 1, or 8 hours with 5 ng/ml of TGFβ1 were analyzed by immunofluorescence with antibodies for PARP1, p65NF-κB, and Snail1. The secondary antibodies used were an anti-mouse Alexa 647 for PARP1 (plotted in blue), an anti-rabbit Alexa 488 for p65NF-κB (green), and an anti-rabbit Alexa 555 for Snail1 (red). Co-localized pixels are

shown in white. We detected neither green nor red signal in the absence of anti-p65NF-κB or anti-Snail1, respectively.

To confirm the necessity of each of the proteins for fibronectin upregulation, we used specific shRNAs targeting PARP1 or p65NF-κB (Figure 16). Posterior to the infection and selection by puromycin, we performed TGFβ1 time course and analyzed the upregulation of fibronectin by Western blot. Even partial depletion of PARP1 was sufficient to prevent the increase in fibronectin levels upon TGFβ1 treatment. Depleting p65NF-κB also prevented the increase. Neither the depletion of PARP1, nor the depletion of p65NF-κB prevented Snail1 protein level increase upon TGFβ1 stimulus.

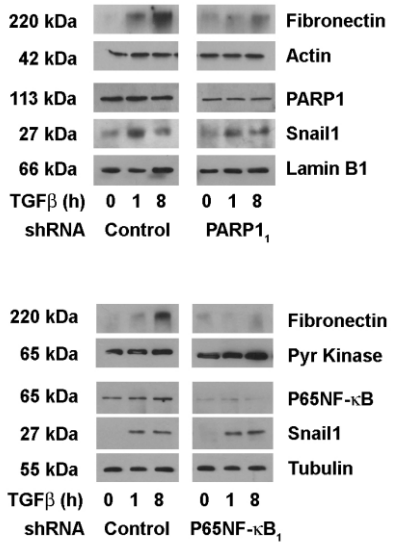


**Figure 16: Depletion of PARP1 or p65NF-κB by shRNA interferes with fibronectin activation by TGFβ1.**
NMuMG cells were infected with a lentivirus carrying a control or a PARP1 shRNA (upper panel). Cells were selected with 2 μg/mL of puromycin and treated for 0, 1, or 8 hours with 5 ng/mL of TGFβ1. The proteins indicated were analyzed by western blot from 10 μg of cytosolic extract or 50 μg of nuclear extracts. NMuMG cells were infected with a lentivirus carrying either a control or a p65NF-κB shRNA (lower panel), and proteins were analyzed by western blot 48 hours after infection. The results were confirmed using two different shRNAs for each of the proteins (not shown).

## 1.6. PARP1, p65NF-κB and Snail1 regulate a set of extracellular matrix proteins during EMT

In order to prove that the regulatory transcription complex we describe is not exclusive for FN1, but a general mechanism of mesenchymal gene regulation, we performed a gene expression microarray analysis (Figure 17). A total of 168 genes showed an increase in their expression by more than two fold after 8 hours of TGFβ1 treatment relative to 1h. 32 of these genes were related with cell movement and migration. We chose to further analyze *HAS2*, *LAMB3* and *THBS1* because of the similarities the three shared with *FN1*. All three encode for proteins of the extracellular matrix and contain p65NF-κB binding site near to their TSS in the 5' UTR.

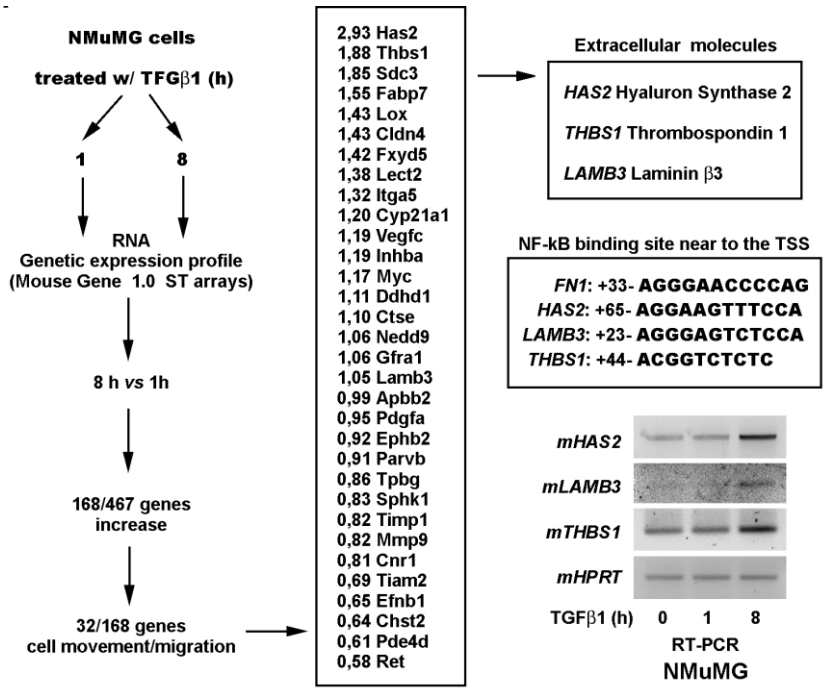


**Figure 17: *HAS2*, *LAMB3*, and *THBS1* promoters recruit p65NF-κB and Snail1 after 8 hours of TGFβ1 treatment.**
*mHAS2*, *mLAMB3,* and *mTHBS1* mRNAs were induced in cells treated with TGFβ1. A mouse gene 1.0 ST array was used to analyze gene expression in the RNA samples obtained from NMuMG cells treated for 1 or 8 hours with 5 ng/ml of TGFβ1. Of the 168 genes whose expression increased with a logFC

higher than 0.5, 32 were related with cell movement and cell migration (Ingenuity Pathway Analysis). sqRT-PCR confirmed the expression of the three indicated genes, which encode secreted extracellular proteins that contain putative p65NF-κB binding sites in their promoters.

Moreover, the expression of all three genes was regulated by a mechanism involving Snail1, since their expression was upregulated in the epithelial cells when Snail1 was overexpressed (Figure 18).

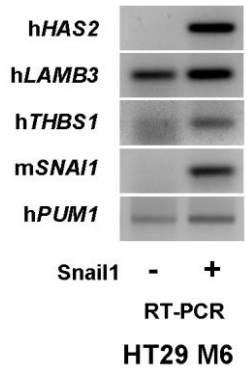


**Figure 18: The levels of *HAS2*, *LAMB3*, and *THBS1* mRNAs increased in HT29 M6 cells that expressed ectopic Snail1.**
Relative mRNA levels were analyzed by sqRTPCR.

Since the mechanism we proposed for the regulation of fibronectin expression required simultaneous binding of p65NF-κB and Snail1 to the proximal promoter, we checked by ReChIP assay if we could detect the proximal promoters of the aforementioned genes in double immunoprecipitates (Figure 19). As expected, the proximal promoters were detected by qPCR only after 8 hours of TGFβ1 treatment, regardless of the order in which the primary antibodies were used.

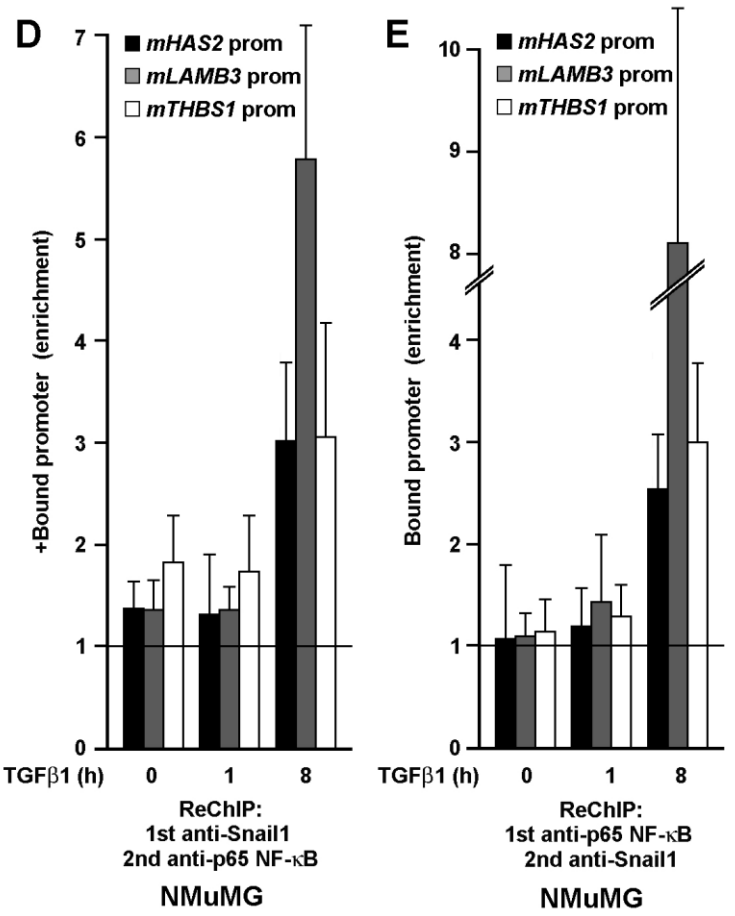


**Figure 19: ReChIP in NMuMG cells treated for 0, 1, or 8 hours with 5ng/ml of TGFβ1.**
NMuMG cell extracts for ChIP were immunoprecipitated with anti-Snail1, and the resulting material was immunoprecipitated again with anti-p65NF-κB. Relative amounts of m*HAS2*, m*LAMB3*, and m*THBS1* promoters in the inputs and the double immunoprecipitated material (using either the specific antibodies or, as a control, IgG) were analyzed by qPCR, using primers that match a promoter region next to the transcription start site (TSS). Bars show promoter enrichment in double immunoprecipitates relative to IgG at 0, 1 or 8 hours of TGFβ1 treatment. Right panel: ReChIP was performed as described, except that anti-p65NF-κB was added first and anti-Snail1 was added second.

## 1.7. Snail1 and TGFβ1 regulate ECM-related genes in fibroblasts through PARP1- p65NF-κB-Snail1 complex

The regulation of mesenchymal gene expression has to take place not only in epithelial cells undergoing EMT, but also in the mesenchymal cells themselves. Therefore, we studied if fibronectin is regulated in the same manner in fibroblasts, the principal source of the extracellular matrix. Fibroblasts are known to express Snail1 *in vitro*[150] and even *in vivo*, in certain embryonic stages and in pathological contexts requiring fibroblast activation[162]. For this purpose we measured *FN1* levels in mouse embryonic fibroblasts (MEFs) that were knock outs for p65NF-κB, Snail1 and PARP1 (Figure 20). All three lines showed decreased levels of *FN1* mRNA compared to their control.

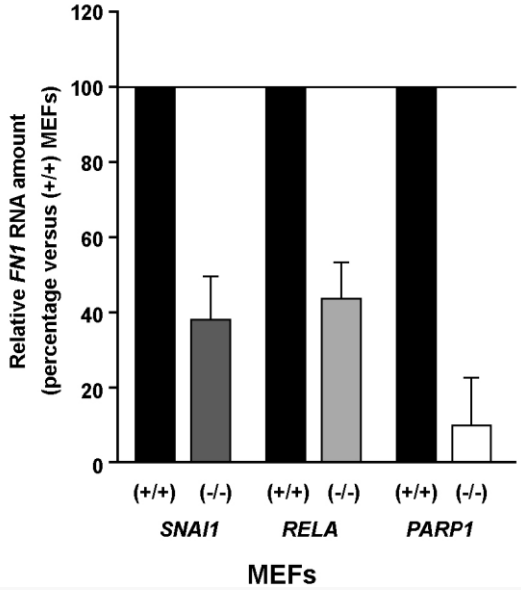


**Figure 20: The amount of FN1 RNA in PARP1, SNAI1, or RELA (+/+) and (-/-) MEFs.**
FN1 and HPRT RNAs were measured by qPCR, and FN1 was normalized to the HPRT value. Bars show the percentage of normalized FN1 RNA in each cell line as compared to that found in PARP1 (+/+) MEFs.

Given that FN1 expression was dependent of the three proteins in mesenchymal system as well, we checked if we could detect their binding to the proximal *FN1* promoter. We transfected

PARP1 KO MEFs transiently with Snail1-HA and performed ChIP assay following qPCR (Figure 21). Proximal FN1 promoter was found co-immunoprecipitating with PARP1, p65NF-κB and Snail1-HA only in the control PARP1 (+/+) MEFs, and not in the KO MEFs, demonstrating that PARP1 is needed for the activation complex to be formed.

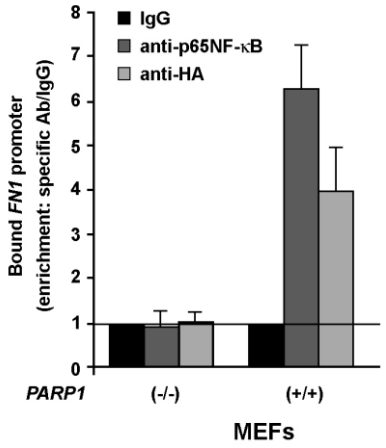


**Figure 21: ChIP in *PARP1* (+/+) and (-/-) MEFs transfected with Snail1-HA.**
*FN1* promoter (+116/+265) that had been co-immunoprecipitated with unspecific IgG, anti-HA, or anti- p65NF-κB, or from inputs, was amplified by qPCR in the indicated cells. Bars show *FN1* promoter enrichment using HA or p65NF-κB antibodies relative to IgG in each cell line, whereby the percentage of input in the IgG in *PARP1* (-/-) and (+/+) MEFs was 0.0033 ± 0.0005% and 0.014 ± 0.002%, respectively.

Next, we checked the formation of the ternary protein complex by co-immunoprecipitation (Figure 22). Snail1 and PARP1 were found in the nuclear immunoprecipitates obtained using the antibody against p65NF-κB. However, no Snail1 was found co-immunoprecipitating with p65NF-κB in the extracts from MEFs KO for PARP1, indicating the importance of PARP1 for the complex formation.

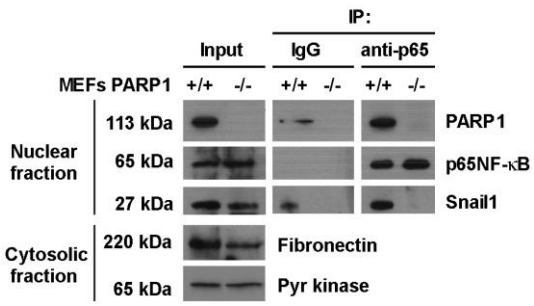


**Figure 22: Co-immunoprecipitation in PARP1 (+/+) and (-/-) MEFs.**
p65NF-κB was immunoprecipitated from nuclear extracts of MEFs. The indicated proteins were detected by western blot. Fibronectin levels present in the cytosolic fractions were also analyzed.

TGFβ1 has an effect and induces changes in mesenchymal cells, too, not only in the epithelial cell lines. Being that we demonstrated that Snail1 is downstream of TGFβ1 when it comes to mesenchymal genes activation in epithelial cells, we wanted to see if Snail1 overexpression will cause the upregulation of ECM genes (as we observed in HT29 M6 epithelial cell line stably expressing Snail1-HA). For this reason, we used a cell line already established in the lab[150], adult human skin fibroblasts, 1BR3G. In this cell line, the three genes regulated in the same manner as fibronectin in the epithelial cells were upregulated when Snail1 was overexpressed, suggesting that the mechanism of Snail1 action is more general (Figure 23).

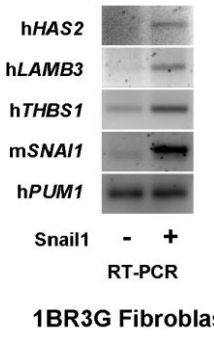


**Figure 23: *HAS2, LAMB3*, and *THBS1* mRNA levels increased in 1BR3G fibroblasts expressing ectopic Snail1.**
Relative RNA levels were analyzed by sqRT-PCR.

Fibronectin expression in these Snail1-overexpressing fibroblasts was checked by Western blot, and was found to be significantly increased compared to control cells (Figure 24). Depletion of PARP1 reduced basal FN levels in control cells, and interfered with the Snail1-induced increase (Figure 24).

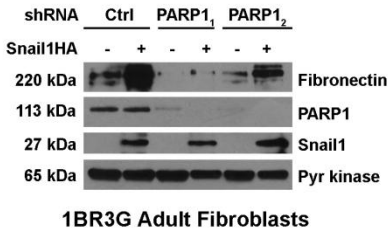


**Figure 24: PARP1 shRNA prevents FN1 activation by Snail1 in 1BR3G adult fibroblasts.**
Fibroblasts were infected with either shRNAs specific for PARP1 or an irrelevant shRNA control for 48 hours. Cells were then lysed, and the expression levels of the indicated proteins were analyzed by western blot.

Human adult skin 1BR3G fibroblasts responded to TGFβ1 treatment increasing the levels of Snail1 and FN (Figure 25). The depletion of p65NF-κB prevented only the upregulation of the former, while the response of Snail1 to the stimulus remained unchanged.

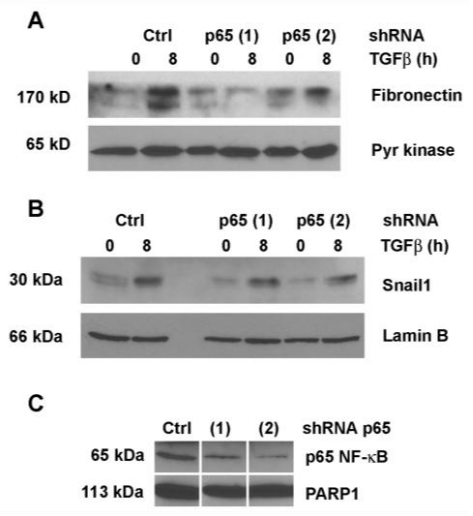


**Figure 25: P65NF-KB is required for Fibronectin expression by TGFβ1 in 1BR3G fibroblasts.**

Depletion of p65NF-κB by shRNA interferes with fibronectin activation by TGFβ1. 1BR3G fibroblasts were infected with a lentivirus carrying control, or two different shRNAs used separately and treated for 0 or 8 hours with 5 ng/ml of TGFβ1 48 hours after the infection. Indicated proteins were analyzed by Western blot from 10μg of cytosolic extract (A) or 50μg of nuclear extracts (B and C).

# 2. Fibroblastic Snail1 promotes myofibroblastic traits that mechanically control tumor malignance and wound healing

## 2.1. TGFβ1 remodels fibroblast-derived 3D matrices in Snail1 dependent manner

Given the capacity of fibroblastic Snail1 to modulate the levels of ECM proteins, we studied how the expression of Snail1 affects the integrity and the architecture of the ECM and analyzed the repercussions of Snail1 expression on the topology of the ECM of the tissues where activated fibroblasts are found- tumor stroma and granulation tissue of skin wound.

To visualize the gross impact of Snail1 loss on the ECM, we generated *in vivo* like 3D extracellular matrices following previously described protocol for fibroblast-derived tridimensional extracellular matrix (3D-ECM) production[169,170]. For this purpose, we used control or Snail1-KO mouse embryonic fibroblasts (MEFs) previously generated in the lab. In agreement with our data that Snail1 modulates a set of ECM genes, MEFs lacking Snail1 produced matrices that were less abundant in collagen (shown by general Masson's trichrome staining of collagen) and acidic polysaccharide-contacting molecules (Alcian blue). Moreover, TGFβ1 caused the increase in all of the aforementioned components that was much less evident in the KO derived 3D-ECMs (Figure 26).

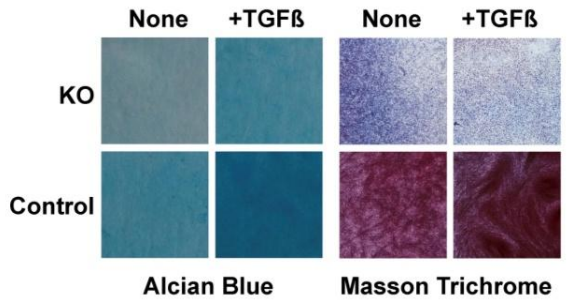


**Figure 26: Masson's trichrome staining and Alcian blue staining of the MEF-derived ECMs.**

Images without magnification show representative regions of the indicated stained matrices.

In fact, TGFβ1 caused major change in the rigidity of 3D-ECMs in Snail1-dependent manner (Figure 27) that we quantified using atomic force microscopy analysis.

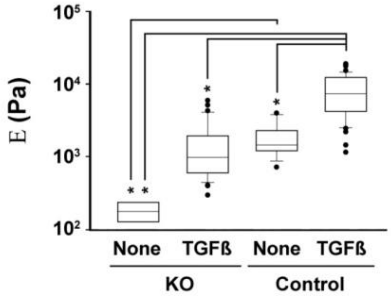


**Figure 27: Stiffness of extracellular matrices derived from control and Snai1 KO MEFs treated or not with TGFβ1.**
Young's modulus, E, was estimated on decellularized matrices by atomic force microscopy and represented in a box plot. Asterisks indicate a statistically significant difference as determined by ANOVA on ranks and Dunn's method ($p < 0.001$).

Western blot analysis showed that the levels of the ECM proteins (fibronectin and thrombospondin) were higher in control MEFs compared to KO cells (Figure 28). In control fibroblasts TGFβ1 induced further increase in fibronectin and thrombospondin amount, but this increase was not evident in KO fibroblasts, in agreement with our observation that 3D-ECMs produced by KO MEFs were less abundant in general (Figure 26). TGFβ1 also induced in the control, but not in KO MEFs higher levels of LOX, extracellular enzyme responsible for the collagen and elastin crosslinking and ECM stiffening, supporting our result that 3D-ECMs deposited by KO MEFs are softer compared to the controls, regardless of the TGFβ1 treatment.

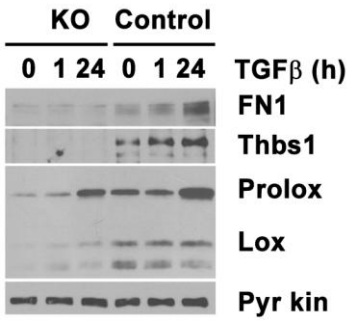


**Figure 28: Time course of ECM protein expression in TGFβ1-treated control and Snail1 KO MEFs.**
Protein levels of thrombospondin, fibronectin and LOX were measured by Western blot from total cell extracts of MEFs treated with TGFβ1 (5 ng/ml) at the indicated time points. Pyruvate kinase levels were measures as a loading control.

## 2.2. Cell commitment is modulated by 3D-ECMs in a Snail1-dependent manner

Matrix rigidity influences the commitment of the progenitor cells[171], so we decellularized our 3D-ECMs and used them as a substrate for murine mesenchymal stem cells (mMSC) and C2C12 cells grown in the presence of the mediums that force their differentiation. C2C12 cells are a well-established model for differentiation and it has been reported that they differentiate towards myoblasts when serum deprived. We could observe nuclei positive for myogenin, a marker of myoblasts, and the formation of F-actin positive structures only when progenitor cells were plated over the matrices produced by KO MEFs (Figure 29), suggesting that soft and compliant substrate, like one progenitor cells would encounter in muscle niche, facilitates and favors the differentiation, while more rigid substrate prevented the process.

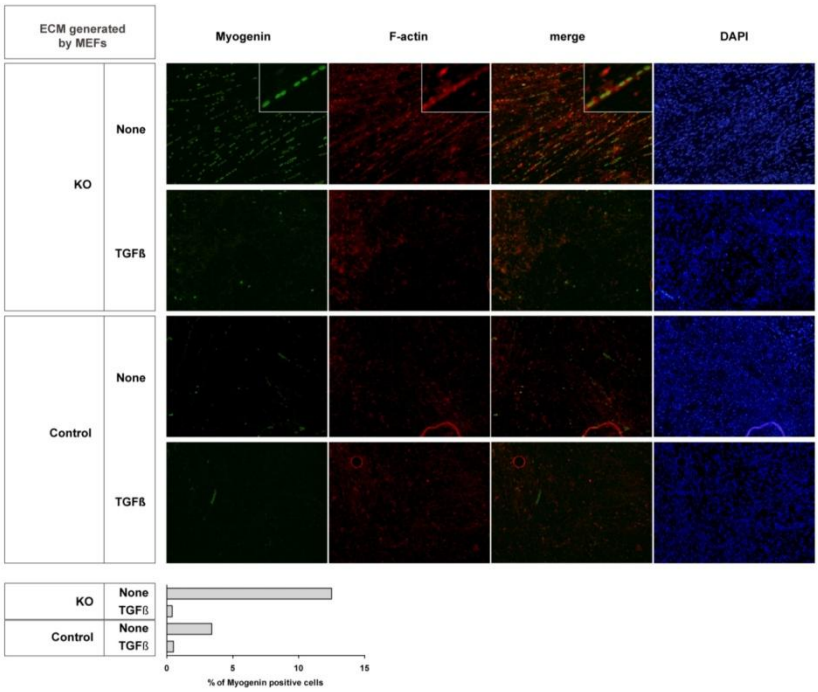


**Figure 29: C2C12 myogenic differentiation on fibroblast-derived matrices.**
C2C12 cells were forced to differentiate toward myogenic lineages on decellularized ECMs from control or *Snail1* KO MEFs treated or not with TGFβ1. Myogenin (green) and F-actin (red) were visualized by immunofluorescence, and nuclei were counterstained with DAPI (blue). The percentage of myogenin-positive cells plotted at the bottom was calculated from a minimum of 1000 cells per condition. While 15% of the C2C12 precursors differentiated towards myogenic lineages on the compliant 3D-ECM generated by *Snai1* KO MEFs, less than 3% of them differentiated on the more rigid matrices.

In contrast, when we forced mMSCs to differentiate towards osteogenic lineages, they remained undifferentiated on softer matrices, while the stiffness of 3D-ECM produced by control MEFs treated with TGFβ1 sustained the differentiation (Figure 30), suggesting that differentiation is accelerated in the conditions similar to that progenitor cells would encounter in bone niche, while softer niche supported undifferentiated state.

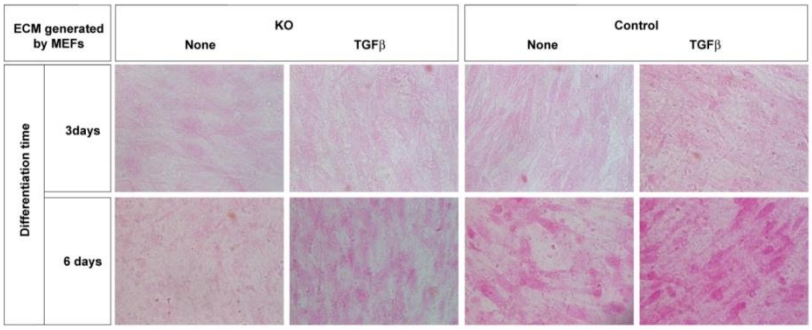


**Figure 30: Osteogenic differentiation of mesenchymal stem cell on fibroblast-derived matrices.**
Mesenchymal stem cells (MSC) were forced to differentiate towards osteogenic lineages on decellularized ECMs from control or *Snai11* KO MEFs treated or not by TGFβ1. Calcific depositions were visualized by alkaline phosphatase staining after 3 and 6 days. MSCs failed to differentiate to osteogenic lineages on the compliant matrix, while the stiffer matrices were more permissive.

## 2.3. Active form of Snail1 is required for TGFβ1 induced ECM alignment and production

In-depth analysis using confocal microscopy of immunofluorescence stained 3D-ECMs showed that KO MEFs produced thinner matrices containing fewer fibronectin and thrombospondin fibers than those produced by control MEFs (Figure 31A), in agreement with our Western blot results. TGFβ1 treatment caused increased thickness in control matrices and parallel orientation of the fibronectin fibers residing in the upper layers of the ECM.

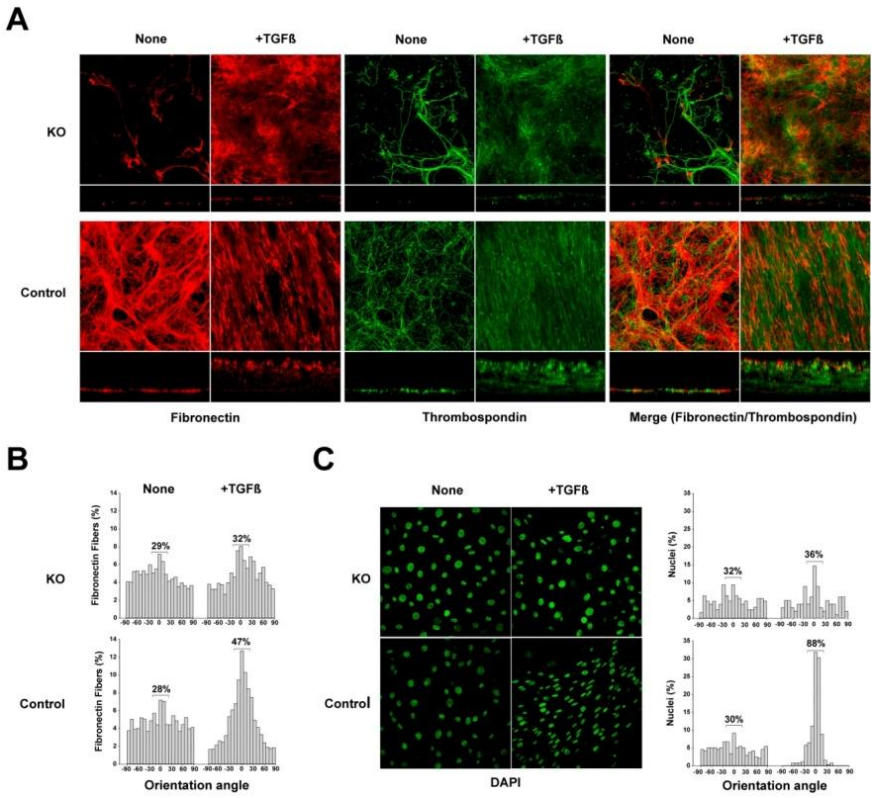


**Figure 31: TGFβ1 remodels the ECM generated by MEFs in a Snail1-dependent manner.**
A) Fibronectin and thrombospondin fibers in ECMs from control and *Snai1* KO MEFs either treated or not with TGFβ1, as indicated. Fibronectin (red) and thrombospondin (green) were visualized by immunofluorescence (at 200×) from the indicated MEFs treated or not with 5 ng/ml of TGFβ1 during 10 days of ECM deposition. Each image is accompanied by a transversal ECM section at the bottom. (B) Fibronectin fibers orientation in ECMs from control and *Snai1* KO MEFs either treated or not with TGFβ1, as indicated. The orientation angle of the fibronectin fibers visualized as in (A) was calculated[172] and plotted as a frequency distribution centered in the modal angle (set as 0°). Percentages indicate oriented fibers accumulated in a range of ± 21° around the modal angle. (C) Nuclei orientation from control and *Snai1* KO MEFs treated or not with TGFβ1, as indicated. Nuclei were stained with DAPI in the indicated MEFs that had been treated as in (A). The nuclei orientation angles were calculated (ImageJ) and plotted as a frequency distribution centered in the modal angle (set as 0°). Percentages indicate oriented nuclei accumulated in a range of ± 21° around the modal angle.

Using previously described algorithm[172], we compared FN1 fiber orientation of the four types of 3D-ECMs (Figure 31B).

While we observed no preferred orientation angle in the untreated matrices, supplementing control MEFs with TGFβ1 during the deposition caused alignment that did not occur in the matrices deposited by TGFβ1 treated KO MEFs. Not just fibers, but also the nuclei of the control MEFs were oriented and become elongated upon TGFβ1 stimulus (Figure 31C).

*In vivo*, soluble factors secreted either by cancer cells or by adjacent fibroblasts influence in paracrine fashion resident fibroblast activity. For this reason, we wondered if Snail1 had an indirect effect on ECM topology, through secreted paracrine factors. We tested if conditioned medium produced by control ECM-depositing MEFs could rescue the phenotype of KO produced 3D-ECMs. Even conditioned medium from control MEFs treated with TGFβ during ECM deposition was not sufficient to produce the increase in thickness, nor the organization of the KO matrix (Figure 32). Supplementing the conditioned medium during ECM deposition with TGFβ1 did not cause the alignment in KO 3D-ECMs. This suggested that Snail1 and intracellular Snail1-dependent processes are directly required for the organization of the extracellular matrix architecture.

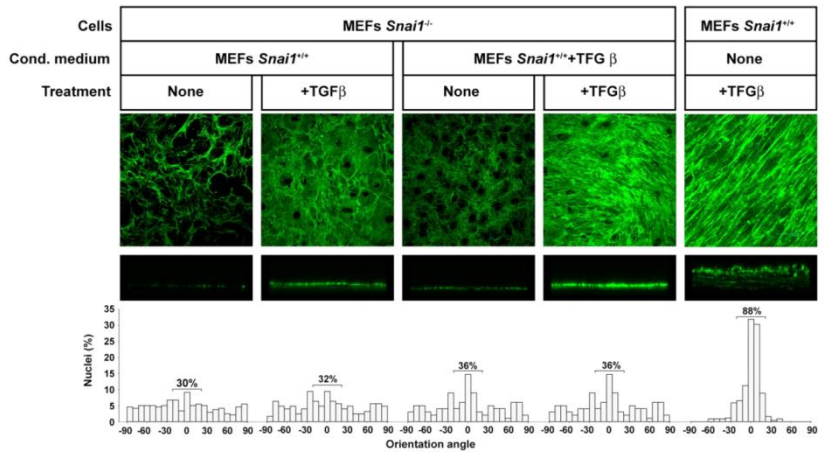


**Figure 32: Effects of WT-conditioned medium on KO-produced ECM.** Fibronectin (green) was visualized by immunofluorescence (at 200x) from KO MEFs treated or not with TGFβ1 using either normal DMEM or conditioned medium from control MEFs treated or not with TGFβ1. Each image is accompanied by a transversal ECM section at the bottom. Nuclei

were counterstained with DAPI and the orientation angles of nuclei were calculated and plotted as in Figure 31.

The necessity of Snail1 as transcription factor in this process was confirmed by reintroducing either dead or active mutant of Snail1 in KO MEFs (Figure 33). We could detect clear nuclear signal for both proteins, but only the active form rescued the phenotype seen in control matrices after TGFβ1 treatment.

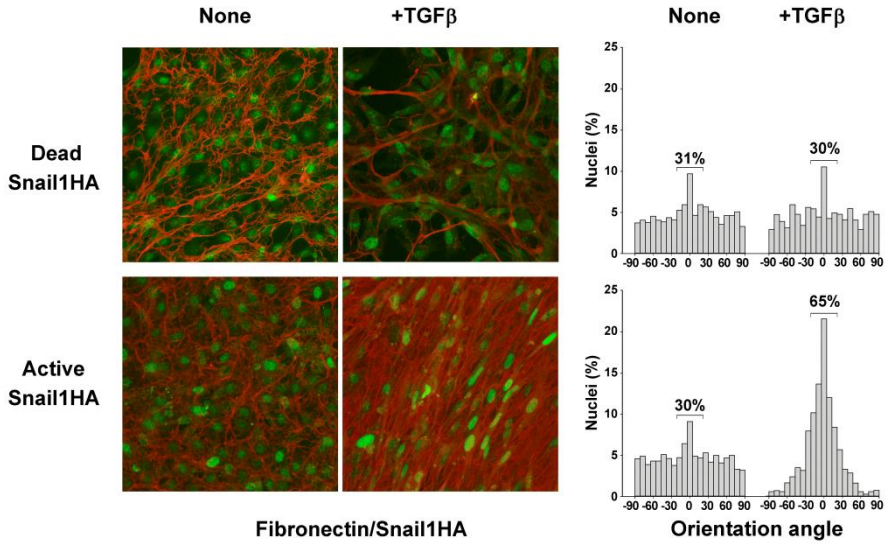


**Figure 33: Transduction of the active Snail1 rescues the phenotype of the KO-deposited ECM.**
Fibronectin (red) and Snail1 (green) were visualized by immunofluorescence (at 200×) from KO MEFs stably expressing a mouse Snail-P2A (dead mutant) or Snail1-SA (active mutant) treated or not with 5 ng/ml of TGFβ1 during 10 days of ECM deposition. Nuclei were counterstained with DAPI and the orientation angles of nuclei were calculated and plotted as in Figure 31.

Not only activated MEFs, but 1BR3G skin fibroblasts overexpressing ectopic Snail1[173] produced aligned 3D-ECMs (Figure 34A), and another mesenchymal cell line where Snail1 was depleted, mesenchymal stem cells, failed to align their nuclei in the absence of Snail1 (Figure 34B).

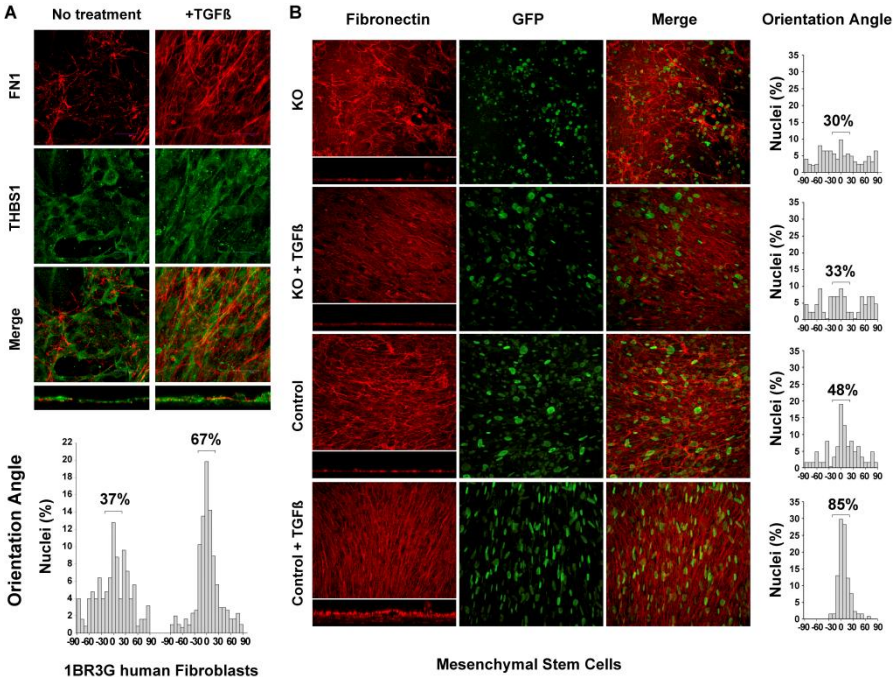


**Figure 34: TGFβ1 remodels the ECM generated by mesenchymal stem cells and 1BR3G cells in a Snail1-dependent manner.**
(A) Fibronectin fibers and nuclei orientation in 3D-ECMs of control or Snail1-depleted mesenchymal stem cells (*Snai1*$^{del/flox}$ mesenchymal stem cells transduced with GFP (control) or CRE-GFP (KO)). Snail1 depletion was confirmed by Western blot. Fibronectin (red) and nuclei (green; from GFP) were visualized by immunofluorescence. Nuclei orientation distribution was calculated and plotted as in Figure 31.
(B) Orientation of nuclei and fibronectin and thrombospondin fibers of control or Snail1 overexpressing 1BR3G human adult fibroblasts. Cells were grown according to the protocol for generating ECMs in the presence or absence of 5 ng/ml of TGFβ1. Fibronectin (red) and thrombospondin (green) were visualized by immunocytochemistry.

## 2.4. Snail1 mediates full fibroblast activation after TGFβ1 treatment

As mentioned in the introduction, activated fibroblasts are positive for α-smooth muscle actin (α-SMA). This feature empowers them with contractility necessary for tissue repair processes they participate in.

During myofibroblast differentiation there is significant elongation of focal adhesions that are associated with α-SMA -

positive stress fibers. Generation of the focal adhesions called fibronexus is dependent on the existence of tensile forces generated inside and outside of the cell. Directional forces generated by α-SMA stress fibers applied on fibronexus control fibronectin fibrillogenesis and fiber orientation in the extracellular compartment. Dynamics of αSMA expression and it posterior incorporation into stress fibers depends on RhoA activity[174].

We tested if Snail1 was remodeling the ECM inducing the activity of the α-SMA cytoskeleton. Control MEFs expressed basal levels of Snail1 that were upregulated after 1h TGFβ1 of treatment (Figure 35). αSMA expression was detectable after 8h of TGFβ1 treatment in the control MEFs, but not in KO MEFs.


**Figure 35: Time course of Snail1 and αSMA expression in TGF β1-treated control and Snai1 KO MEFs.**
Snail1 and αSMA protein levels were measured by Western blot from total cell extracts of MEFs treated with TGFβ1 (5 ng/ml) at the indicated time points. Pyruvate kinase levels were measures as a loading control.

KO MEFs not only produced less αSMA, but failed to incorporate it into stress fibers (Figure 36). There were almost no KO MEFs with αSMA-positive stress fibers and after TGFβ1 treatment only a slight increase was detected. In control MEFs, around 85% of the cells were detected after TGFβ1 treatment as positive in immunofluorescence analysis (Figure 36, right panel).

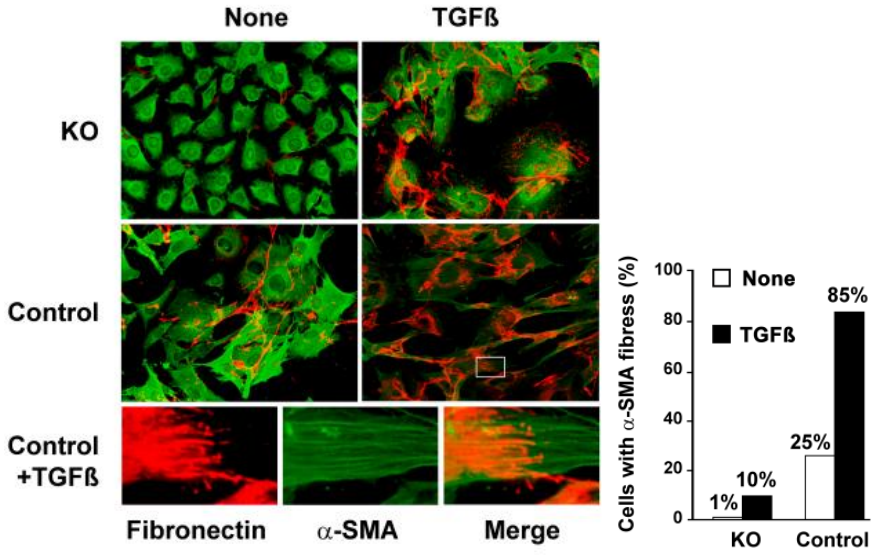


**Figure 36: Snail1 is required for TGFβ1-induced αSMA expression and αSMA-dependent events.**
Left panel: αSMA and fibronectin from control and *Snai1* KO MEFs treated or not with TGFβ1. αSMA (green) and fibronectin (red) were visualized by immunofluorescence (200×) from indicated MEFs grown in the presence or absence of 5 ng/ml of TGFβ1 for 60 hr. Bottom images correspond to electronically amplified areas from control MEFs treated with TGFβ1 and display co-aligning of fibronectin and αSMA fibers. Right panel: Percentage of control and *Snail1* KO MEFs treated or not with TGFβ1 with αSMA-positive fibers. The percentage of cells with αSMA-stained fibers was calculated by counting a minimum of 500 cells per condition from immunofluorescence images as those shown in the right panel.

The contractile power of αSMA positive stress fibers governs the fibronectin fibrilogenesis and fiber orientation[175] transmitting tension to ECM. In immunofluorescence analysis, we observed that extracellular fibronectin fibers co-aligned with the intracellular αSMA positive stress fibers only in TGFβ-treated control MEFs (Figure 36, amplification). In control and KO MEFs cultured for 24h in the presence or absence of TGFβ1, we measured the percentage of long and very long focal contacts (paxillin-stained) and we found that in control MEFs it was higher (Figure 37).

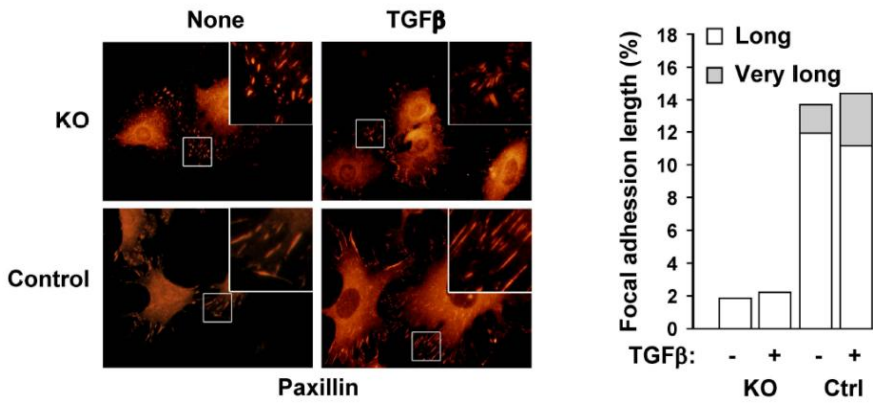


**Figure 37: Paxillin-stained focal junctions from control and Snail1 KO MEFs treated or not with TGFβ1.**
Paxillin was visualized by immunofluorescence (400×) after 24 hr of culturing the indicated MEFs. The lengths of the paxillin contacts were measured with ImageJ, and the percentage of contacts in each condition that were long (ranging from 25 to 50% relative to the longest contact) or very long (more than 50%) were plotted. Electronic amplification (3x) is shown in the boxes.

Fibronectin fibrilogenesis assay reflects the capacity of fibroblasts to polymerize offered soluble fibronectin. Control and TGFβ1-treated control MEFs were significantly more efficient in this process, quantified by the zones left with no fibronectin staining (Figure 38).

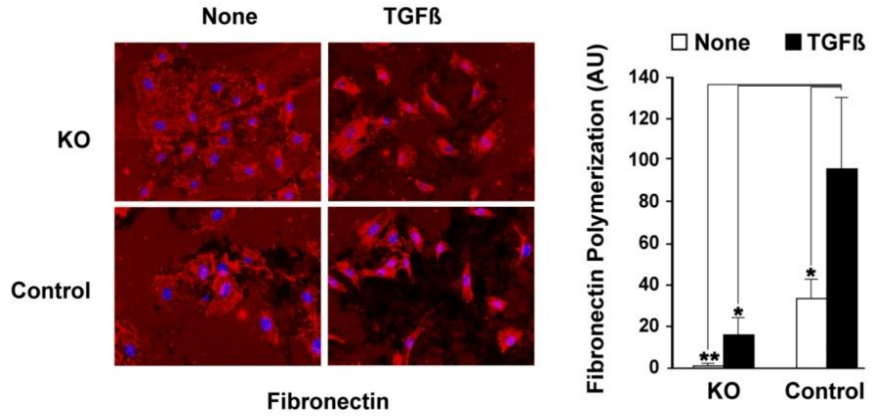


**Figure 38: Fibronectin fibrillogenesis from control and Snai1 KO MEFs treated or not with TGFβ1.**
Fibronectin was visualized by immunofluorescence (200×) after MEFs had been cultured on fibronectin-coated cover slips for 16 hr. The plotted

fibrillogenesis estimation in each condition was quantified as the surface glass areas with an intensity value lower that a background threshold level (ImageJ). Bars represent the mean ± SD from at least ten different fields.

Using rhotekin pull-down assay, we compared the amount of active RhoA in KO and control MEFs (Figure 39). More active RhoA was present in the control fibroblasts and the upregulation following TGFβ1 treatment occurred to a lesser degree in KO MEFs, suggesting that RhoA activation is downstream of Snail1.

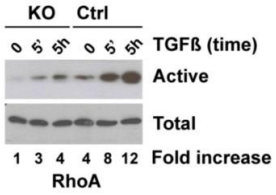


**Figure 39: Amount of the active RhoA in control and Snai1 KO MEFs treated with TGFβ1.**
MEFs were treated with TGFβ1 (5 ng/ml) for the time indicated (5 min or 5 hr). RhoA-GTP in the pull-down assays (active RhoA) and input samples (total RhoA) were analyzed by Western blot and quantified by densitometry. RhoA-GTP values were normalized by the total RhoA value in the corresponding input sample and are indicated at the bottom as fold increase relative to the amount in non-treated KO MEFs.

Treating the control MEFs with the inhibitor of ROCK1, known downstream kinase of RhoA, prevented the accumulation of αSMA, but did not prevent rapid response of Snail1 to TGFβ1 treatment (Figure 40), suggesting that Snail1 activation by TGFβ1 is an upstream event.

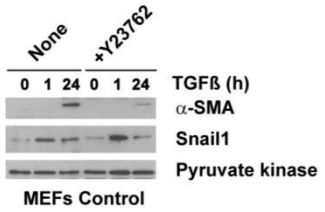


**Figure 40: Snail1 and αSMA expression in TGF β1-treated control MEFs in the presence or absence of ROCK1 inhibitor (Y23762).**
Snail1 and αSMA protein levels were measured by Western blot from total cell extracts of MEFs treated with TGFβ1 (5 ng/ml) at the indicated time

points and grown in the presence or absence of 10 μM of Y23762. Pyruvate kinase levels were measured as a loading control.

We supposed that impeding αSMA upregulation in response to TGFβ1 treatment would have repercussions in all the processes where mechanical signaling is needed. Indeed, the use of the inhibitor during the deposition of 3D-ECMs by control MEFs with or without TGFβ1 had an effect similar to Snail1 depletion, preventing the fiber alignment (Figure 41).

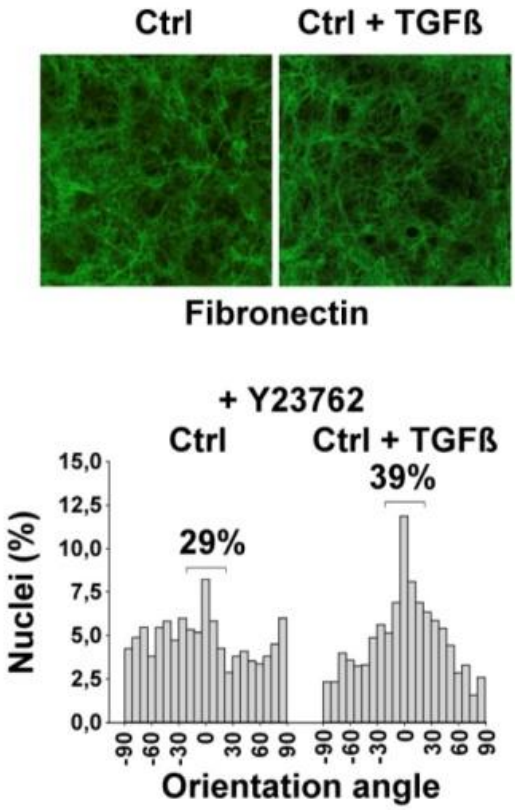


**Figure 41: Control MEFs deposited ECMs treated or not with TGFβ1 in the presence or absence of ROCK1 inhibitor (Y23672).**
Fibronectin fibers (green) were visualized (at 200×), and their orientation was calculated and plotted as in Figure 31.

The contractile activity of αSMA positive stress fibers in fibroblasts also forces maturation of adherens junctions, cell-to-cell contacts that myofibroblasts use to signal each other about mechanical stress. Transmembrane protein forming the

adherens junctions is N-cadherin[176]. By immunofluorescence, we could observe elongated N-cadherin positive structures in control TGFβ1 treated MEFs, but not in KO MEFs (Figure 42).

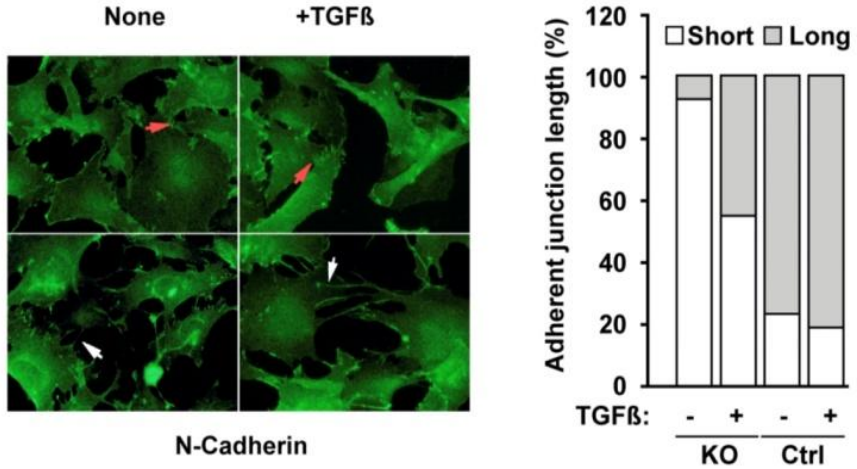


**Figure 42: N-cadherin stained adherens junctions in control and Snail1 KO MEFs treated or not with TGFβ1.**
N-cadherin (green) was visualized by immunofluorescence (400×) in the indicated MEFs grown for 60 hr on plastic dishes. Length of contacts was measured with ImageJ and classified as short or long contacts, depending if they were shorter or longer than 20% of the longest contact. Red and white arrowheads indicate short and long contacts, respectively. Percentages of short and long contacts in the indicated MEFs are plotted in the left panel. A minimum of 500 contacts per condition were analyzed.

We checked by Western blot the levels of N-cadherin in the absence of Snail1 (Figure 43). KO MEFs expressed less N-cadherin and failed to upregulate its levels in response to TGFβ1 the way control cells did.

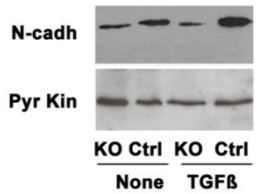


**Figure 43: N-cadherin protein levels in control and Snai1 KO MEFs treated or not with TGF β1.**
N-cadherin protein levels were quantified from total cell extracts obtained from the indicated MEFs treated or not with TGFβ 1 (5 ng/ml for 60 hr). Pyruvate kinase was analyzed as a loading control.

β-catenin binds N-cadherin directly on the cytoplasmatic side of the junction[177,178]. Stress fibers are also connected intracellularly via adherens junctions. In control MEFs we observed αSMA positive fibers of the two adjacent cells co-localizing with β-catenin present in the junctions (Figure 44), supporting our model.

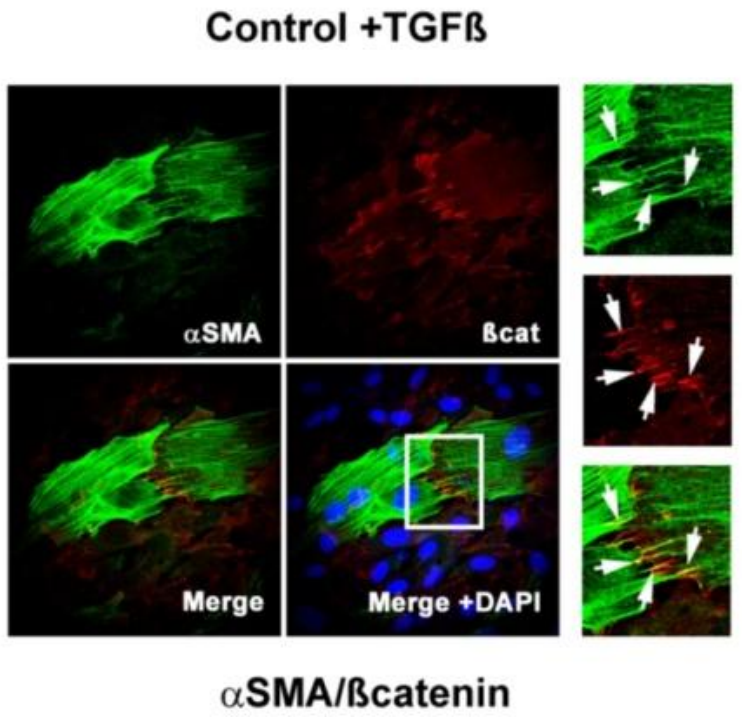


**Figure 44: αSMA and β-catenin staining in two adjacent control MEFs treated with TGFβ1.**
αSMA (green), β-catenin (red) and nuclei (blue) were visualized by immunofluorescence (200x) in control MEFs treated with TGFβ1. Three panels on the right show a zone of cell-cell contacts. Arrows point to co-localization.

Presence of ROCK1 inhibitor prevented the proper formation of N-cadherin stained adherens junctions (Figure 45), indicating that Snail1 dependent αSMA increase and posterior incorporation into stress fibers via RhoA is also necessary for cell-cell contacts formation and maturation.

Altogether, our data suggest that myofibroblast activation is not taking place in MEFs that are KO for Snail1.

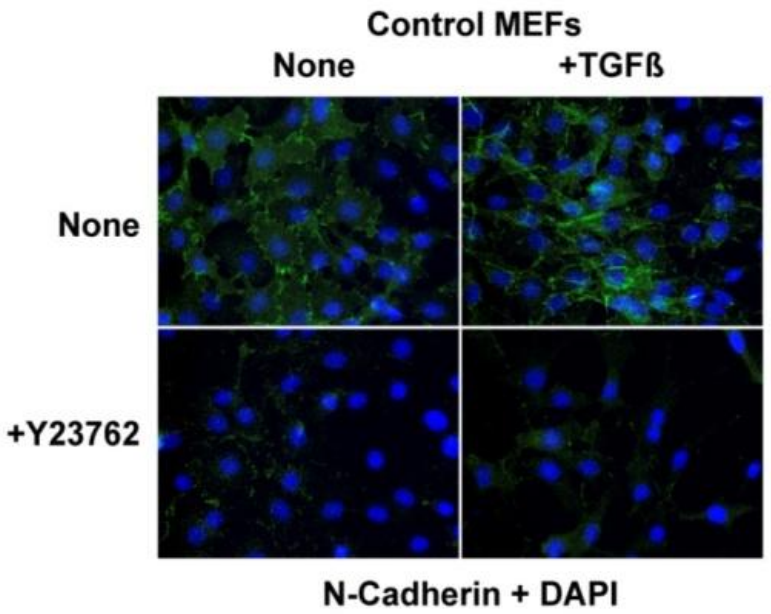


**Figure 45: N-cadherin stained adherens junctions in control MEFs treated or not with TGF β1 in the presence or absence of the ROCK1 inhibitor (Y23762).**
N-cadherin (green) and nuclei (blue) were visualized by immunofluorescence (200×) in the indicated MEFs grown for 24 hr on cover slips in the presence or absence of 10 μM of Y23762.

## 2.5. ECM organizing capacity of CAFs correlates with their Snail1 levels

Fibroblasts present in reactive stroma surrounding the growing tumor are found in active state and are usually called cancer-associated fibroblasts (CAFs). We used human primary CAFs from surgical colon tumors (obtained in collaboration with Dr. Cristina Peña from Hospital Universitario Puerta de Hierro de Majadahonda, Madrid) in order to check the expression of Snail1 (Figure 46) and their capacity to generate and organize 3D-ECMs (Figure 47).

Three different established CAF lines (77, 120 and 148) presented different levels of Snail1 protein. CAF-120 expressed higher levels of Snail1 than the other two lines and the levels of

the marker of fibroblast activation, αSMA, as well as N-cadherin and fibronectin were significantly increased compared to the other two lines of CAFs.

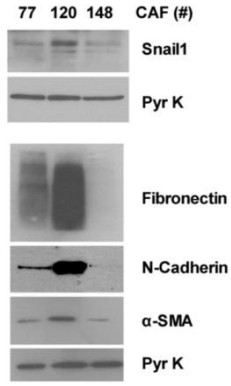


**Figure 46: Protein expression in primary CAF lines established from surgical human tumors.**
Fibronectin, αSMA, Snail1, N-cadherin, and pyruvate kinase from indicated CAF lines were measured from total cell extracts by Western blot.

Snail1 levels expressed by CAFs were directly proportional with their capacity to organize 3D-ECM. CAF-120 line nuclei alignment in mature 3D-ECMs was similar to the one observed in control MEFs treated with TGFβ1. CAF-77 and CAF-148 nuclei acquired higher orientation compared to unactivated MEFs, but less than CAF-120 (Figure 47).

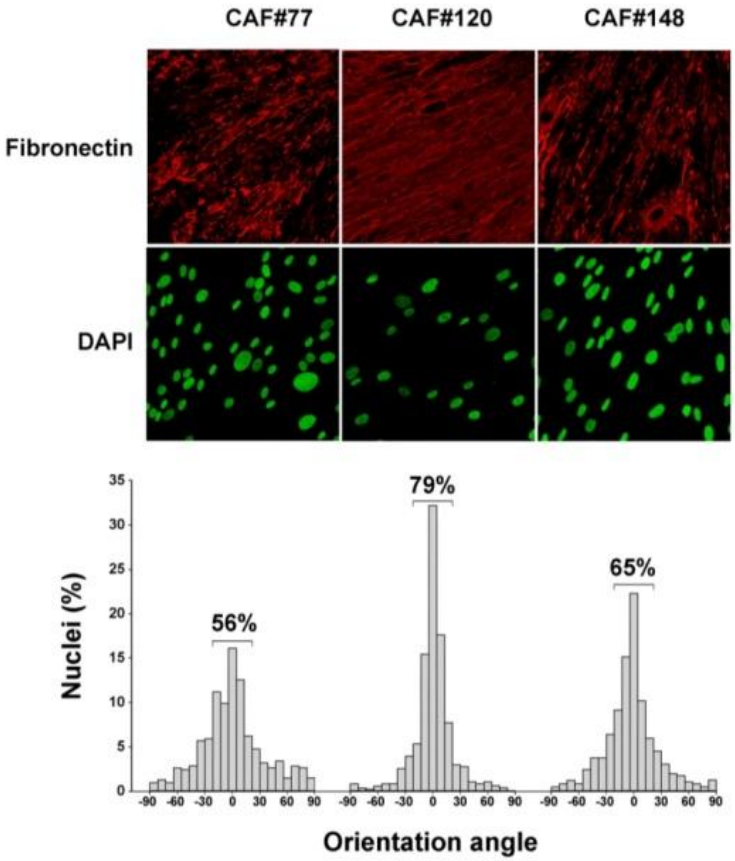


**Figure 47: Fibronectin fibers and nuclei orientation of ECM deposited by primary CAF lines established from surgical human tumors.**
Fibronectin (red) in ECMs generated by the indicated CAF lines was visualized by immunofluorescence, and CAF nuclei (green) by DAPI staining (200×). Nuclei orientation angles were calculated and plotted as in Figure 31.

Since activated fibroblasts represent only a small portion of all the fibroblasts present in the tumor stroma, we mimicked this situation *in vitro* co-cultivating CAFs with unactivated fibroblasts (control MEFs) to test if the few CAFs could impose matrix organization. Murine fibroblasts organize their chromatin in structures called chromocenters that are stained with DAPI and this allowed us to easily distinguish the two cell types in immunofluorescence (Figure 48). A proportion of 30% of CAF-120 line imposed 3D-ECM organization on control MEFs,

whose nuclei alignment reached the degree of organization observed in CAFs.

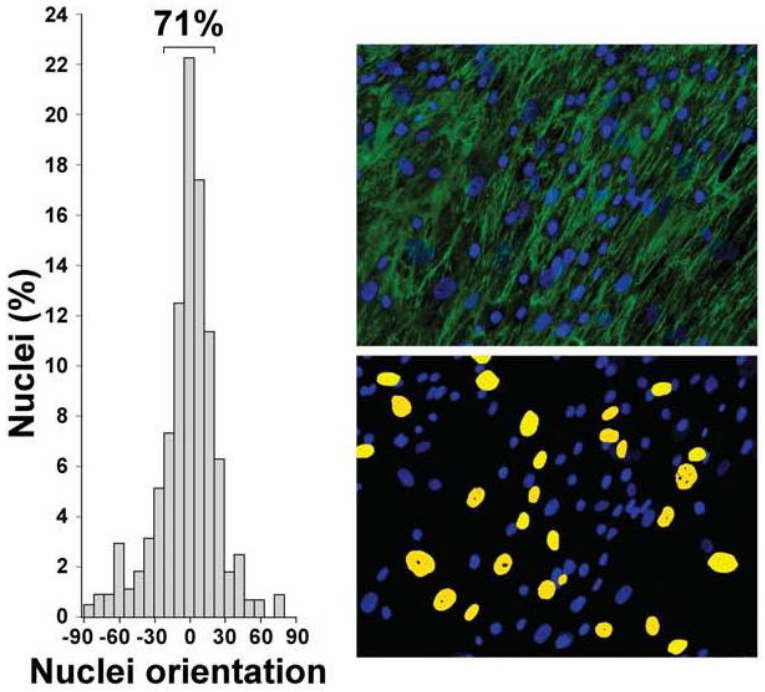


**Figure 48: Presence of primary CAF lines during ECM deposition by control MEFs causes nuclei alignment.**
Control MEFs (70%) and CAF #120 (30%) were co-cultured according to the standard protocol for generating ECMs. Fibronectin (green) was visualized by immunofluorescence, and nuclei were counterstained with DAPI. In contrast to murine MEFs nuclei, human CAFs nuclei (highlighted in yellow) did not present chromocenter staining (DAPI dots) and could be discarded from the analysis (ImageJ). Nuclei orientation angles of MEFs were calculated and plotted as in Figure 31.

We repeated the experiment using the other two CAF lines (Figure 49). The capacity of CAFs to impose matrix organization was in proportion with the levels of Snail1 cells expressed.

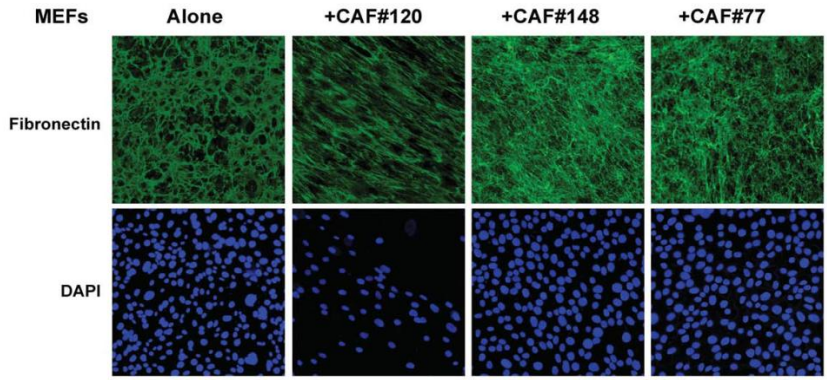


**Figure 49: MEF nuclei and fibronectin fibers in cocultures of MEFs with CAF lines.**
Fibronectin (green) was visualized by immunofluorescence, and nuclei were visualized with DAPI, from co-cultures of control MEFs and the indicated CAF lines (to a final amount of about 30%) grown according to the standard protocol for generating ECMs. CAF nuclei were deleted as indicated in Figure 44.

We confirmed this observation quantifying nuclei orientation of MEFs in each of the cocultures with CAFs (Figure 50).

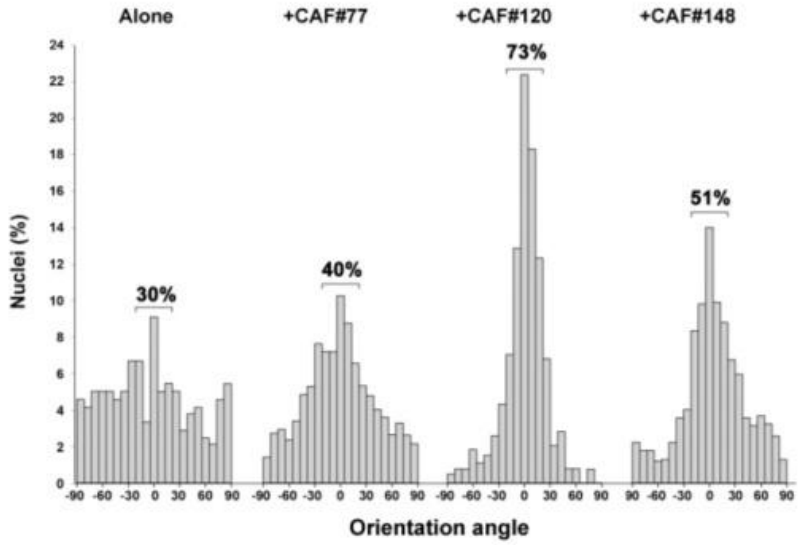


**Figure 50: Nuclei orientation of MEFs grown in the presence of primary CAF lines.**

Nuclei were stained with DAPI from co-cultures of control MEFs and the indicated CAF lines. The nuclei orientation angles of MEFs were calculated and plotted as in Figure 31.

To determine the limiting amount of CAFs needed to organize the extracellular matrix, we seeded in co-culture with control MEFs decreasing amounts of CAF-120 cells (Figure 51). 1% of CAFs sufficed to cause local matrix alignment.

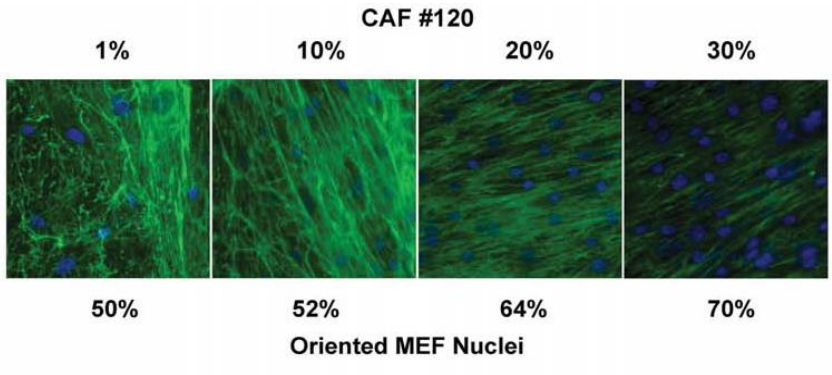


**Figure 51: MEF nuclei reorientation in the presence of increasing amounts of CAF #120.**
Control MEFs were grown according to the standard protocol for generating 3D-ECMs in the presence of increasing amounts of CAF #120. The final percentage of CAFs relative to the total amount of fibroblasts (the number is indicated above the corresponding image) in the co-culture was estimated by counting a minimum of 500 nuclei per condition. MEF nuclei angles were calculated (as described in Figure 31) and orientation frequencies are showed below the corresponding images.

## 2.6. 3D-ECM produced by Snai1-lacking fibroblasts fails to promote anisotropic cancer cell migration and invasion

It has been proposed that stiff and perpendicular collagen fibers around breast cancers facilitate the invasion[179]. For this reason, we tested the capacity of 3D-ECMs to support breast cancer cells invasion and migration. We plated MDA MB231 over decellularized 3D-ECMs from control and KO MEFs treated or not with TGFβ1 during deposition.

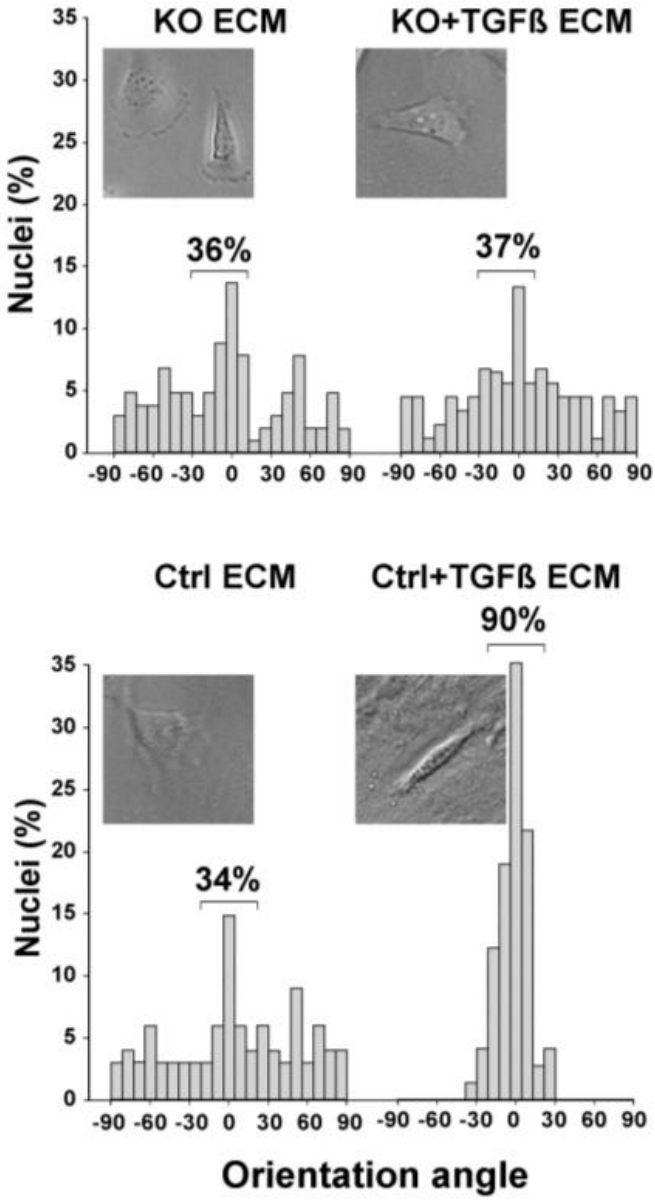


**Figure 52: Nuclei orientation of MDA-MB 231 tumor cells grown on ECMs from TGFβ1-treated control and Snai1 KO MEFs.**
Cells plated on the indicated decellularized matrices were allowed to attach for 24 hr. Nuclei of tumor cells were stained with DAPI, and nuclei orientation angles were calculated and plotted as in Figure 31. A light

transmitted image of a representative cell grown in the indicated ECM is shown.

Cells obtained typical amoeboid morphology (Figure 52) and were moving without preferential direction (Figure 53) when plated over the untreated control matrices or KO matrices treated or not with TGFβ1. Only when plated over TGFβ1 treated control matrices MDA MB231 cells adopted elongated, bipolar morphology and showed anisotropic movements (Figures 52 and 53).

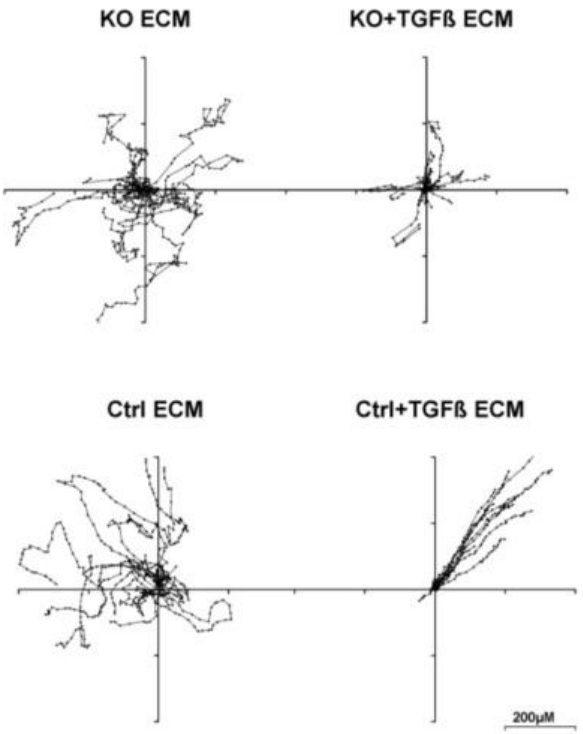


**Figure 53: Single cell tracks of MDA-MB 231 tumor cells moving on ECM from TGF β1-treated control and Snai1 KO MEFs.**
Cell tracker–labeled cells plated on decellularized matrices generated by the indicated MEFs were allowed to attach for 24 hr and then photographed every 15 min. Single-cell coordinates at each time point were calculated with ImageJ, and tracks of ten representative cells per condition relative to the initial position were plotted.

To test if stromal Snail1 supports invasion *in vitro*, the four types of matrices (control and KO treated or not with TGFβ1) were deposited on Boyden chamber inserts and were

decellularized prior to the plating of the cancer cells (Figure 54). Stiff and highly organized 3D-ECMs produced by TGFβ1-treated control MEFs promoted the invasion, and significant decrease in invasion capacity was observed for MDA MB 231 cells on 3D-ECMs produced by KO MEFs.

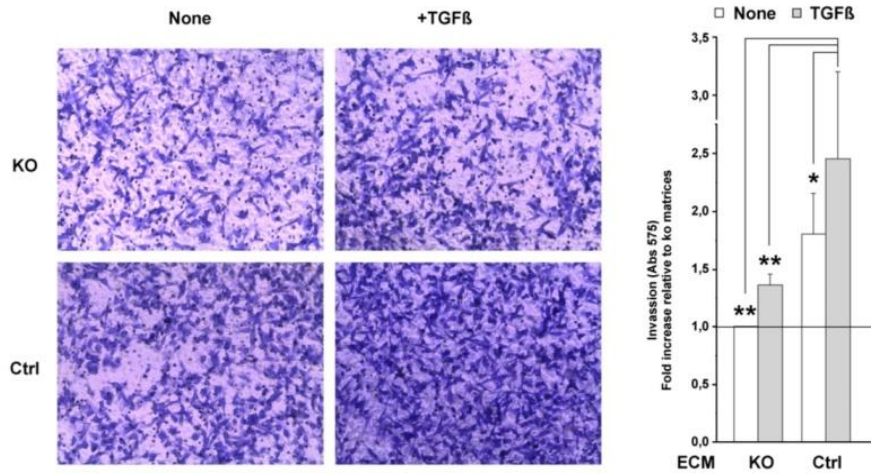


**Figure 54: Invasive capacity of MDA-MB 231 cells on ECM from TGF β1-treated control and Snai1 KO MEFs.**
Cell tracker–labeled green cells were plated over decellularized matrices generated on invasion inserts by the indicated MEFs. Tumor cells were seeded and allowed to invade the matrices for 24 hr. Images (100×) of violet crystal stained cells attacked to the lower side of the membrane are shown. Cells were then quantified by measuring the A575 of the cells solubilized with an HCl solution. Values represent the mean ± SD from three independent experiments. Asterisks indicate a statistically significant difference as determined by the Student's test with a p value <0.05 (*) and 0.01 (**).

## 2.7. Snail1 expression in breast cancer stroma induces local anisotropic fibronectin and collagen alignment and is associated with worse outcome

To study the relevance of our findings about the effect of Snail1-positive CAFs on migration and invasion capacities of breast cancer cells, we analyzed Snail1 expression in stroma of human infiltrating early breast carcinomas (from a TMA obtained in collaboration with Dr. Joan Albanell from the Hospital del Mar).

16,4% (61 out of 371 cases) presented nuclear Snail1 signal in spindle-shaped stromal cells (Figure 55).

We chose a set of tumors (15 positive and 15 negative for Snail1 in stroma) to further analyze Snail1 expression and the architecture of stromal fibers. Snail1 and fibronectin expression was visualized by immunofluorescence (Figure 55). Uppermost and the middle part of the panel are the cases of Snail1 positive stroma, while the bottom panel represents area of the stroma negative for Snail1 expression. There was heterogeneity for Snail1 positive cells amount, but fibronectin alignment and perpendicular organization could have been observed even when only a few Snail1 positive cells were stained, while there were no aligned fibers in the zones negative for Snail1.

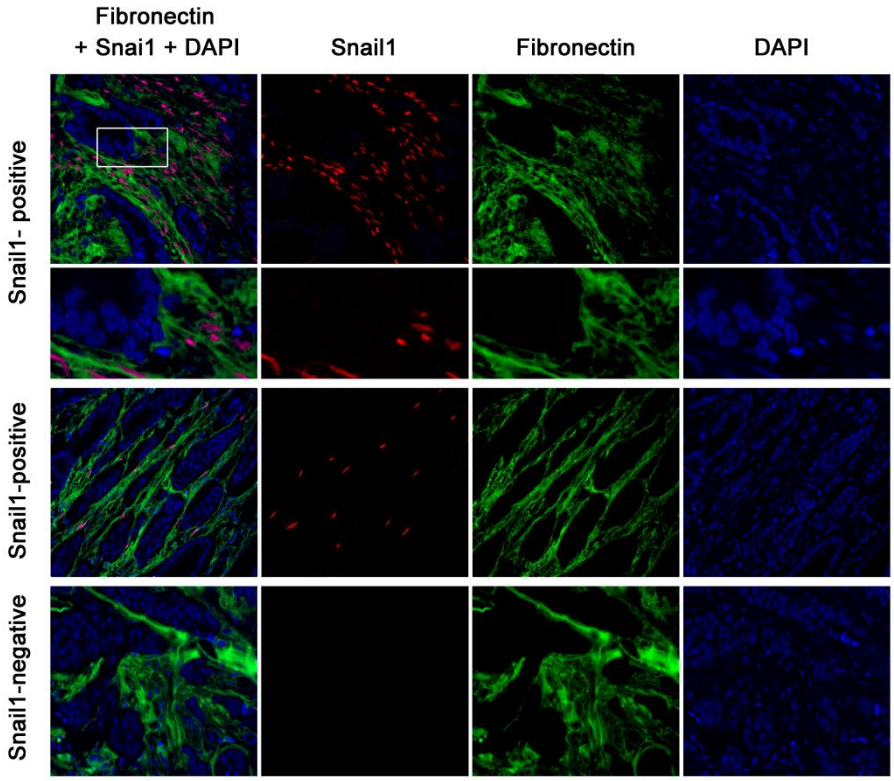


**Figure 55: Fiber organization in stromal areas of representative tumors (400x) with positive (upper and middle panel) and negative (lower panel) Snail1 staining.**

Fibronectin (green) and Snail1 (red) were visualized by multispectral immunofluorescence. DAPI was used to visualize the nuclei. For the upper panel an electronic amplification (3×) of the indicated box is shown.

Using second harmonic generation to visualize collagen fibers in the samples of the same tumors that were used in Figure 55, we observed that collagen was also aligned and perpendicular only in tumors with Snail1 positive stroma (Figure 56).

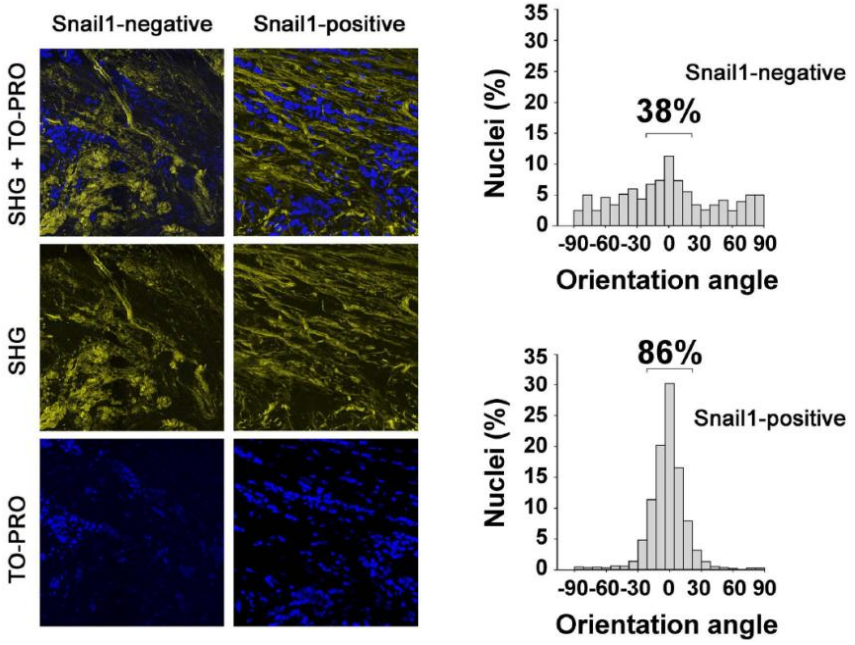


**Figure 56: Fiber and nuclei organization in stromal areas of the representative tumors (400x) with positive (upper panel) and negative (lower panel) Snail1 staining.**
Samples from the same tumors as in Figure 54 were used to visualize collagen fibers by second harmonic generation (SGH, yellow). TO-PRO (blue) was used to visualize nuclei. The nuclei orientation angles of fibroblasts from eight tumors per condition (over 500 fibroblasts) were calculated and plotted as in Figure 31.

The presence of Snail1 in stromal compartment was directly correlated with lymph node involvement at diagnosis ($p = 0.033$) (Figure 57).

| Characteristics | Complete series (n=371) | | Snail1 non-expression in stroma (n=310) | | Snail1 expression in stroma (n=61) | | P |
|---|---|---|---|---|---|---|---|
| | No. of patients | % | No. of patients | % | No. of patients | % | |
| Age (median, range) | 58, 26-90 | | 58, 28-90 | | 58, 26-83 | | |
| Menopausal status | | | | | | | 0.555 |
| Premenopausal | 109 | 29.4 | 93 | 30.0 | 16 | 26.2 | |
| Postmenopausal | 262 | 70.6 | 217 | 70.0 | 45 | 73.8 | |
| Tumor size, mm | | | | | | | 0.245 |
| ≤20 | 191 | 51.5 | 166 | 53.5 | 25 | 41.0 | |
| 21-50 | 139 | 37.5 | 113 | 36.5 | 26 | 42.6 | |
| >50 | 41 | 11.0 | 31 | 10.0 | 10 | 16.4 | |
| Tumor grade | | | | | | | 0.062 |
| I | 61 | 16.4 | 56 | 18.1 | 5 | 8.2 | |
| II | 169 | 45.6 | 143 | 46.1 | 26 | 42.6 | |
| III | 141 | 38.0 | 111 | 35.8 | 30 | 49.2 | |
| Lymph nodes | | | | | | | 0.033 |
| None | 212 | 57.1 | 178 | 57.4 | 34 | 55.7 | |
| 1-3 | 91 | 24.5 | 79 | 25.5 | 12 | 19.7 | |
| 4-9 | 44 | 11.9 | 38 | 12.3 | 6 | 9.8 | |
| >9 | 24 | 6.5 | 15 | 4.8 | 9 | 14.8 | |
| Histology | | | | | | | 0.236 |
| Ductal | 345 | 93.0 | 287 | 92.7 | 58 | 94.4 | |
| Lobular | 20 | 5.2 | 19 | 6.3 | 0 | 0.0 | |
| Others | 7 | 1.8 | 3 | 1.0 | 3 | 5.6 | |
| Estrogen receptor status | | | | | | | 0.007 |
| Negative | 100 | 27.0 | 75 | 24.2 | 25 | 41.0 | |
| Positive | 271 | 73.0 | 235 | 75.8 | 36 | 59.0 | |
| Progesterone receptor status | | | | | | | 0.075 |
| Negative | 139 | 37.5 | 110 | 35.5 | 29 | 47.5 | |
| Positive | 232 | 62.5 | 200 | 64.5 | 32 | 52.5 | |
| HER2 status | | | | | | | 0.029 |
| Negative | 294 | 79.2 | 252 | 81.3 | 42 | 68.9 | |
| Positive | 77 | 20.8 | 58 | 18.7 | 19 | 31.1 | |
| Proliferation (Ki-67) | | | | | | | 0.975 |
| Low proliferation (<15%) | 267 | 72.0 | 223 | 71.9 | 44 | 72.1 | |
| High proliferation (≥15%) | 104 | 28.0 | 87 | 28.1 | 17 | 27.9 | |

Abreviations: HER2, human epidermal growth receptor 2

**Figure 57: Baseline characteristics according to Snail1 expression in the stroma**

More importantly, the presence of Snail1 in stromal compartment of breast tumors was directly correlated with poor overall survival (OS) (Hazard ratio, HR: 5.31; 95% CI: 3.14-8.99; p=0.001) (Figures 58 and 59) and the significance of Snail1 expression in stroma was maintained in a Cox Multivariate analysis for OS (HR: 4.54; 95% CI: 2.53-8.15; p=0.001) (Figure 59). Snail1 expression in cancer cells themselves was in no correlation with overall survival.

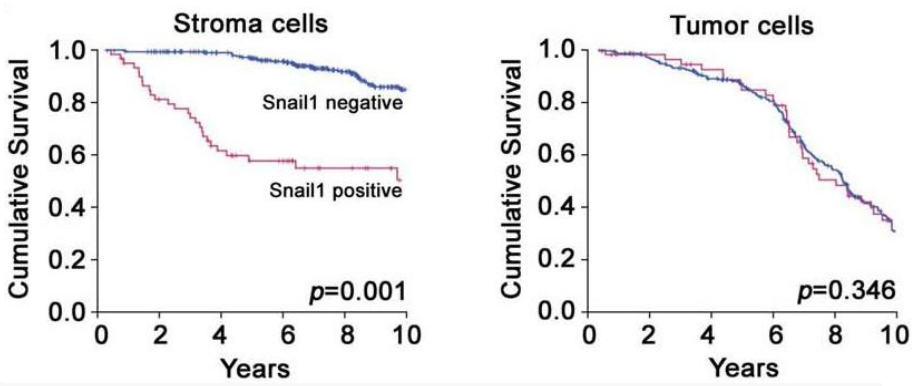


**Figure 58: Kaplan-Meier cumulative curves for Overall Survival (OS) in early breast cancer patients according to Snail1 expression in the stroma (left) and in the tumor (right).**
The p values are indicated.

| Variable | Univariate (n=371) | | | Multivariate (n=371) | | |
|---|---|---|---|---|---|---|
| | HR | 95% CI | *P* | HR | 95% CI | *P* |
| Age | | | 0.096 | | | - |
| Premenopausal | 1.00 | | | - | | |
| Postmenopausal | 1.69 | 0.91 to 3.14 | | - | | |
| Tumor size, mm | | | 0.001 | | | 0.001 |
| ≤20 | 1.00 | | | 1.00 | | |
| 21-50 | 2.63 | 1.45 to 4.81 | | 1.37 | 0.71 to 2.66 | |
| >50 | 3.24 | 1.39 to 7.52 | | 1.05 | 0.84 to 2.74 | |
| Tumor grade | | | 0.058 | | | - |
| I | 1.00 | | | - | | |
| II | 1.27 | 0.51 to 3.13 | | - | | |
| III | 2.23 | 0.92 to 5.39 | | - | | |
| Lymph nodes | | | <0.001 | | | 0.001 |
| None | 1.00 | | | 1.00 | | |
| 1-3 | 1.71 | 0.88 to 3.29 | | 2.17 | 1.07 to 4.40 | |
| 4-9 | 2.13 | 0.93 to 4.84 | | 1.67 | 0.62 to 4.52 | |
| >9 | 7.26 | 3.66 to 14.38 | | 6.23 | 2.81 to 8.18 | |
| Histology | | | 0.784 | | | - |
| Ductal | 1.00 | | | - | | |
| Lobular | 0.44 | 0.33 to 1.15 | | - | | |
| Others | 0.44 | 0.31 to 1.12 | | - | | |
| Hormonal receptor status | | | 0.014 | | | 0.093 |
| Negative | 1.00 | | | 1.00 | | |
| Positive | 0.51 | 0.28 to 0.87 | | 0.61 | 0.34 to 1.08 | |
| HER2 status | | | 0.035 | | | 0.218 |
| Negative | 1.00 | | | 1.00 | | |
| Positive | 1.58 | 0.89 to 2.82 | | 1.27 | 0.58 to 1.76 | |
| Proliferation (Ki-67) | | | 0.711 | | | - |
| Low proliferation (<15%) | 1.00 | | | - | | |
| High proliferation (≥15%) | 1.19 | 0.51 to 1.65 | | - | | |
| Adjuvant chemotherapy | | | 0.609 | | | - |
| No | 1.00 | | | - | | |
| Yes | 0.78 | 0.37 to 1.63 | | - | | |
| Adjuvant hormonotherapy | | | 0.375 | | | - |
| No | 1.00 | | | - | | |
| Yes | 0.76 | 0.42 to 1.37 | | - | | |
| Snail1 in stroma | | | 0.001 | | | 0.001 |
| Non-expression | 1.00 | | | 1.00 | | |
| Expression | 5.31 | 3.14 to 8.99 | | 4.54 | 2.53 to 8.15 | |

Abreviations: OS, overall survival; HR, hazard ratio; CI, confidence interval; HER2, human epidermal growth factor receptor 2

**Figure 59: Overall survival analysis in patients with Snail1 expression in stroma**

## 2.8. Snail1 conditional knock-out mice display delayed skin wound healing due to defects in myofibroblast activity in the granulation tissue

Myofibroblasts are present during physiological wound healing process[174] and their activation is maintained via TGFβ signaling. Therefore, in order to study the importance of Snail1 in myofibroblasts recruited during skin wound healing *in vivo*, we took advantage of the experiment already conducted in the lab. Puncture wounds inflicted to a dorsal skin of control and Snail1 inducible KO mice were photographed during the process of wound closure (Figure 60). A clear delay was observed in the animals that were knockouts for Snail1, differences being most remarkable at day five.

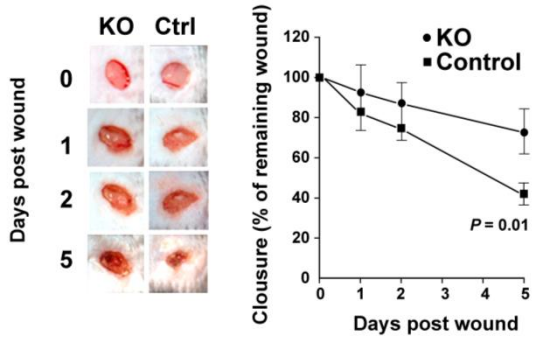


**Figure 60: Skin wound healing in control and Snai1-deficient mice.** Experiment was kindly performed by Jordina Loubat-Casanovas. *Snai1*$^{+/flox}$ (Control) and *Snai1*$^{+/flox}$ (KO) mice were treated with tamoxifen, and skin wounds (6 mm in diameter) were performed after 10 days. Wound diameters were measured and photographed on the indicated days. Plot represents the mean ± SD for the percentage of closure from a minimum of 6 wounds performed on different animals. The student's test p value is indicated.

For this reason, we studied closely the histology of the tissue surrounding the forming scab where the presence of cells positive for Snail1 has been reported before[162]. Spindle-shaped cells positive for Snail1 and α-SMA were present in the granulation tissue of the control animals, but not in the KO animals. Masson's trichrome staining revealed that Snail1

depletion decreased the deposition of collagen and caused disorganization of its fibers (Figure 61).

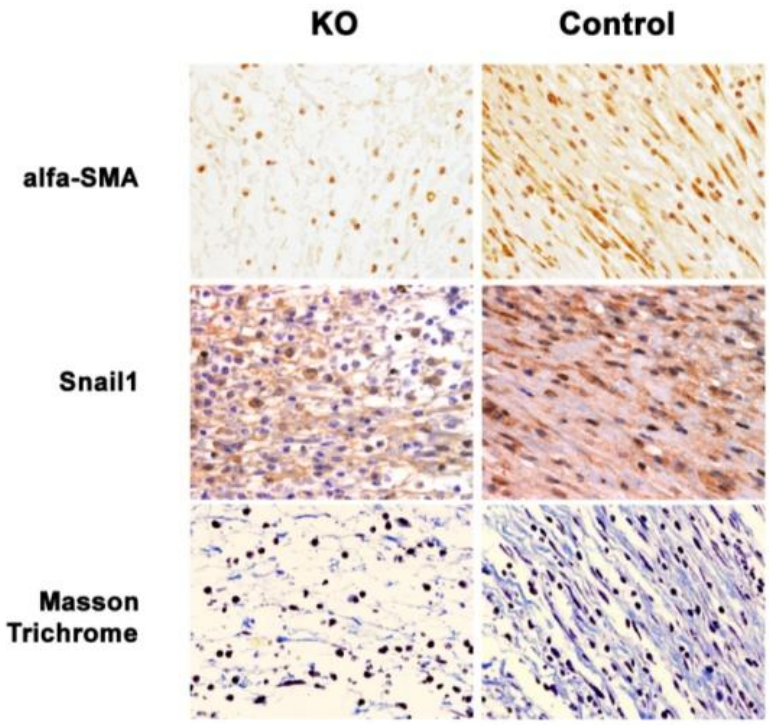


**Figure 61: Snail1, αSMA and Masson's trichrome staining of the granulation tissue adjacent to the scab of the wound.**
Five-day wounds from tamoxifen-treated control (right) and KO (left) mice were analyzed by immunohistochemistry and visualized at 400×.

Using immunofluorescence, we observed that depletion of Snail1 caused the loss of fibronectin and oriented nuclei alignment observed in control animals (Figure 62). Using nuclei orientation as estimation of fibroblast organization and alignment in the granulation tissue, we found that in KO animals cells were orientated randomly, while in the control animals around 80% of the cells co-aligned with the fibronectin fibers. We conclude that Snail1 has an essential role in the organization of the granulation tissue required for wound repair.

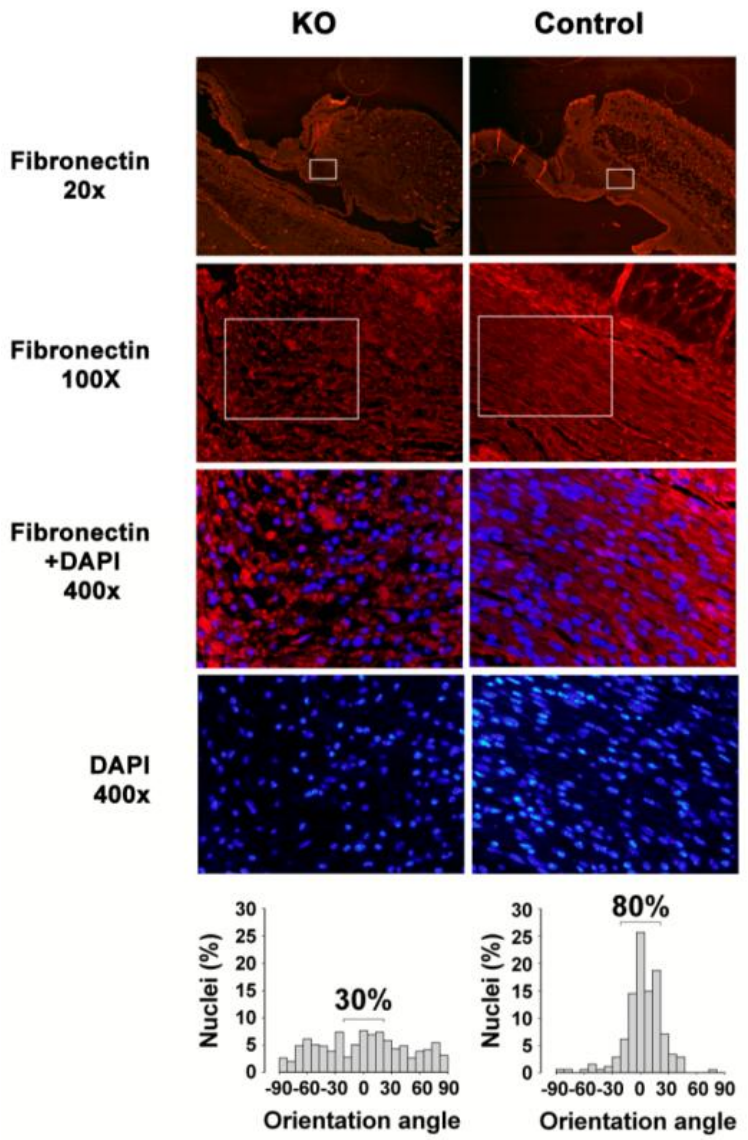


**Figure 62: Fibronectin and nuclei staining of the granulation tissue adjacent to the scab of the wound.**
Five days wounds from tamoxifen-treated control (right) and KO (left) mice were analyzed by immunofluorescence. Fibronectin (red) and DAPI-stained (blue) were visualized at the indicated magnifications. The orientation angles of DAPI-visualized nuclei were estimated with ImageJ, and a frequency distribution centered in the modal angle was represented as in Figure 31.

# Discussion

# Discussion

## Physico-mechanical aspects of the stroma influence cancer progression

Palpation is routinely used in diagnostics of cancers of soft organs, since tumors exhibit increased stiffness compared to surrounding tissue. The major cause of this physical hardening is prominent fibrosis within collagenazed stroma that the scirrhous (skirrhos- hard), or sclerotic cancers have. Scar-resembling desmoplasia is a common feature in most stroma-abundant invasive adenocarcinomas of breast, ovaries, prostate, lung, and gastrointestinal tract and in squamous cell carcinoma, but its manifestation and degree is highly variable even within one cancer type and molecular mechanisms are largely unknown.

For breast cancer, collagen structure and density are shown to be independent prognostic factor regardless of the breast cancer subtype[180]. Three distinct tumor-associated collagen signatures (TACS, Figure D 1) have been defined; TACS1 is characterized by the presence of dense collagen at region near the tumor that even may not be palpable yet. TACS2 is related to non-invading regions and is represented by strained collagen fibers (most likely due to a tumor growth) whose angle is distributed tangentially along the smooth edge of the tumor, wrapped around the tumor. TACS3 is present in regions of invasion, where collagen fibers aligned perpendicular to irregular-shaped tumor edge. The mechanism behind the stromal reorganization remained to be elucidated, but the authors speculated that it must be through Rho/ROCK mediated contractility.

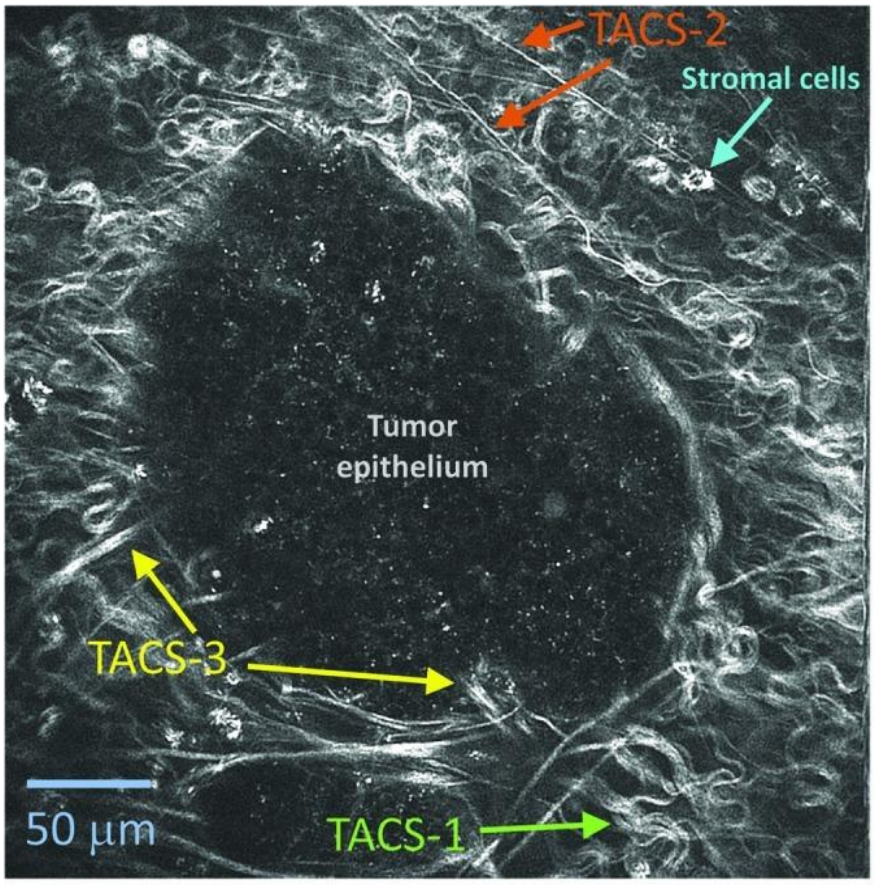


**Figure D 1: Three types of TACS in mouse breast tumors**[181]**.**

## Fibroblastic Snail1 predicts poor prognosis in breast cancer and causes stromal reorganization

Our results demonstrate that some of the stromal cells in the zones where collagen and FN1 fibers lay organized and perpendicular to the irregular tumor edge express Snail1. The expression of Snail1 correlates with lymph node involvement and has robust prognostic value for early breast infiltrating carcinomas. This finding is in agreement with the previous result from our group reporting the correlation between stromal Snail1 and colorectal cancer prognosis[163].

In contrast with our findings, several papers reported no correlation between Snail1 expression and cancer progression[182,183,184]. Three concerns regarding those studies must be raised. First, they focus their attention on epithelial compartment of the cancer, not on the stroma. Our own analysis indicates no correlation between Snail1 expression in cancer cells and prognosis. While we do believe that Snail1 expression in epithelial cells themselves plays a very important role in cancer invasion, we must not forget that, even in culture, the response of Snail1 to various stimuli is rapid and robust, but transient. Snail1 plays a role of a trigger, while subsequently activated factors such as Zeb1, or Twist, maintain the induced change. Experiments *in vitro* take place over hours, or days most, while it takes months or years for full-blown metastasis to develop, and the precise and punctual moment when Snail1 could be found in epithelial cells, initiating EMT, is easily missed. In turn, in the stromal compartment Snail1 levels seem to be sustained.

Second, Snail1 protein stability is tightly regulated and mRNA levels that some studies use must be considered with caution, since Snail1 mRNA and protein levels do not always coincide.

Third, detecting Snail1 by immunohistochemistry is tricky. While others and us consider only nuclear staining as relevant, in one particular work reporting that Snail1 expression in colorectal cancer epithelium promotes lymph node metastasis[185], the authors consider cytoplasmatic staining as

significant. Furthermore, we have discarded cross-reaction of our antibody in particular, but most commercially available antibodies either recognize other Snail family members as well, or do not detect the protein in paraffin sections.

## Snail1 is the architect of the ECM

Our hypothesis that Snail1 may play a role in ECM organization was formed based on our observation described in the first part of the thesis that a set of ECM-related genes was under the control of newly described Snail1/PARP1/p65NF-κB complex in fibroblasts. To test the hypothesis, we used fibroblasts that lack Snail1 and we demonstrated that Snail1 controls both stromal rigidity and ECM fiber organization. Most of the work in this thesis that demonstrates the requirements of Snail1 for ECM remodeling uses *in vivo*-like stromal system consisting of fibroblast-derived three-dimensional extracellular matrices (3D-ECMs), a valid model to study the physical properties of stroma[170,186,169] like its organization and architecture and its mechanical properties, like rigidity.

### Influence on rigidity and rigidity's influence

The values we have obtained employing atomic force microscopy for extracted (decellularized) 3D-ECMs produced by TGFβ-treated control MEFs are in range with those reported for stroma of breast cancer[63] and are associated with bad prognosis[187]. The lack of Snail1 results in a decreased rigidity regardless of the TGFβ treatment. Compliant and poor aspect of Snail1-KO 3D-ECMs was not caused by slower proliferation of the KO fibroblasts, since plating five times higher starting amounts of KO MEFs did not rescue the observed phenotype (not shown). Western blot analysis supported the differences in ECM amount, since KO MEFs expressed less ECM proteins, including LOX, the enzyme responsible for collagen cross-linking. Some levels of LOX were still detected in the KO MEFs, suggesting that factors other than Snail1 may be involved in its

control. We did, however, detect p65NF-κB binding sites and Snail1 binding to LOX promoter in control MEFs treated with TGFβ (Figure D 2), indicating that Snail1/p65NF-κB/PARP1 complex (discussed ahead) may be involved in its activation. LOX has been reported to be involved in hypoxia-induced Snail1 stabilization[188], and feed-forward loop linking Snail1 expression and ECM rigidity may be in action.

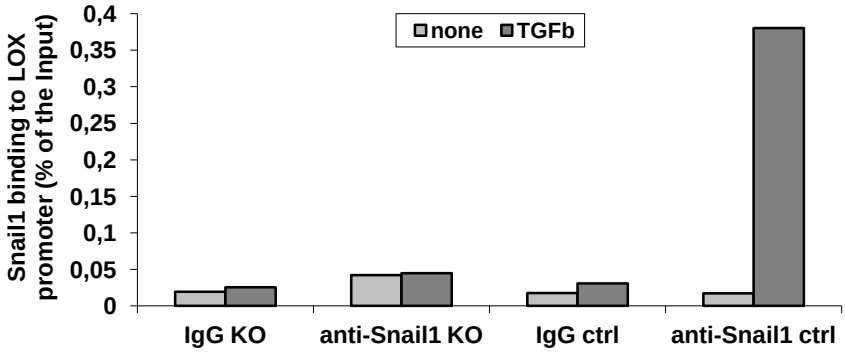


**Figure D 2: *In vivo* binding of Snail1 to the promoter of LOX.**
ChIP assay was performed in mMSCs control and KO for Snail1 treated or not with TGFβ1 (5ng/ml) for 24h. LOX promoter from the immunoprecipitates of the indicated antibodies and assay inputs were analyzed by qPCR.

In epithelial cells, LOX was found among the genes upregulated after TGFβ treatment in the microarray analysis we performed. TGFβ dependent LOX upregulation[189] takes place in normal and in neoplastic breast epithelial cells, suggesting that both stromal and parenchymal compartment participate in collagen stiffening increase.

Matrix rigidity may trigger EMT in epithelial cells[190]. Our group has reproduced the result using normal mammary epithelial cells and several cancer epithelial cells grown on synthetic polyacrilamyde gels of controlled rigidity (these results were part of Alba Azagra's diploma thesis). Switching to *in vivo*-like system, we observed that NMuMG cells plated over stiff extracted 3D-ECMs produced by control MEFs treated with TGFβ1 responded quicker to TGFβ treatment, accumulating nuclear Snail1 (Figure D 3, experiments performed mainly by

Josué Curto Navarro). Upregulation of mRNAs of ECM genes also occurred faster in this condition (not shown, included in Josué Curto Navarro's Master thesis), suggesting that the rigid ECM deposited by activated fibroblasts primes the cells to undergo EMT, possibly initiating the escape from the primary cancer in *in vivo* scenario. The result also indicates that 3D-ECMs could present a useful tool for testing cellular response in varying stiffness condition. Our preliminary results suggest that the 3D-ECM's stiffness also affects the chemoresistance of cancer cells (not shown).

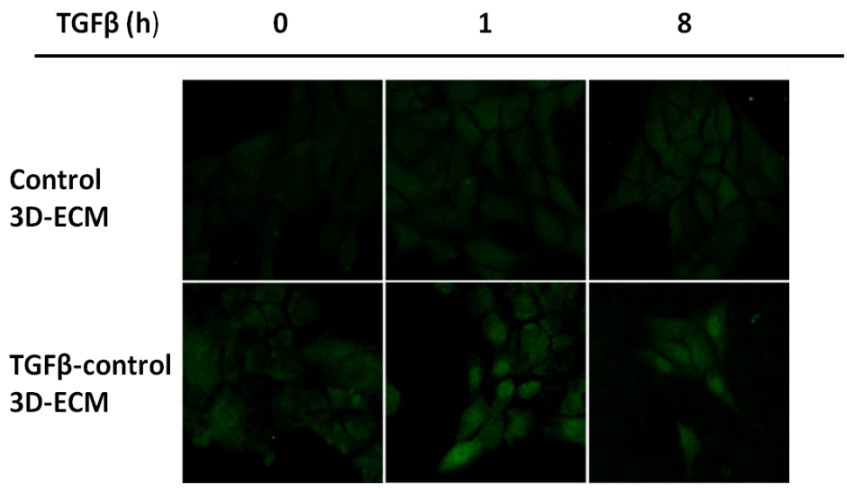


**Figure D 3: ECM rigidity primes epithelial cells for EMT.**
Control MEFs deposited 3D-ECMs following standard protocol either with or without TGFβ1 treatment (5ng/ml). After 10 days, fibroblasts were extracted from the 3D-ECMs and NMuMG cells were plated over the matrices, allowed to adjust for 24h and then treated or not with TGFβ1 (5ng/ml) to induce EMT. Snail1 expression (green) was detected using standard immunofluorescence protocol. Experiment performed by Josué Curto Navarro.

Plastic represents for the cells a substrate of infinite rigidity, a situation that normally cell would never encounter *in vivo*. For this reason, it is plausible that even non-activated MEFs in culture express Snail1, due to mechanical activation signals they perceive. The rigidity of the plastic may as well be the signal that sustains the activated, tumor-promoting phenotype of the CAFs in culture others[191] and us observed, where the ongoing interaction with the carcinoma cells is not taking place. Another

option is that epigenetic alterations, such as DNA methylation or histone modifications, are behind the stable phenotype. Direct genetic alterations probably are not the cause, since they have been detected only sparsely in primary CAF cultures[192,193,194]. Further studies are needed to fully explore how this stability may be abrogated and how the underlying mechanisms could be therapeutically exploited.

It has been described that matrix rigidity and elasticity directs stem cell lineage specification[171,195], and we show that Snail1/TGFβ induced rigidity determines the fate of mesenchymal stem cells. While stiff 3D-ECM produced by TGFβ-treated control fibroblasts sustained the differentiation to osteoblasts, compliant matrices sustained the differentiation to muscle lineages, demonstrating that *in vivo*-like system mimics the rigidity of real niches and highlighting the potential use in tissue engineering and regenerative medicine.

*In vivo*, rigidity may determine the fate of mesenchymal stem cells coming from the bone marrow, recruited by the growing cancer. BM-derived mesenchymal stem cells can also be a source of CAFs, not only resident stromal fibroblasts[196]. It has been reported that TGFβ is the factor responsible for the homing of the BM-derived mesenchymal stem cells to tumor stroma[197]. Snail1-positive CAFs would recruit more MSCs via elevated TGFβ production and, and, once there, MSCs would be in niche where Snail1-induced stromal rigidity would support their differentiation to fibroblasts. Apart from TGFβ, durotaxis, rigidity-guided cell migration[69,198], could also be the reason why BM-derived MSCs home to wounds and scars[199].

Rigidity is particularly relevant factor in breast tissue, where high mammographic density increase the risk of breast cancer 4 to 6 fold[200]. Breast fibroblasts isolated from healthy women with either low or high mammographic density that were propagated *in vitro*, in conditions promoting differentiation to adipocytes, accumulated fat significantly more coming from low density, compliant tissue[201], demonstrating the dominancy of the stroma. The authors identified CD36 as the molecule downregulated in dense breast tissue and in CAFs originating from invasive cancer tissues and show that CD36 KO mice have

significant decrease in fat accumulation and increase in collagen and FN1 deposition. We expect that Snail1 is repressing CD36 in fibroblasts. In fact, CD36 levels are significantly decreased in fibroblasts that lack Snail1 (microarray results)[202]. ChIP assays showing Snail1 binding to CD36 promoter and staining for CD36 in breast cancers samples showing inverse correlation with Snail1 are needed to support our idea.

## Influence on fiber organization

Using the same *in vivo* like stromal system, we demonstrate that TGFβ treatment during the deposition of the 3D-ECMs causes aligned and highly organized 3D architecture similar to the one obtained using tumor-derived fibroblasts[169] and the one we observed in breast cancer tissue samples in Snail1-dependent manner. Moreover, in 3D-ECMs produced by CAF lines isolated from human tumors we found that the Snail1 levels CAFs expressed correlated with the degree of nuclei alignment.

We demonstrate that the fiber organization actually requires functionally active nuclear Snail1, because conditioned medium from control MEFs could not rescue the phenotype of KO 3D-ECMs, while re-introducing Snail1 did. Re-introducing the Snail1 version with point mutation (P2A[102]) that abrogates the interaction with protein partners (e.g. co-repressors) we did not rescue the phenotype, suggesting that for the proper ECM topology, Snail1 could be needed acting as a repressor in fibroblasts.

One open question is how the fibroblasts decide upon direction of the ECM they deposit, resulting in literally parallel local structures. In living tissues, multiple chemical and mechanical gradients exist and evolve with the organ. We report that lymph node involvement in breast cancer correlates with stromal Snail1 and it has been described that lymph nodes are the source of SDF1 chemoattractant. Both SDF1 and its receptor CXCR4 have been reported to be involved in lymph node metastasis in breast cancer[203], but also colon[204] and gastric carcinoma[205]. SDF1 gradient from the lymph vessels could be a

cue fibroblasts require to align the ECM in the direction of the lymph node, as well as the signal for the cancer cells migrating along the ECM fibers. Experiments using SDF1 inhibitor during 3D-ECM deposition, or SDF1 as a stimulus instead of TGFβ would serve to show if SDF1-driven fibroblast activation depends on Snail1 and if SDF1 signaling affects ECM organization. *In vitro*, we speculate that the direction is randomly determined by first-to-reply-to-the-stimulus fibroblast.

While we expect that LOX inhibition or downregulation would have an effect on 3D-ECM rigidity, no effect on topology and fiber orientation was observed when we used either a general inhibitor of LOX enzymatic action, or specific shRNAs (not shown). LOX exerts its action on collagen, and collagen fibrilogenesis comes second, after the FN fibers have been stretched and aligned[206]. FN polymerization is crucial regulator of ECM organization and stability[207].We demonstrate that Snail1 regulates FN transcription and governs proper FN fibrilogenesis through RhoA and expect that collagen alignment occurs concomitantly as a direct consequence.

There may be another level of Snail1 control over FN fibrilogenesis, since it has been reported that in fibroblasts lacking Snail1, levels of FN1 receptor, integrin alpha V, are significantly decreased. Ectopic Snail1 expression in epithelial cells increased Integrin αV promoter activity[208]. We found p65NF-κB binding site after the transcription start site, precisely where it is positioned in ECM-related genes regulated via our mechanism. Integrin αV is also a component of integrin complex involved in TGFβ activation and it was shown that its deletion in myofibroblasts in multiple organs protected mice from hepatic, pulmonary and renal fibrosis, and pharmacological blockade of αV-containing integrins attenuated liver and lung fibrosis[209]. Integrin αV promoter activity is regulated by Sp1[210], Zinc-finger transcription factor that interacts with Snail1, upregulating transcription[211]. Moreover, overexpression of Snail1 upon TGFβ-induced EMT upregulates Sp1 levels[212]. Future experiments should include ChIP assays to test if Snail1 regulates integrin αV directly.

Since FN fibrillogenesis is a coordinated action involving many elements, we expect that removing any of the players participating in FN fibrillogenesis would produce similar consequences. For example, defective FN fibrillogenesis was observed in cells with impaired proteoglycan synthesis[213]. Using the same *in vivo* like system of 3D-ECMs, it was demonstrated that the lack of Syndecan-1 (Sdc1), cell surface proteoglycan overexpressed in stromal fibroblasts of infiltrating breast carcinomas[214,215], causes the deposition of unorganized 3D-ECM, while overexpression of Sdc1 caused 3D-ECM to be organized in parallel patterns[216]. Snail1 may be regulating either directly or indirectly Sdc1 levels, promoting its stability. Sdc1 levels correlate with TACS3[180], and zones where we detect Snail1 in breast cancer patient samples resemble TACS3. The authors, however, do not provide any molecular mechanism.

*In vivo*, aligned collagen of TACS3 correlates with invasion[217]. Disorganized and compliant KO-produced 3D-ECMs did not sustain directional tumor cell migration or efficient invasion, while the aligned and stiff 3D-ECMs produced by TGFβ-treated control MEFs promoted migration in a persistent and anisotropic way. Moreover, cancer cells on these matrices adopted elongated, spindle shaped phenotype. Hence, Snail1 is behind ECM topography, which, in combination with Snail1-controled rigidity, supports the initiation of cancer invasion. We believe that 3D-ECMs could present a useful tool for testing putative pharmacological molecules that disturb stroma-potentiated invasion.

## Few Snail1 positive CAFs dominate stroma locally

CAFs are heterogeneous population and we confirm that in the context of Snail1 levels that different isolated CAF lines express in culture. Ongoing experiments in the lab with murine model of breast cancer support our results, since different population of murine CAFs show different Snail1 amount (experiments mainly performed by Lorena Alba-Castellon). Levels of Snail1 in cultured CAFs seem to be stable, suggesting that, once isolated, they maintain themselves through autocrine mechanisms in a

certain degree of activation. We assume that Snail1 levels in CAFs also are in direct correlation with the rigidity of ECM, but we had not performed the measurements to prove the hypothesis.

In agreement with self-promoted activation idea, isolated CAFs needed no exogenous TGFβ to align their 3D-ECMs and the degree of nuclei alignment was proportionate to their Snail1 levels. However, both MEFs and CAFs are sensitive to exogenous TGFβ1 and respond even to short treatments through fast and transient upregulation of Snail1, and later upregulation of ECM related proteins (not shown for CAFs), suggesting that the phenotype in culture is stable, but not fixed. *In vivo*, this makes CAFs in a ready state, perceiving their surroundings where levels of growth factors fluctuate.

Although high number of activated fibroblasts present in the stroma has been reported for several types of cancer, the breast cancer samples we analyzed had TACS3-resembling aspect and aligned FN1 and collagen fibers even in zones with only few Snail1 positive stromal cells. Additional staining using other markers of CAFs, such as αSMA, S100A4, FSP1, or vimentin, would be useful to define the entire CAF population within the studied zone. As described in the introduction and revised by others[218], CAFs act as a cohort, a single tensegrity unit of fibronexus-connected cells and full activation of each unit member may not be needed for efficient stromal reorganization.

Mimicking the conditions *in vitro* by co-culturing CAFs with non-activated control MEFs, we demonstrate that CAFs are capable of fibroblast education, imposing stromal organization on non-activated majority of the population. This is in agreement with the findings that the resident normal mammary fibroblasts have the capacity to be educated and to co-evolve with juxtaposed carcinoma cells in xenograft experiments upon the establishment of autocrine TGFβ signaling loops[191]. A simple way to demonstrate if non-activated fibroblasts require Snail1 to be educated would be co-culture experiment with KO MEFs. Since KO MEFs can form actin stress fibers and short contacts, we would expect that sufficient amount of Snail1-expressing CAFs will dominate over the KO cells.

Fibroblasts can be educated by the stroma alone, as recently shown in elegant experimental approach where untreated fibroblasts obtained activated phenotype when grown on 3D-ECMs generated by TGFβ-pulsed fibroblasts[219]. Both parameters we describe to be dependent of fibroblastic Snail1 expression, rigidity and 3D fiber organization, are involved in this education. Same authors show that full myofibroblast activation can be achieved through short pulses of TGFβ, and we speculate that such short TGFβ pulses sustain myofibroblastic phenotype through Snail1. Our group reported that ectopic Snail1 expression in normal fibroblasts upregulates TGFβ at both mRNA and protein levels[150], and this may be the initial spark that sets feed-forward loop on. Others reported that two autocrine signaling loops, mediated by TGF-β and SDF1, are needed for fibroblast activation in the stroma, both acting in autostimulatory and cross-communicating manner. [191]

## Snail1 forms ternary protein complex regulating transcription activation

In order to understand what are the downstream effects of Snail1's quick upregulation at both protein and mRNA levels upon TGFβ treatment, we analyzed the kinetics of Snail1 promoter binding in epithelial cells undergoing EMT. Its rapid union to E-cadherin promoter was observed, followed by later switch to mesenchymal promoters, coinciding with the onset of p65NF-κB nuclear accumulation. E-cadherin downregulation releases sequestered pools of β-catenin and p65NF-κB[82] that aid Snail1 in mesenchymal gene activation, but only 8hrs of TGFβ treatment would not suffice to downregulate a protein as highly expressed as E-cadherin is. Cortical actin, in close contact with E-cadherin and β-catenin and p65NF-κB membrane pools, suffers profound reorganization upon TGFβ treatment, and may release p65NF-κB to go to the nucleus, where it would, along with its co-factors, guide Snail1 to mesenchymal promoters where PARP1 would promote the formation and the stabilization of promoter-bound complex. Members of PRMT family interact with Snail1 in the contexts of both repression

and activation. PRMT5 was described to interact with Snail1[123], introducing its repressive histone mark. We show that known co-factors of p65NF-κB, PRMT1 and CARM1 (PRMT4), also interact with Snail1, and we expect that the activating histone mark is left behind.

During EMT, the exclusion of Snail1 from epithelial promoters after several hours of TGFβ treatment may be due to the appearance of another E-cadherin repressor, Zeb1, responding slower to TGFβ stimulus, as we observed in our microarray and as other members of our group have reported[220]. An interesting experiment would be to follow the dynamics of Zeb1 binding to E-cadherin promoter. Zeb1 shows very tight posttranscriptional regulation via the members of miR200 family, particularly miR200c[221,222]. Another mesenchymal self-stimulatory loop exists here, since Zeb1 itself directly represses miR200c[223]. miR200c is one possible target for Snail1 as repressor in fibroblasts (Figure D 9). Apart from Zeb1/2, other mesenchymal genes, such as N-cadherin, contain putative miR-200c binding site in their 5' UTRs (Figure D 4, top left corner). Through miR200c repression, Snail1 could control N-cadherin and Zeb1 levels.

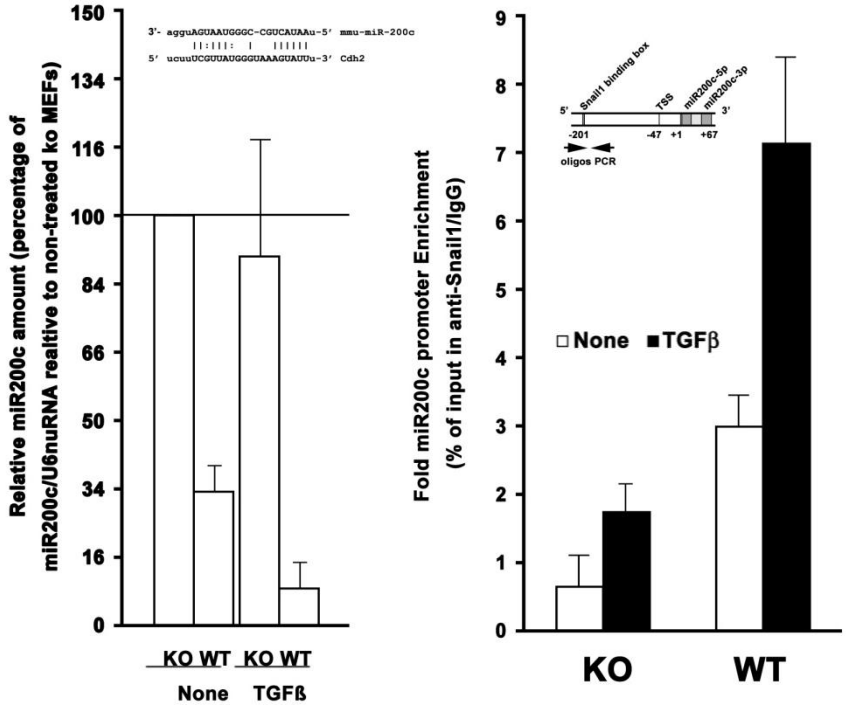


**Figure D 4: Snail1 represses miR200c.**
Left panel: MEFs control and KO for Snail1 were treated with TGFβ1 (5ng/ml) and miR200c and U6nuRNA levels were measured by qPCR. miR200c levels were normalized to U6nuRNA value. Bars show the percentage of normalized miR200c levels in each cell line as compared to that found in untreated KO MEFs.
Right panel: ChIP assay was performed in mMSCs control and KO for Snail1 that were treated or not with TGFβ1 (5ng/ml) for 24h. The levels of miR200c promoter (amplified region is shown in detail in the top right corner) in anti-Snail1 or irrelevant IgG immunoprecipitates and assay inputs were analyzed by qPCR. Bars show promoter enrichment in anti-Snail1 relative to IgG.

Various experiments are still missing to corroborate the finding. It would be interesting to check if downregulation of miR200c in the KO MEFs would rescue the phenotype, or if overexpressing miR200c in control cells would have an effect on 3D-ECM topology and rigidity. Partial downregulation of N-cadherin in control MEFs using specific shRNAs had no effect over the organization of 3D-ECMs caused by TGFβ (not shown).

In myofibroblasts with stable levels of Snail1 regardless of their origin, Snail1-activator complex action most likely has

prolonged effect, sustaining affected promoters in active state. p65NF-κB binding sites that the complex occupies are always found near the transcription start site, where RNA polymerase II (RNA pol II) binds. Snail1 is DNA-binding transcription factor and a way to reconcile this fact with the indirect interaction of Snail1 with mesenchymal genes promoters is to envision Snail1 as master gene regulator binding super-enhancer specific for mesenchymal lineage. The concept of super-enhancers was introduced in 2013 by Richard A. Young's lab[224,225,226]. They identified a set of powerful gene regulators controlling cell identity via transcriptional regulation through super-enhancer regions occupied by lineage-specific master regulators. The binding to super-enhancer region promotes the formation of enhancer protein complex including a bridge protein named mediator and RNA pol II at the proximal promoter site. If our hypothesis is correct, Snail1 would bind directly to super-enhancer regions. Undergoing ChIP-seq and biochemical analysis could substantiate this idea. A special class of long non-coding RNAs, ncRNA-activating (ncRNA-a) function to activate genes through interaction with Mediator[227] and Snail1 has been shown to be regulated by one such ncRNA, namely, ncRNA-7a[228]. In conclusion, as mesenchymal master gene regulator, Snail1 would drive the expression of ECM-related genes, its own expression, and the expression of genes such as Integrin αV, or Sdc1, determining myofibroblastic traits.

## The involvement of Snail1 in molecular mechanism controlling myofibroblastic traits

Apart from ECM proteins, we demonstrate that αSMA and active RhoA and TGFβ induced upregulation of both proteins is Snail1 dependent in fibroblasts. Others have reported that in fibroblasts that are KO for Snail1, mRNA levels of RhoA and ROCK1 were significantly decreased[202], but we could not convincingly reproduce the result using MEFs. We do not provide exact molecular mechanism that would explain how active RhoA levels are decreased in the absence of Snail1, since the network of GAPs, GEFs and GDIs involved in its regulation is

vast, but we speculate that Snail1 may be directly repressing one of them, controlling RhoA activity through a fast and TGFβ-independent pathway. TGFβ and Snail1, hence, would promote further RhoA activation and αSMA synthesis and incorporation into stress fibers. Loss of Caveolin1 (Cav1), for example, causes disorganized stromal tissue architecture in mice[229] and the authors demonstrate that Cav1 promotes Rho-dependent matrix alignment and matrix stiffening via p190RhoGAP. We could not establish any correlation between Snail1 and Cav1, or p190RhoGAP. Ongoing ChIP-seq analysis performed in control and KO MEFs treated or not with TGFβ would provide us with answers that are more definite.

Differences in ECM protein levels were reproduced at mRNA levels only after shorter treatments with TGFβ (8hrs), while longer treatments (24h, 48h) mRNA levels increased even in the absence of Snail1 (not shown). These observations suggest that Snail1-independent mechanism can upregulate ECM genes after the initial Snail1-dependent transcription, but the incorporation of these proteins into maturing complexes forming cell-cell and cell-substrate junctions fails without Snail1/RhoA framework.

3D-ECMs produced by MEFs KO for p65NF-κB and MEFs KO for PARP1 do present similar topological disorganization observed in 3D-ECMs deposited by Snail1 KO fibroblasts, supporting our finding that this ternary protein complex regulates directly ECM genes expression (Figure D 5). Moreover, in 1BR3G skin fibroblasts where we depleted PARP1 using shRNAs, the increase of αSMA in response to Snail1 overexpression and TGFβ treatment was abrogated (not shown). Others reported the same result[230].

Unlike Snail1 KO mice, both PARP1[231] and p65NF-κB[232] mice form normal mesoderm, suggesting that only the Snail1 repressor role is indispensable for gastrulation. One hypothesis about the need for so many EMT-TFs with seemingly redundant actions says that they serve to ensure the survival of the embryo in the earliest stages of development, and such tight control is most likely inactivated in adult tissues, where sparse need for EMT relies on action of individual factors.

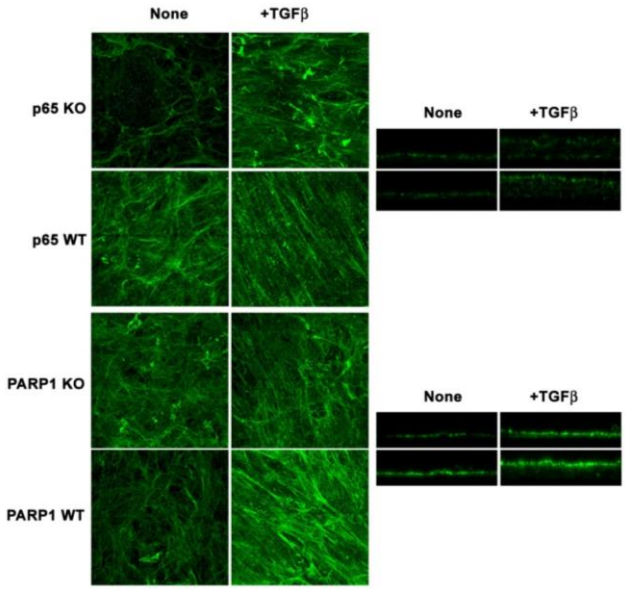


**Figure D 5: TGFβ1 does not induce fiber alignment in p65NF-κB and PARP1 KO MEFs.**
3D-ECMs were generated following described protocol and FN1 was stained using standard immunofluorescence protocol. Pictures on the right represent transversal sections.

We abrogated TGFβ-induced organization in control 3D-ECMs using protein arginine N-methyl-transferase inhibitor AMI1[233] (inhibits the action of PRMT1 and, to a lesser extent, CARM1) during the 3D-ECM deposition (Figure D 6). The use of shRNAs against individual PRMTs had less effect (not shown; described in Josué Curto Navarro's Master thesis). For that reason, AMI1 may have potential therapeutic use, targeting the physical aspects of the stromal compartment.

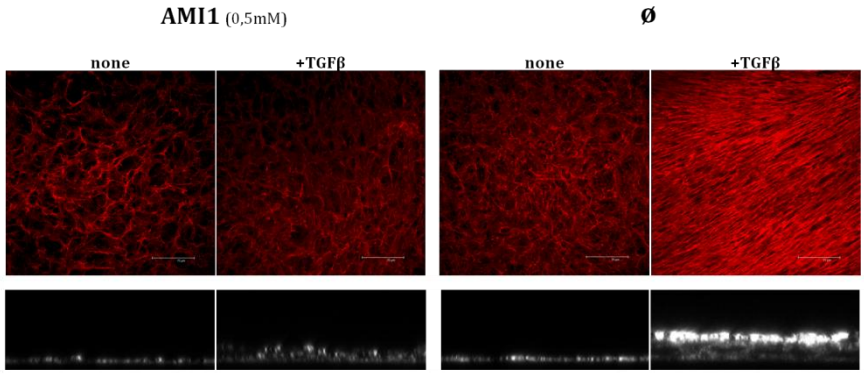


**Figure D 6: The effect of AMI1 on 3D-ECM deposition.**
Control MEFs were used to deposit 3D-ECM following the standard protocol, either in the presence or absence of TGFβ1 (5ng/ml) and AMI1 (0,5mM). Matrices were stained for FN1 (red) following the standard immunofluorescence protocol. Bottom images represent z-sections.

## Wound healing myofibroblasts express Snail1

The main molecule driving partial EMT process during wound closure seems to be Snail2[234,235]. The fact that Snail2 is a much weaker repressor of E-cadherin[236] explains why only a partial EMT takes place in keratinocytes. We did not study the changes in wound's epithelial compartment in our work. As mentioned in the introduction, the fact that fibroblast present plasticity in phenotype was observed first during wound healing[7]. We show that delayed skin wound closure in mice that are conditional KO for Snail1 is due to the failure in myofibroblast activation, since no αSMA positive spindle shaped cells were present in the granulation tissue of KO animals, while the same spindle-shaped cells observed to be positive for αSMA in control animals expressed nuclear Snail1. Myofibroblasts act as a tensegrity unit, highly complex hyper-structure of tightly interconnected cells and surrounding ECM that sustains the stability of incorporated proteins (Figure D 7). mRNAs and proteins produced in fibroblasts lacking Snail1 via unknown alternative rescue mechanisms (possibly involving β-catenin[82] or TFCP2c[237] in the case of FN1) cannot incorporate into functional structures. In the cells lacking Snail1, the tension

element does not provide the compression element with sufficient attraction, compromising fatally structure's stability. Snail1 may be directly activating the expression of only a few of the key factors, its absence causing the collapse of the whole system, because stability through complex formation was not achieved.

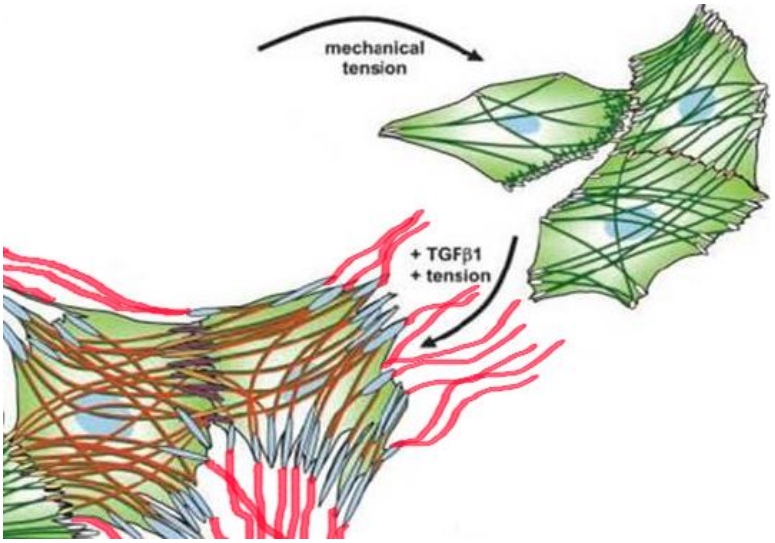


**Figure D 7: The maturation of myofibroblast framework.**
Green lines- actin stress fibers, orange lines- αSMA-positive stress fibers, red- ECM. Adapted from Hinz et al[238].

αSMA KO mice, however, apart from being viable, present normal wound healing, due to the redundancy among different members of the actin family[239]. This would suggest that Snail1 might be regulating the dynamics of other forms of actin as well. The fact that the wounds inflicted to KO mice eventually do close may be because the model is not a perfect one; the efficiency of Snail1 depletion in our conditional KO mice varies from organ to organ, and the emergency situation (such wound is) may eventually recruit some myofibroblasts or bone marrow derived mesenchymal stem cells that express Snail1. Differences we report are nonetheless evident and clear.

Poetically referred to as "wounds that do not heal[240]", carcinomas exploit the same mechanism of stromal activation necessary for tissue repair. Stromal activation is also a common

occurrence in chronic fibrosis resulting from prolonged healing response. We put Snail1 in the center of the activation cascade, mediating TGFβ signaling arm that controls physical and mechanical properties of the stroma (Figure D 8). This would provide the epithelial compartment with necessary signals for wound closure/fibrotic EMT/onset of invasion.

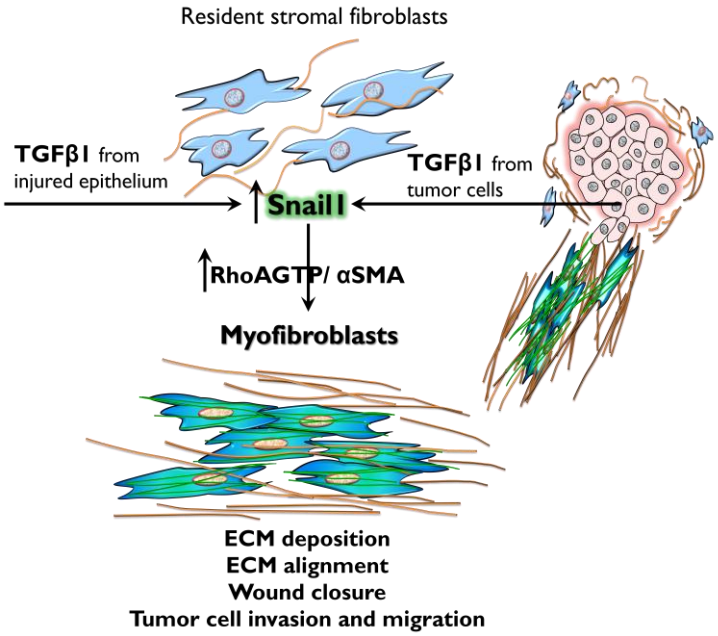


**Figure D 8: Course of action during the activation of stroma.**

# Model summary

Based on all the data discussed above, we propose a model of cancer progression that could be extrapolated to any situation involving stromal activation (Figure D 9) where Snail1 plays simultaneous roles in parenchyma and stroma through reciprocal reprogramming of the two compartments, exploiting their plasticity. We base the model on the concept of bilateral dialogue between cells interacting with and thereby changing the ECM, first described in wound healing cell-ECM interactions[241], and corroborated by Mina Bissell's early work on epithelial development[242]. Unlike in those physiological programs with well-defined end-points, cancer-stroma co-evolution is constantly fueled by promoting cues, and adaptive stroma participates continuously in molecular mechanotransduction.

Cancer progression is heterogeneous within the same malignancy[243], and is reflected in different degree of local activation response in the connective tissue. Cancer cells derived growth factors like TGFβ, and environmental signals such as hypoxia or oxidative stress, trigger fibroblast-to-myofibroblast transdifferentiation, during which Snail1 controls RhoA activity and αSMA induction. Snail1 activates TGFβ, and this feed-forward loop, along with Snail1-induced ECM rigidity, sustains CAFs in an active state- ready to sense orientation-determining gradients of chemoattractants such as lymph node-derived SDF1 might be. Via mature adherens junctions stabilized by Snail1 activity, the decision about the direction can be transmitted to non-activated fibroblasts. In this way, coordination between Snail1's roles of activator/repressor turns local fibroblasts in powerful contractile tensegrity units and allows them increased ECM deposition and protein stabilization within mature contacts, resulting in rigid and parallel three-dimensional ECM typical for desmoplastic areas. In turn, Snail1-positive CAFs are capable of inducing migration and proliferation in cancer and cancer-associated cells in paracrine manner[244].

Cancers cells mechanosense self-provoked environmental changes and undergo functional adaptation to cope with them. Snail1 upregulation in cancer cells initiates EMT, or partial EMT. Snail1 represses E-cadherin and subsequently activates mesenchymal genes, promoting motility. Leaving the tumor, cells come in direct contact with rigid collagen fibers, further stabilizing Snail1 protein through the action of collagen receptor DDR2[245], sustaining EMT. The fact that the surrounding stroma may be more rigid due to the increased levels of LOX in the presence of Snail1 does not have to represent a barrier for the invading cancer cells; rigidity has been related with EMT induction[190] and higher production of matrix metallopreoteinases[246]. Nonetheless, not all invading cells opt for chop-through strategy of invasion, like ambulance car turning on emergency lights to budge through a traffic jam; instead, some carcinomas contract CAFs to build them their private highway of oriented fibers perpendicular to the cancer edge, guiding the invading cells up the chemo and mechanogradients. In fact, it has been reported that in collectively invading cocultures of cancer cells and fibroblasts, fibroblast is always a leading cell, causing force-mediated matrix remodeling[247], while cancer cells collectively follow along, probably in metastable, in-between state, expressing both epithelial and mesenchymal markers. In another visually beautiful and elegant work on EMT in development, it was shown that chemogradient is not only pre-established, but self-generated by epithelial followers via receptor-mediated internalization of SDF1 chemokine[248]. Snail1 may be regulating the expression of the receptor, establishing yet another level of invasion process control.

Our findings highlight Snail1/RhoA framework in stromal cells as a relevant pharmacological target, since the changes in the physical properties of the niche directly affect the cancer cells, modulating their metastasis-related capacities. One of the benefits of this approach is that stromal cells are rarely genetically altered and for this reason, resistance to therapy due to mutations is improbable.

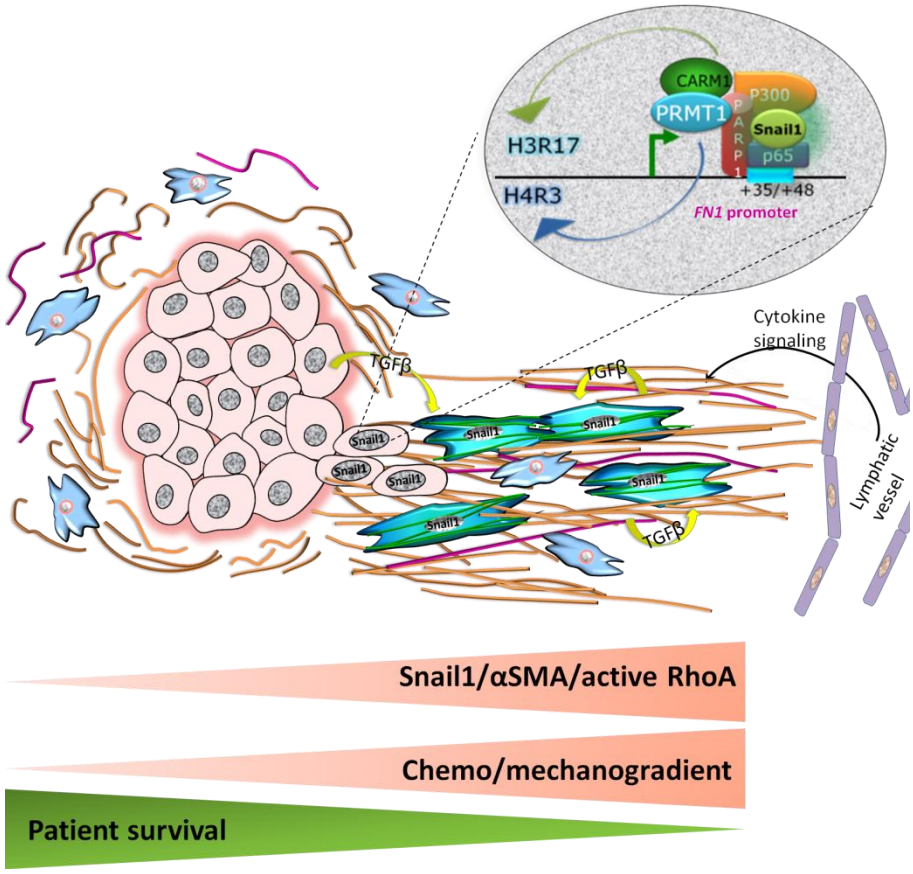


**Figure D 9: Simplified model of Snail1 role in cancer progression.**

# Materials and Methods

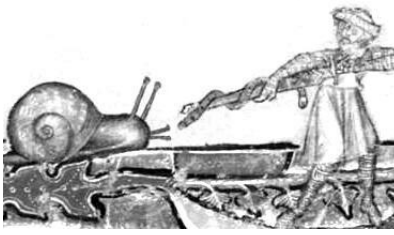

# Materials and methods

## Cell culture

All cells were maintained at 37°C in a humid atmosphere containing 5% $CO_2$ and grown in Dulbecco's modified Eagle's medium (DMEM, Invitrogen) supplemented with 4.5 g/l glucose (Life Technologies), 2mM glutamine, 56U/ml penicillin, 56µg/l streptomycin and 10% foetal bovine serum (FBS, GIBCO) unless stated otherwise. Where indicated, cells were treated with 5ng/ml of TGFß1 (Peprotech).

C2C12, 3T3-L1, MDA MB231, SW620, 1BR3G, NMuMG (growth medium supplemented with 10µg/ml insulin), HEK 293T, and HEK 293 Phoenix cells were acquired from the repository stock of our center. Stable HT29 M6 clones for mSnail1-HA were generated[102] and maintained in our laboratory. Stable expression of mSnail1-HA was conserved by adding the antibiotics G418 (500µg/ml) and hygromycin (200µg/ml) to the culture medium. PARP1 (-/-) and (+/+) MEFs were kindly provided by Dr. Zhao-Qi Wang, from the Fritz Lipmann Institute, Germany, while RELA (-/-) and (+/+) MEFs were provided by Dr. A. Hofmann, from the University of California, USA. SNAI1 KO and control MEFs and mesenchymal stem cells (MSCs) were established in our laboratory from a conditional KO mouse[150]. SW480 cells expressing Snail1-HA, E-cadherin, or Snail1-HA/E-cadherin were previously described[118,82]. 1BR3G human fibroblasts were infected with retroviruses using pBABE mSnail1-HA (cDNA) and GFP vectors and then selected with puromycin (2µg/ml). Where indicated, ROCK1 inhibitor (SIGMA, Y27632) was added to the medium at final concentration of 10µM 24h prior to the experiment.

## Retroviral and lentiviral infection

Phoenix cells were transfected with the indicated RNA interference plasmids expression as well as an adjuvant vector (pVSVG). Subsequently, 1BR3G and MEFs were infected twice with viral supernatant in the presence of polybrene (4mg/ml; Sigma). To knockdown PARP1 and p65NF-κB in MEFs, 1BR3G and NMuMG cells, shRNA vectors (human or murine), as well as the three adjuvant vectors: pMDLg/pRRE, pRSVREV, and pVSVG, were transiently transfected into HEK293T cells. Viral supernatants were collected 48h and 72h later, clarified by filtration and used to infect cells with 4mg/ml polybrene. Infected cells were processed 48h after the initial infection, or were selected with puromycin (2,5μg/ml) and further treated with TGFβ when indicated.

## Cell differentiation procedures

For all the differentiation experiments the indicated cell line was grown over extracted fibroblast-derived extracellular matrices (see below). As a control, cells were allowed to differentiate grown on normal culture dish.

In order to differentiate C2C12 cells to myoblasts, they were allowed to reach full confluence and then were cultured during 5 days in low serum conditions (DMEM supplemented with 2% FBS). Since the cells committed to myogenic lineage express myogenin II, its expression was analyzed following the immunofluorescence protocol in DAPI counterstained samples.

Osteogenic differentiation of MSCs was performed adding 100nM dexamethasone, 10mM β-glycerophosphate, 50mM L-ascorbic acid-2-phosphate to a medium of a confluent culture during 3 days. Cells were grown in DMEM with 10% FBS for 3 or 6 additional days and then stained with alizarin red. Cells were washed twice with PBS, fixed with 4% PFA for 15 minutes at room temperature, washed twice with dH2O prior to addition of 40mM ARS (Sigma) (pH 4.1). The plates were incubated at

room temperature for 20 minutes. After aspiration of the unincorporated dye, the wells were washed four times with dH2O and photos were taken using transmitted light microscopy.

## ChIP

Cells seeded the day before were washed with warm phosphate buffered saline (PBS) and then cross-linked for 10 minutes at 37°C with 1% formaldehyde in serum free DMEM. To stop the reaction, cells were incubated for 2 minutes more after adding glycin at final concentration of 0.125M. Cells were washed twice with cold PBS scrapped off with cold soft lysis buffer (50mM Tris pH 8.0, 2mM EDTA, 0.1% Nonidet P-40, 10% glycerol). Lysates were incubated 10 minutes on ice and then centrifuged for 15 minutes at 3000rpm in cold. Pellet was resuspended in SDS lysis buffer (1% SDS, 10mM EDTA, 50mM Tris pH 8.0) and sonicated using 40% of the sonicator's amplitude (Branson DIGITAL Sonifier® UNIT Model S-450D) in order to generate DNA fragments ranging from 200 to 1000 kb in length. Lysates were incubated for 20 minutes on ice and centrifuged at maximum speed for 10 minutes. Optionally, the length of the fragments was confirmed running a small volume of the sample on 0.5% agarose gel.

Protein concentration was determined by Lowry and the desired amount of protein per immunoprecipitation (usually between 250µg and 1mg) was diluted ten times in dilution buffer (0.001% SDS, 1.1% Triton X-100, 16.7mM Tris pH 8.0, 2mM EDTA, 2mM EGTA, 167mM NaCl).

In order to reduce background, samples were incubated for 3 hours at 4°C with IgGs of the same species as the used antibody and protein G or protein A magnetic beads (Upstate). Beads were removed using magnetic racks, 100µl for the input was kept apart and the samples were divided in half and incubated with either the specific antibody or the IgG of the same species overnight at 4°C with agitation. Magnetic beads that were blocked overnight with BSA and sheared salmon sperm were

added to all the samples and incubated 1 hour at 4°C with agitation. Afterwards, five washes were performed on ice with each in each of the given buffers: low salt buffer (0.1% SDS, 1% Triton X-100, 2mM EDTA, 20mM Tris, pH 8.0, and 150mM NaCl), high salt buffer (the same as low salt but with 500 mM NaCl), LiCl Buffer (250mM LiCl, 1% Nonidet P-40, 1% Sodium deoxycholate, 1mM EDTA, and 10mM Tris, pH 8.0), and TE buffer. Beads were recovered using magnetic racks and samples were eluted with the elution buffer (100mM $Na_2CO_3$, 1% SDS)0 at 37°C. Elutes were recovered by centrifugation (3 minutes, 2000rpm). To each sample and to the inputs NaCl was added at final concentration of 250mM and both the samples and the inputs were decrosslinked by incubation at 65°C overnight, following by digestion with proteinase K for additional 2 hours. DNA was purified using GFX PCR DNA and Gel Band Purification kit (GE healthcare) and quantitative PCR was performed. In ReChIP assays, a second IP was performed: eluates were brought to a final volume of 1ml with the dilution buffer and re-incubated with either specific antibody or the proper control overnight with agitation. The precipitation process was then repeated as described for the first IP.

## EMSA

Cells were washed twice and scraped with cold PBS and centrifuged for 10 minutes at 1000 rpm at 4°C. Pellet was resuspended in buffer 1 (10mM Hepes pH 7.6, 1.5mM $MgCl_2$, 10mM KCl, 0.5% NP-40, 0.5mM DTT), incubated on ice for 10 minutes and centrifuged for 10 minutes at 5000 rpm (4°C). Pellet containing nuclear fraction was then resuspended with the buffer 2 (20mM Hepes pH 7.6, 1.5mM $MgCl_2$, 840mM KCl, 0.2mM EDTA, 25% glycerol, 0.5mM DTT), incubated on ice for 20 minutes and centrifuged at 5000 rpm for 30 minutes (4°C). The supernatant, now containing the nuclear fraction, was dialyzed overnight against 1l of buffer 3 (20mM Hepes pH 7.6, 100mM KCl, 0.2mM EDTA, 20% glycerol, 0.5mM DTT) at 4°C. Samples were quantified by Bradford and stored at -80°C.

Sense and antisense oligonucleotides of the probe were annealed in TEN buffer (10mM Tris pH 7.5, 50mM NaCl, 1mM EDTA) for 10 minutes at 70°C and allowed to cool until they reached room temperature. Probe was then labelled with gamma $^{32}P$ using T4 polynucleotide kinase (Invitrogen) following manufacturer's instructions. Excess of unincorporated radioactive ATP was removed using Microspin TM G-25 columns (Amersham Pharmacia Biotech Inc). One microliter was used for cpm quantification. 10mg of nuclear extract was incubated with 100,000 cpm of $^{32}P$ labelled probe in binding buffer (20mM HEPES pH 7.6, 150mM KCl, 3mM $MgCl_2$, 10% glycerol, 0.3mg/ml BSA, 0.2mM ZnSO, 10 µg of poly dI-dC, 1mM DTT) for 30 minutes on ice. When competition was performed the stated amount of cold probe was added to the reaction. When the antibody specific for PARP1 was used, the binding reaction was supplemented with the indicated amounts of irrelevant or specific antibody and incubated for 15 minutes prior to the addition of the radiolabelled probe. A non-denaturing TBE-polyacrylamide gel (0.5X TBE [TBE (10x): 1M Tris, 1M Boric acid, 10mM EDTA pH 8.0], 8% polyacrylamide, 0.02% APS, 0.0012% TEMED) was prepared and left polymerizing overnight at 4°C. Pre-running was performed for at least one hour prior to loading the gel (100V). Samples were loaded in the gel and additional lane was left for loading buffer (20% Ficoll 400, 0.1mM EDTA, 1% SDS, 0.25% Bromophenol blue, 0.25% Cyanol xylene). Gel was run at constant voltage (125 V), dried and exposed to an autoradiography.

## Reporter assay

Cells were seeded in 24-well culture plates at a density of $1x10^5$ cells per well and were transfected 24 hours afterwards with the indicated promoter sequence cloned in the PGL3* reporter plasmids and 10ng of thymidine kinase-Renilla luciferase plasmid as a control (Promega). 48 h post-transfection the activities of Firefly and Renilla were measured using the Dual Luciferase Reporter Assay System (Promega) with an FB12 luminometer (Berthold Detection Systems, Pforzheim,

Germany). Luciferase activity was normalized by Renilla luciferase activity and empty reporter vector. Triplicates were systematically included, and experiments were repeated at least three times.

## Immunofluorescence

Cells grown on ethanol sterilized glass coverslips were washed three times with phosphate-buffered saline (PBS) and incubated with 4% paraformaldehyde (PFA) for 15 minutes at room temperature, washed again with PBS and incubated for 5 minutes more with 50 mM NH4Cl to quench PFA's autofluorsecence. Blocking and permeabilization were performed at the same time for 1 hour at room temperature in PBS containing 3% BSA and 0.3% Triton X-100. Coverslips were first incubated in a humid chamber overnight at 4°C with the primary antibody diluted in the blocking/permeabilization solution, and after extensive washing, for 1 hour more in a dark, humid chamber with the secondary antibody. In the case of the co-staining, both primary and the secondary antibodies were mixed and used at the same time. Coverslips were mounted with DAPI-Fluoromount-G and fluorescence was observed and captured through a Leica TCS-SP2 confocal microscope.

## Immunohistochemistry

Harvested tissue samples were fixed in formalin and embedded in paraffin. Sections of 4μm were obtained with a microtome and were subsequently dewaxed and rehydrated. Antigens were retrieved by boiling the samples in Tris/EDTA (50mM Tris/HCl, 1mM EDTA and 10mM NaCl, pH 9.0) for 15 min. Endogenous peroxidase activity was quenched with 4% hydrogen peroxide in PBS containing 0.1% sodium azide for 15 min. After several rinses with PBS, sections were incubated with PBS containing 1% BSA to block non-specific binding and were washed with PBS. Sections were incubated with indicated antibodies (10μg/ml of purified anti-Snail1 monoclonal antibody EC3 or

1/800 SIGMA anti-αSMA antibody) overnight at 4°C. After several further rinses with PBS, bound antibody was detected using anti-mouse or anti-rabbit Envision (Envision System Peroxidase; DAKO). Sections were counterstained with haematoxylin and mounted for microscopy analysis. Some paraffin sections were stained with a Masson Trichrome Reagent kit following the manufacturer's instructions.

## Fibronectin fibrillogenesis

Ethanol-sterilized glass coverslips in 24 well plates were coated overnight with purified soluble fibronectin (2µg/ml) in PBS at 4°C. Unbound protein was washed off with PBS and cells were seeded over. 16, 24 and 60 hours afterwards cells were washed twice with PBS, fixed with 4% PFA in PBS and fibronectin was stained following standard immunofluorescence protocol. Using ImageJ software, fibronectin fibrilogenesis was measured as fibronectin-clear black area normalized by the number of cells. A minimum of 100 cells per condition was analyzed.

## Extracellular matrices (3D-ECMs)

Preparation of three-dimensional extracellular matrices produced by cultured fibroblasts was performed following a standard protocol[249]. All steps were performed under sterile conditions. Ethanol sterilized glass coverslips, 96 well plates and Boyden chamber inserts were incubated with 0.2% (w/v) gelatine solution for 1 hour at 37°C. Extra gelatine was washed off with PBS, PBS aspirated and 1% glutaraldehyde (prediluted in PBS) was added and incubated 30 min at room temperature to crosslink the gelatine. Coverslips or culture dishes were washed three times for 5 min each with PBS. 1M ethanolamine was added to each dish and incubated for 30 min more at room temperature. Washes with PBS were repeated and plates were kept in PBS. For 24 wells plates, $5x10^5$ fibroblasts were seeded per well, for 96 wells plates $1x10^5$ fibroblasts per well and for Boyden Chamber inserts $1x10^5$ fibroblasts were seeded in 100

µl of medium to prevent leaking through the insert pores due to gravity. Cell culture media was replaced with fresh one supplemented with 50 µg/ml of ascorbic acid and with 5 ng/ml of TGFβ1 when indicated every 48 hours during 10 days. For the analysis of the matrix structure, matrices were finally washed with warm PBS and fixed with 4% PFA following standard immunofluorescence protocol. Otherwise, intact matrices were washed gently with warm PBS and then incubated with warm extraction buffer at 37°C until no cells could be visualised. PBS was added slowly avoiding turbulence to dilute the cellular debris and extracted matrices were stored overnight at 4°C. Diluted debris was removed the next day, extracted matrices were carefully washed two more times with PBS and were kept at 4°C in PBS supplemented with 100U/ml penicillin, 100µg/ml streptomycin, and 0.25µg/ml fungizone until they were used.

Alcian blue staining was used to assess the formation of extracellular matrix. Extracted fibroblast-derived extracellular matrices were fixed for 20 minutes at room temperature with 4% PFA and incubated with 4% Alcian Blue/AcOH (Sigma) for 15 minutes at room temperature. The samples were washed with distilled water and photos were taken with digital camera.

## Young's modulus (E)

Rigidity of decellularized extracellular matrices was analysed by atomic force microscopy. Complete elimination of cells from matrices was confirmed by fluorescent microscopy in parallel MEFs-labelled cultures (Cell Tracker™ Green CMFDA).

Decellularized ECMs were extensively washed with (37°C) PBS, and Young's Modulus was measured with a custom-built AFM attached to an inverted optical microscope (TE2000, Nikon, Tokyo, Japan) by using a previously described method.[250,251] The matrices were probed with V-shaped pyramidal cantilevers with nominal spring constant (k) of 0.01 and 0.03 N/m (MLCT, Bruker, Mannheim, Germany). The cantilever was displaced in 3D with nanometric resolution (z) and the defection of the

cantilever (d) was measured using the optical lever method. The force (F) on the cantilever was computed as $F = k(d - d_{off})$ being $d_{off}$ the offset of the photodiode. The indentation of the sample ($\delta$) was computed as $\delta = (z - z_c) - (d - d_{off})$, where $z_c$ is the position of the tip-matrix contact point. ECM samples were measured at 9-13 points separated by 20μm. At each measurement point, 5 F-$\delta$ curves were recorded (1 Hz triangular displacement, peak-to-peak amplitude of 5 μm), which were analysed with the pyramidal Hertz model

---

where $\theta$ is the semi-included angle of the tip and $\sigma$ is the Poisson's ratio, assumed to be 0.5. Nonlinear least-squares fit (Matlab, The MathWorks, Natick, MA) was used to estimate E from the loading branch of the F-$\delta$ curve for a maximum indentation of 1 μm. The average E obtained from the five force curves recorded at each measurement point was computed.
E values were presented in a box plot. Boxes represent the median and the 25%–75% interquartile range, and whiskers mark the 1.5× interquartile range. Circles denote outlying values. The asterisk indicates a statistically significant difference ($p > 0.001$) between groups as determined by ANOVA on ranks and Dunn's method (for the ECMs from KO–, KO+TGFβ–, control–, and control+TGFβ1– MEFs, n equals 7, 38, 16, and 49, respectively).

## *In vivo* wound healing

Snail1+/flox and Snai1-/flox mice were treated with tamoxifen both intraperitoneally and cutaneously. A solution of 0.2mg tamoxifen in corn oil solution per gram of body weight was injected intraperitoneally every 48 hr 4 times. 24 hr after the first injection, a cutaneous application of 4-hydroxytamoxifen in acetone (200μl of 10 mg/ml) on a shaved dorsal hair area was applied; this was repeated after every injection. Ten days after the first tamoxifen injection, mice were anesthetized with isoflurane (FORANE®, Abbot Laboratories, Abbot Park, IL, USA)

for skin wounding. After cleaning the exposed skin with 70% ethanol, full-thickness excision skin wounds were made aseptically on either side of the dorsal midline using a 6mm biopsy punch. Two wounds were usually made on the same animal. Wounds were photographed and measured at days 1, 2, and 5. The wound tissue and surrounding skin from the wound margin were harvested from mice at five days post-wounding, fixed in formalin, embedded in paraffin, and sectioned in 4μM slices for immunohistological analysis. This study was approved by the Animal Experimentation Ethical Committee of IMAS (Barcelona, Spain).

## Migration assay

Tumor cells plated the day before were washed once with PBS and incubated for 1 hour at 37°C with serum free DMEM containing Cell Tracker™ Green CMFDA (5-chloromethyl fluorescein diacetate) at final concentration of 5nM (10mM stock in DMSO). The excess dye was rinsed with PBS and cells were allowed to recover in DMEM supplemented with 10% FBS for 30 minutes at 37°C. After that, cells were trypsinized, counted and seeded (1000 cells per well) on extracted fibroblast-derived extracellular matrices generated previously on 96 well plates. Cells were allowed to attach overnight and then bright field and fluorescence images were taken every 10 minutes over 18 hours using Cell Observer HS system (Zeiss). Position coordinates for 10 single cells were calculated using ImageJ software and the movement over time is represented relative to the each cell's initial position.

## Invasion assay

Tumor cells were trypsinized, counted and seeded (50.000 cells per well) on extracted fibroblast-derived extracellular matrices generated previously over 8 μm-pore membranes of Boyden chamber inserts in serum-free DMEM while 10% serum-containing medium was placed in the lower part as

chemoattractant. After 24 hours, both the lower and the upper part of the membrane were washed once with PBS, incubated 20 minutes at room temperature with 4% PFA, washed again with tap water and stained with crystal violet. All the cells from the upper part were swabbed using a cotton tip and invaded cells were photographed using transmitted light microscopy.

## RNA Analysis

RNA was extracted with the GenElute TM Mammalian Total RNA Miniprep Kit (Sigma-Aldrich). For quantitative analysis, 1µg of RNA was retro-transcribed with the Transcriptor First Strand cDNA Synthesis Kit (Roche), and 100 ng of the cDNA obtained was used as the template for quantitative SYBR Green-based PCR with specific oligonucleotides. Correct product size was confirmed in agarose gels. The amount of RNA calculated was systematically normalized to the amount of HPRT or pumillio RNA. For microarray analyses, amplification, labeling, and hybridizations were performed according to the protocols from Ambion and Affymetrix. Briefly, 250 ng of total RNA were amplified using the Ambion® WT Expression Kit (Ambion/Applied Biosystems, Foster City, CA, USA), labelled using the WT Terminal Labeling Kit (Affymetrix Inc, Santa Clara, CA, USA), and then hybridized to Mouse Gene 1.0 ST Array (Affymetrix) in a GeneChip® Hybridization Oven 640. Washing and scanning were performed using the Hybridization Wash and Stain Kit and the GeneChip® System of Affymetrix (GeneChip® Fluidics Station 450 and GeneChip® Scanner 3000 7G).

## RhoA-GTP pull-down assay

Activated RhoA was quantified in cell extracts by capturing RhoA-GTP form onto a bead support including the RhoA-GTP specific interacting protein as a GST fusion. For the purification of GST-rhotekin, LB broth supplemented with 100µg/ml ampicillin was inoculated with a single colony of *E. coli*

containing the GST-rhotekin construct and incubated overnight at 37°C shaking. The overnight culture was diluted 1:10 in LB broth containing 100µg/ml ampicillin and grown until $OD_{600}$ reached 0.6. Isopropyl-β-d-thiogalactopyranoside (IPTG) was added at the final concentration of 0.1mM to induce the protein expression. After more 2h of incubation, the culture was centrifuged for 10 minutes and bacteria pellet was resuspended in PBS and sonicated on ice seven times. TX-100 was added at final concentration of 1% followed by the incubation during 30 minutes at 4°C. The lysed cells were clarified by centrifugation at 10.000rpm at 4°C for 10 minutes. Glutathion-Sepharose beads were added to the supernatant followed by the incubation at 4°C for 1h. Beads were washed at least three times with cold PBS and finally resuspended in the PBS containing 10% glycerol. The purity of the fusion protein was assessed by SDS-PAGE.

For the GST pull-down assay, cells starved 24h prior to the experiment were treated with TGFβ1 (5ng/ml) for the indicated period of time and then washed with cold PBS. Cold lysis buffer (50mM Tris-HCl pH 7.5, 1% Triton X-100, 0.5% sodium deoxycholate, 0.1% SDS, 500mM NaCl, 10mM $MgCl_2$, 10 µg/ml aprotinin, and 1mM PMSF) was added and the cells were rapidly scraped off the plates. Lysates were transferred to Eppendorf tubes, syringed five times and centrifuged at 13,000 rpm for 10 min at 4°C. The protein amount in the supernatant was quantified: 25 µg of lysate was separated to be analysed as input and 1mg was incubated with 20µg of GST-rhotekin for 1h at 4°C. The beads were washed five times with 1ml of cold washing buffer (50mM Tris-HCl pH 7.5, 1% Triton X-100, 150mM NaCl, 10mM MgCl2, 10µg/ml aprotinin, and 0.1mM PMSF). SDS-PAGE sample buffer was added to each sample and inputs then heated at 95°C for 5 min. Total RhoA and RhoA-GTP amounts were detected by western blot and quantified with Quantity-one analysis software (BIORAD) and represented as relative RhoA-GTP/total RhoA.

## Protein analysis

### 1. Total protein extraction

In order to obtain a total protein extracts, cells were washed twice with cold PBS and were scraped off the dish in SDS buffer (2% SDS, 50mM TRIS pH 7.5, 10% glycine). Lysates were syringed 5 times and then centrifuged for 10 minutes at top speed. Protein concentration in the supernatant was determined by Lowry.

### 2. Cellular subfractionation

Nuclear extracts were prepared using a variation of the Dignam procotol[252]. Cells were washed twice with cold PBS and then scraped in cytoplasmic extraction buffer A (10mM Hepes pH 7.8, 1.5mM $MgCl_2$, 10mM KCl and 0.5mM DTT). After 10 minutes of incubation on ice, Triton X-100 was added to a volume of 1/30 of the extract, and the samples were vortexed for 30 seconds. Subsequently, samples were centrifuged for 1 minute at 11000rpm, and cytosolic fraction was purified from the supernatant, while the nuclear extracts were prepared from pellet. Buffer B (0.3mM Hepes, pH 7.8, 1.4 MKCl, 30mM $MgCl_2$) was added at 0.11x the volume of the cytosolic fraction, and the mixture was incubated for 30 minutes under agitation at 4°C. The mixture was then centrifuged at maximum speed for 30 minutes at 4°C, and the supernatant was kept. To prepare the nuclear fraction, the pellet containing nuclei was washed three times with buffer A, and then resuspended in nuclear extraction buffer C (20mM Hepes, pH 7.8, 25% glycerol, 0.42M NaCl, 1.5mM $MgCl_2$, 0.2mM EDTA, and 0.5mM DTT). Samples were incubated at 4°C for 30 minutes with agitation and then centrifuged at maximum speed for 15 minutes at 4°C. The obtained supernatant contained the nuclear fraction.

For immunoprecipitation assays, the indicated antibody was added to 0.5-1 mg of nuclear extracts pre-cleared with protein A

or G magnetic beads and incubated overnight at 4°C. Antibody-bound proteins were pulled-down with 15 µl of protein A or G combined magnetic beads, washed 3 times with buffer C, and then 3 times with buffer A with 0.1% Triton. Washed beads were resuspended in 15µl of sample buffer, boiled and used for western blot analysis.

## Analysis by western blot

Electrophoresis in SDS polyacrylamide gels was used for the analysis of the results. 1.5mm thick glasses of Mini-Protean III/Tetra system (Bio-Rad) with 7.5-15% acrylamide gels were used to load the samples boiled for 5 minutes in the sample buffer and gels were run at constant voltage in Tris-Glycin-SDS (TGS) buffer. To determine the molecular weight Precission Plus Protein Dual Color Strand (Bio-Rad) was loaded on each gel. Resolved proteins were either visualized directly using Comassie Briliant Blue staining, or electrotransfered to a Protran™ nitrocellulose (NC) membrane (GE healthcare) in humid cuvette (Bio-Rad) in Transfer Buffer at constant amperage for 1 to 2.5 hours, depending of the molecular weight of the analyzed protein. Membranes were blocked for 1 hour at room temperature in 5% non-fat milk in TBS-T and then incubated with the primary antibody either 1 hour at room temperature, or overnight at 4°C, depending of antibody's quality, following by three washes 10 minutes each with TBS-T and 1 hour more at room temperature with the appropriate secondary antibody (Horse-radish peroxidise conjugated anti-IgG). Membranes were washed two times for 10 minutes with TBS-T and 10 minutes with TBS prior to developing using the Immobilion™ Western Chemiluminiscent HRP Substrate (Millipore) and were exposed on Agfa-Curix autoradiographic films.

The following primary antibodies were used in this work: Snail1 was hybridoma[162] or it was polyclonal antibody produced in CRG-TTO, Fibronectin1 from DAKO, P65NF-KB and RhoA from Santa Cruz, PARP1 was a kind gift from Dr. Jose Yelamos[253], myogenin a kind gift from Dr. Pura Muñoz, Pyruvate kinase

from Chemicon, actin, HA and αSMA from SIGMA, Lamin B1, Thrombospondin1, LOX, and N-cadherin from Abcam, β-catenin and paxillin from BD Transduction Labs, GST from GE healthcare.

**Primers (qPCR and sqPCR):**

Human FN1 promoter:

5'-CGTCCCCTTCCCCACC-3'
5'-GTTGAGACGGTGGGGGAGA-3'

Murine FN1 promoter:

5'-CTGCTCTTGGGGCTCAACC-3'
5'-AAGGAGATGGAAGGAGAGGACC-3'

Murine FN1 mRNA:

5'-CGAAGCCGGGAAGAGCAAG-3'
5'-CGTTCCCACTGCTGATTTATCTG-3'

Human FN1 mRNA:

5'-CCCGACCCTGACCGAAG-3'
5'-GTGCCTGGGCAACGGA-3'

Murine CDH1 promoter:

5'-TTCTAAGGCCGGCCCCATGC-3'
5'-GGCCGGGCAGGAGTCTAGCA-3'

Pumilio mRNA (both human and murine):

5'-CGGTCGTCCTGAGGATAAAA-3'
5'-CGTACGTGAGGCGTGAGTAA-3'

Murine THBS1 promoter:

5'-GGACTTCTGCAGGCAATCG-3'
5'-GACGCTGAGTCCGGTGAAG-3'

Murine THBS1:

5’-AAGCAACCGCATTCCAGAG-3’
5’-TGGCCCTTCACCAGTCG-3’

Murine HAS2 promoter:

5’-GCAACCACAGCGAAGAAGAAG-3’
5’-AGAATGAAGAAGTCTTTGGCTGG-3’

Murine HAS2:

5’-GTCATGTACACAGCCTTCAGAGC-3’
5’-CACGCTGCTGAGGAAGGAG-3’

Murine Lamb3 promoter:

5’-TGAGGCCGCCAGCAG-3’
5’-GAGAGCTCCCTGGGAATGTG-3’

Murine Lamb3:

5’-CCCAATATGGACAGTGGCAG-3’
5’-TGCCACCAGCGCATG-3’

HPRT mRNA (both human and murine):

5’-GGCCAGACTTTGTTGGATTTG-3’
5’-TGCGCTCATCTTAGGCTTTGT-3’

Murine LOX promoter:

5’-CGCCCTTCTCCTCCCTG -3’
5’-CGGGGAGGACGTGGCTA -3’

Murine miR200c promoter:

5’-GCTCGCAGGTGGATAGTAGAGG -3’
5’-CACTTCCGGGAGAGCCTG -3’

Murine pre-miR200c:

5’-CCCTCGTCTTACCCAGCAGTG-3’
5’-CCTCCATCATTACCCGGCAG-3

# Bibliography

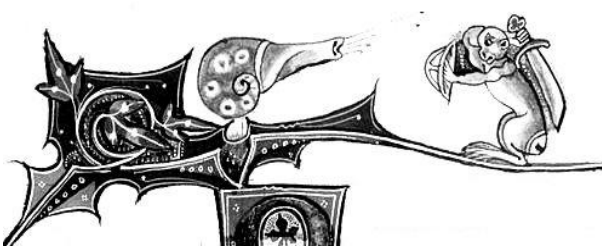

# Bibliography


1. American Cancer Society. The History of Cancer.

2. Binder, M., Roberts, C., Spencer, N., Antoine, D. & Cartwright, C. On the Antiquity of Cancer: Evidence for Metastatic Carcinoma in a Young Man from Ancient Nubia (c. 1200BC). *PLoS One* **9,** e90924 (2014).

3. Hanahan, D. & Weinberg, R. A. The hallmarks of cancer2. *Cell* **100,** 57–70

4. Hanahan, D. & Weinberg, R. R. a. Hallmarks of cancer: the next generation. *Cell* **144,** 646–74 (2011).

5. Bissell, M. J. & Hines, W. C. Why don't we get more cancer? A proposed role of the microenvironment in restraining cancer progression. *Nat. Med.* **17,** 320–9 (2011).

6. Tarin, D. & Croft, C. B. Ultrastructural studies of wound healing in mouse skin. II. Dermo-epidermal interrelationships. *J. Anat.* **106,** 79–91 (1970).

7. Hirschel, B. J., Gabbiani, G., Ryan, G. B. & Majno, G. Fibroblasts of granulation tissue: immunofluorescent staining with antismooth muscle serum. *Proc. Soc. Exp. Biol. Med.* **138,** 466–9 (1971).

8. Ryan, G. B. *et al.* Myofibroblasts in human granulation tissue. *Hum. Pathol.* **5,** 55–67 (1974).

9. Majno, G., Gabbiani, G., Hirschel, B. J., Ryan, G. B. & Statkov, P. R. Contraction of granulation tissue in vitro: similarity to smooth muscle. *Science* **173,** 548–50 (1971).

10. Goffin, J. M. *et al.* Focal adhesion size controls tension-dependent recruitment of alpha-smooth muscle actin to stress fibers. *J. Cell Biol.* **172,** 259–68 (2006).

11. Hinz, B. Formation and function of the myofibroblast during tissue repair. *J. Invest. Dermatol.* **127,** 526–37 (2007).

12. Grivennikov, S. I., Greten, F. R. & Karin, M. Immunity, inflammation, and cancer. *Cell* **140,** 883–99 (2010).

13. Olumi, A., Grossfeld, G. & Hayward, S. Carcinoma-associated fibroblasts direct tumor progression of initiated human prostatic epithelium. *Cancer Res.* 5002–5011 (1999).

14. Sen, R. & Baltimore, D. Multiple nuclear factors interact with the immunoglobulin enhancer sequences. *Cell* **46,** 705–16 (1986).

15. Hagemann, T. *et al.* "Re-educating" tumor-associated macrophages by targeting NF-kappaB. *J. Exp. Med.* **205,** 1261–8 (2008).

16. Erez, N., Truitt, M., Olson, P., Arron, S. T. & Hanahan, D. Cancer-Associated Fibroblasts Are Activated in Incipient Neoplasia to Orchestrate Tumor-Promoting Inflammation in an NF-kappaB-Dependent Manner. *Cancer Cell* **17,** 135–47 (2010).

17. Sieweke, M. H., Thompson, N. L., Sporn, M. B. & Bissell, M. J. Mediation of wound-related Rous sarcoma virus tumorigenesis by TGF-beta. *Science* **248,** 1656–60 (1990).

18. Vaughan, M. B., Howard, E. W. & Tomasek, J. J. Transforming growth factor-beta1 promotes the morphological and functional differentiation of the myofibroblast. *Exp. Cell Res.* **257,** 180–9 (2000).

19. Montesano, R. & Orci, L. Transforming growth factor beta stimulates collagen-matrix contraction by fibroblasts: implications for wound healing. *Proc. Natl. Acad. Sci. U. S. A.* **85,** 4894–7 (1988).

20. Chaudhry, S. S. *et al.* Fibrillin-1 regulates the bioavailability of TGFbeta1. *J. Cell Biol.* **176,** 355–67 (2007).

21. Wipff, P.-J., Rifkin, D. B., Meister, J.-J. & Hinz, B. Myofibroblast contraction activates latent TGF-beta1 from the extracellular matrix. *J. Cell Biol.* **179,** 1311–23 (2007).

22. Hawinkels, L. J. A. C. *et al.* Active TGF-β1 correlates with myofibroblasts and malignancy in the colorectal adenoma-carcinoma sequence. *Cancer Sci.* **100,** 663–670 (2009).

23. Löhr, M., Schmidt, C., Ringel, J., Kluth, M. & Müller, P. Transforming growth factor-β1 induces desmoplasia in an experimental model of human pancreatic carcinoma. *Cancer Res.* 550–555 (2001).

24. Naba, A., Clauser, K. R., Lamar, J. M., Carr, S. A. & Hynes, R. O. Extracellular matrix signatures of human mammary carcinoma identify novel metastasis promoters. *Elife* **3,** e01308 (2014).

25. Calon, A. *et al.* Dependency of colorectal cancer on a TGF-β-driven program in stromal cells for metastasis initiation. *Cancer Cell* **22,** 571–84 (2012).

26. Hawinkels, L. J. A. C. *et al.* Interaction with colon cancer cells hyperactivates TGF-β signaling in cancer-associated fibroblasts. *Oncogene* **33,** 97–107 (2014).

27. Orimo, A. *et al.* Stromal fibroblasts present in invasive human breast carcinomas promote tumor growth and angiogenesis through elevated SDF-1/CXCL12 secretion. *Cell* **121,** 335–48 (2005).

28. Olive, K. P. *et al.* Inhibition of Hedgehog signaling enhances delivery of chemotherapy in a mouse model of pancreatic cancer. *Science* **324,** 1457–61 (2009).

29. Pavlides, S. *et al.* The reverse Warburg effect: aerobic glycolysis in cancer associated fibroblasts and the tumor stroma. *Cell Cycle* **8,** 3984–4001 (2009).

30. Martinez-Outschoorn, U. E., Lisanti, M. P. & Sotgia, F. Catabolic Cancer-Associated Fibroblasts (CAFs) Transfer Energy and Biomass to Anabolic Cancer Cells, Fueling Tumor Growth. *Semin. Cancer Biol.* 1–13 (2014). doi:10.1016/j.semcancer.2014.01.005

31. Singer, I. I. The fibronexus: a transmembrane association of fibronectin-containing fibers and bundles of 5 nm microfilaments in hamster and human fibroblasts. *Cell* **16,** 675–85 (1979).

32. Singer, I. & Kawka, D. co-distribution of fibronectin and actin fibers in granulation tissue: immunofluorescence and electron microscope studies of the fibronexus at the myofibroblast surface. *J. cell …* (1984).

33. Estes, J. M. *et al.* Phenotypic and functional features of myofibroblasts in sheep fetal wounds. *Differentiation.* **56,** 173–81 (1994).

34. Eyden, B. The fibronexus in reactive and tumoral myofibroblasts: further characterisation by electron microscopy. *Histol. Histopathol.* **16,** 57–70 (2001).

35. Lu, P., Weaver, V. M. & Werb, Z. The extracellular matrix: a dynamic niche in cancer progression. *J. Cell Biol.* **196,** 395–406 (2012).

36. Yamada, K. M. & Cukierman, E. Modeling tissue morphogenesis and cancer in 3D. *Cell* **130,** 601–10 (2007).

37. Vogel, V. & Sheetz, M. Local force and geometry sensing regulate cell functions. *Nat. Rev. Mol. Cell Biol.* **7,** 265–75 (2006).

38. Singh, P., Carraher, C. & Schwarzbauer, J. E. Assembly of fibronectin extracellular matrix. *Annu. Rev. Cell Dev. Biol.* **26,** 397–419 (2010).

39. Erickson, H. P. & Carrell, N. A. Fibronectin in extended and compact conformations. Electron microscopy and sedimentation analysis. *J. Biol. Chem.* **258,** 14539–44 (1983).

40. Huveneers, S., Truong, H., Fässler, R., Sonnenberg, A. & Danen, E. H. J. Binding of soluble fibronectin to integrin alpha5 beta1 - link to focal adhesion redistribution and contractile shape. *J. Cell Sci.* **121,** 2452–62 (2008).

41. Wu, C., Bauer, J. S., Juliano, R. L. & McDonald, J. a. The alpha 5 beta 1 integrin fibronectin receptor, but not the alpha 5 cytoplasmic domain, functions in an early and essential step in fibronectin matrix assembly. *J. Biol. Chem.* **268,** 21883–8 (1993).

42. Zhong, C. *et al.* Rho-mediated contractility exposes a cryptic site in fibronectin and induces fibronectin matrix assembly. *J. Cell Biol.* **141,** 539–51 (1998).

43. Lee, S. H. & Dominguez, R. Regulation of actin cytoskeleton dynamics in cells. *Mol. Cells* **29,** 311–25 (2010).

44. Wierzbicka-Patynowski, I. & Schwarzbauer, J. E. The ins and outs of fibronectin matrix assembly. *J. Cell Sci.* **116,** 3269–76 (2003).

45. Serini, G. *et al.* The fibronectin domain ED-A is crucial for myofibroblastic phenotype induction by transforming growth factor-beta1. *J. Cell Biol.* **142,** 873–81 (1998).

46. Muiznieks, L. D. & Keeley, F. W. Molecular assembly and mechanical properties of the extracellular matrix: A fibrous protein perspective. *Biochim. Biophys. Acta* **1832,** 866–75 (2013).

47. Shadwick, R. E. Elastic energy storage in tendons: mechanical differences related to function and age. *J. Appl. Physiol.* **68,** 1033–40 (1990).

48. Kadler, E. & Prockops, J. Assembly of Collagen Fibrils de Novo by Cleavage of the Type I PC- Collagen with Procollagen C-Proteinase. **260,** 15696–15701 (1987).

49. Li, S., Van Den Diepstraten, C., D'souza, S. J., Chan, B. M. C. & Pickering, J. G. Vascular Smooth Muscle Cells Orchestrate the Assembly of Type I Collagen via α2β1 Integrin, RhoA, and Fibronectin Polymerization. *Am. J. Pathol.* **163,** 1045–1056 (2003).

50. McDONALD, J. of fibronectin in collagen deposition: Fab'to the gelatin-binding domain of fibronectin inhibits both fibronectin and collagen organization in fibroblast extracellular matrix. *J. cell …* (1982).

51. Siegel, R. C., Fu, J. C. C., Uto, N., Horiuchi, K. & Fujimoto, D. Collagen cross-linking: Lysyl oxidase dependent synthesis of pyridinoline in vitro: Confirmation that pyridinoline is derived from collagen. *Biochem. Biophys. Res. Commun.* **108,** 1546–1550 (1982).

52. Csiszar, K. Lysyl oxidases: a novel multifunctional amine oxidase family. *Prog. Nucleic Acid Res. Mol. Biol.* **70,** 1–32 (2001).

53. Pinnell, S. R. & Martin, G. R. The cross-linking of collagen and elastin: enzymatic conversion of lysine in peptide linkage to alpha-aminoadipic-delta-semialdehyde (allysine) by an extract from bone. *Proc. Natl. Acad. Sci. U. S. A.* **61,** 708–16 (1968).

54. Mäki, J. M. *et al.* Inactivation of the lysyl oxidase gene Lox leads to aortic aneurysms, cardiovascular dysfunction, and perinatal death in mice. *Circulation* **106,** 2503–9 (2002).

55. Gacheru, S. N. *et al.* Transcriptional and post-transcriptional control of lysyl oxidase expression in vascular smooth muscle cells: effects of TGF-beta 1 and serum deprivation. *J. Cell. Biochem.* **65,** 395–407 (1997).

56. Fogelgren, B. *et al.* Cellular fibronectin binds to lysyl oxidase with high affinity and is critical for its proteolytic activation. *J. Biol. Chem.* **280,** 24690–7 (2005).

57. Schietke, R. *et al.* The lysyl oxidases LOX and LOXL2 are necessary and sufficient to repress E-cadherin in hypoxia: insights into cellular transformation processes mediated by HIF-1. *J. Biol. Chem.* **285,** 6658–69 (2010).

58. Le, Q.-T. *et al.* Validation of lysyl oxidase as a prognostic marker for metastasis and survival in head and neck squamous cell carcinoma: Radiation Therapy Oncology Group trial 90-03. *J. Clin. Oncol.* **27,** 4281–6 (2009).

59. Erler, J. T. *et al.* Lysyl oxidase is essential for hypoxia-induced metastasis. *Nature* **440,** 1222–6 (2006).

60. Albinger-Hegyi, A. *et al.* Lysyl oxidase expression is an independent marker of prognosis and a predictor of lymph node metastasis in oral and oropharyngeal squamous cell carcinoma (OSCC). *Int. J. Cancer* **126,** 2653–62 (2010).

61. Baker, A.-M., Bird, D., Lang, G., Cox, T. R. & Erler, J. T. Lysyl oxidase enzymatic function increases stiffness to drive colorectal cancer progression through FAK. *Oncogene* **32,** 1863–8 (2013).

62. Cox, T., Bird, D., Baker, A. & Barker, H. LOX-mediated collagen crosslinking is responsible for fibrosis-enhanced metastasis. *Cancer Res.* 1721–1732 (2013). doi:10.1158/0008-5472.CAN-12-2233

63. Butcher, D. T., Alliston, T. & Weaver, V. M. A tense situation: forcing tumour progression. *Nat. Rev. Cancer* **9,** 108–22 (2009).

64. Wolfe, J. N., Saftlas, A. F. & Salane, M. Mammographic parenchymal patterns and quantitative evaluation of mammographic densities: a case-control study. *AJR. Am. J. Roentgenol.* **148,** 1087–92 (1987).

65. Ingber, D. E. The architecture of life. *Sci. Am.* **278,** 48–57 (1998).

66. Gallant, N. D., Michael, K. E. & García, A. J. Cell adhesion strengthening: contributions of adhesive area, integrin binding, and focal adhesion assembly. *Mol. Biol. Cell* **16,** 4329–40 (2005).

67. Zaidel-Bar, R., Cohen, M., Addadi, L. & Geiger, B. Hierarchical assembly of cell-matrix adhesion complexes. *Biochem. Soc. Trans.* **32,** 416–20 (2004).

68. Helmke, B. P. & Davies, P. F. The cytoskeleton under external fluid mechanical forces: hemodynamic forces acting on the endothelium. *Ann. Biomed. Eng.* **30,** 284–96 (2002).

69. Lo, C. M., Wang, H. B., Dembo, M. & Wang, Y. L. Cell movement is guided by the rigidity of the substrate. *Biophys. J.* **79,** 144–52 (2000).

70. Mao, Y. & Schwarzbauer, J. E. Fibronectin fibrillogenesis, a cell-mediated matrix assembly process. *Matrix Biol.* **24,** 389–99 (2005).

71. Ingber, D. E. Cancer as a disease of epithelial-mesenchymal interactions and extracellular matrix regulation. *Differentiation.* **70,** 547–60 (2002).

72. Huang, S. & Ingber, D. E. A non-genetic basis for cancer progression and metastasis: self-organizing attractors in cell regulatory networks. *Breast Dis.* **26,** 27–54 (2007).

73. López-Novoa, J. M. & Nieto, M. A. Inflammation and EMT: an alliance towards organ fibrosis and cancer progression. *EMBO Mol. Med.* **1,** 303–14 (2009).

74. Thiery, J. J. P., Acloque, H., Huang, R. R. Y. J. & Nieto, M. A. Epithelial-mesenchymal transitions in development and disease. *Cell* **139,** 871–90 (2009).

75. Hinz, B. *et al.* The myofibroblast: one function, multiple origins. *Am. J. Pathol.* **170,** 1807–16 (2007).

76. Block, E. R., Matela, A. R., SundarRaj, N., Iszkula, E. R. & Klarlund, J. K. Wounding induces motility in sheets of corneal epithelial cells through loss of spatial constraints: role of heparin-binding epidermal growth factor-like growth factor signaling. *J. Biol. Chem.* **279,** 24307–12 (2004).

77. Ahmed, N. Molecular pathways regulating EGF-induced epithelio-mesenchymal transition in human ovarian surface epithelium. *Am. J. ...* 1532–1542 (2006). doi:10.1152/ajpcell.00478.2005.

78. Thiery, J. P. Epithelial-mesenchymal transitions in tumour progression. *Nat. Rev. Cancer* **2,** 442–454

79. Ledford, H. Cancer theory faces doubts. *Nature* **472,** 273 (2011).

80. Yoshida, R., Kimura, N., Harada, Y. & Ohuchi, N. The loss of E-cadherin, α- and β-catenin expression is associated with metastasis and poor prognosis in invasive breast cancer. *Int. J. Oncol.* **18,** 513–520 (2001).

81. Becker, K. F. *et al.* Functional allelic loss detected at the protein level in archival human tumours using allele-

specific E-cadherin monoclonal antibodies. *J. Pathol.* **197,** 567–574

82. Solanas, G. & Porta-de-la-Riva, M. E-cadherin controls β-catenin and NF-κB transcriptional activity in mesenchymal gene expression. *J. cell …* (2008).

83. Yilmaz, M. & Christofori, G. EMT, the cytoskeleton, and cancer cell invasion. *Cancer Metastasis Rev.* **28,** 15–33 (2009).

84. Van Aelst, L. & Symons, M. Role of Rho family GTPases in epithelial morphogenesis. *Genes Dev.* **16,** 1032–54 (2002).

85. Siderovski, D. P. & Willard, F. S. The GAPs, GEFs, and GDIs of heterotrimeric G-protein alpha subunits. *Int. J. Biol. Sci.* **1,** 51–66 (2005).

86. Lawson, C. D. & Burridge, K. The on-off relationship of Rho and Rac during integrin-mediated adhesion and cell migration. *Small GTPases* **5,** (2014).

87. Amano, M. *et al.* Formation of actin stress fibers and focal adhesions enhanced by Rho-kinase. *Science* **275,** 1308–11 (1997).

88. Lamouille, S., Xu, J. & Derynck, R. Molecular mechanisms of epithelial–mesenchymal transition. *Nat. Rev. Mol. Cell Biol.* **15,** 178–196 (2014).

89. Savagner, P., Yamada, K. M. & Thiery, J. P. The zinc-finger protein slug causes desmosome dissociation, an initial and necessary step for growth factor-induced epithelial-mesenchymal transition38. *J.Cell Biol.* **137,** 1403–1419 (1997).

90. Lo, H.-W. *et al.* Epidermal growth factor receptor cooperates with signal transducer and activator of transcription 3 to induce epithelial-mesenchymal

transition in cancer cells via up-regulation of TWIST gene expression. *Cancer Res.* **67,** 9066–76 (2007).

91. Graham, T. R. *et al.* Insulin-like growth factor-I-dependent up-regulation of ZEB1 drives epithelial-to-mesenchymal transition in human prostate cancer cells. *Cancer Res.* **68,** 2479–88 (2008).

92. Acevedo, V. D. *et al.* Inducible FGFR-1 activation leads to irreversible prostate adenocarcinoma and an epithelial-to-mesenchymal transition. *Cancer Cell* **12,** 559–71 (2007).

93. Shintani, Y., Maeda, M., Chaika, N., Johnson, K. R. & Wheelock, M. J. Collagen I promotes epithelial-to-mesenchymal transition in lung cancer cells via transforming growth factor-beta signaling. *Am. J. Respir. Cell Mol. Biol.* **38,** 95–104 (2008).

94. Zoltan-Jones, A., Huang, L., Ghatak, S. & Toole, B. P. Elevated hyaluronan production induces mesenchymal and transformed properties in epithelial cells. *J. Biol. Chem.* **278,** 45801–10 (2003).

95. Wrana, J. L. *et al.* TGF beta signals through a heteromeric protein kinase receptor complex. *Cell* **71,** 1003–14 (1992).

96. Xu, J., Lamouille, S. & Derynck, R. TGF-beta-induced epithelial to mesenchymal transition. *Cell Res.* **19,** 156–72 (2009).

97. Zheng, H. & Kang, Y. Multilayer control of the EMT master regulators. *Oncogene* **33,** 1755–63 (2014).

98. Grau, Y., Carteret, C. & Simpson, P. Mutations and Chromosomal Rearrangements Affecting the Expression of Snail, a Gene Involved in Embryonic Patterning in DROSOPHILA MELANOGASTER. *Genetics* **108,** 347–60 (1984).

99. Hemavathy, K., Ashraf, S. I. & Ip, Y. T. Snail/slug family of repressors: slowly going into the fast lane of development and cancer. *Gene* **257,** 1–12 (2000).

100. Smith, D. E., Franco del Amo, F. & Gridley, T. Isolation of Sna, a mouse gene homologous to the Drosophila genes snail and escargot: its expression pattern suggests multiple roles during postimplantation development. *Development* **116,** 1033–9 (1992).

101. LaBonne, C. & Bronner-Fraser, M. Snail-related transcriptional repressors are required in Xenopus for both the induction of the neural crest and its subsequent migration. *Dev. Biol.* **221,** 195–205 (2000).

102. Batlle, E. *et al.* The transcription factor Snail is a repressor of E-cadherin gene expression in epithelial tumour cells. *Nat. Cell Biol.* **2,** 84–89

103. Cano, A. *et al.* The transcription factor Snail controls epithelial-mesenchymal transitions by repressing E-cadherin expression. *Nat. Cell Biol.* **2,** 76–83 (2000).

104. Carver, E. A., Jiang, R. L., Lan, Y., Oram, K. F. & Gridley, T. The mouse snail gene encodes a key regulator of the epithelial-mesenchymal transition. *Mol. Cell. …* **21,** 8184–8188 (2001).

105. Poser, I. *et al.* Loss of E-Cadherin expression in melanoma cells involves upregulation of the transcriptional repressor snail. *J. Invest. Dermatol.* **117,** 777 (2001).

106. Guaita, S. *et al.* Snail induction of epithelial to mesenchymal transition in tumor cells is accompanied by MUC1 repression and ZEB1 expression. *J. Biol. Chem.* **277,** 39209–16 (2002).

107. Peinado, H., Olmeda, D. & Cano, A. Snail, Zeb and bHLH factors in tumour progression: an alliance against the epithelial phenotype? *Nat. Rev. Cancer* **7,** 415–28 (2007).

108. Yang, M.-H. *et al.* Direct regulation of TWIST by HIF-1alpha promotes metastasis. *Nat. Cell Biol.* **10,** 295–305 (2008).

109. Viñas-Castells, R. *et al.* The hypoxia-controlled FBXL14 ubiquitin ligase targets SNAIL1 for proteasome degradation. *J. Biol. Chem.* **285,** 3794–805 (2010).

110. Bachelder, R. E., Yoon, S.-O., Franci, C., de Herreros, A. G. & Mercurio, A. M. Glycogen synthase kinase-3 is an endogenous inhibitor of Snail transcription: implications for the epithelial-mesenchymal transition. *J. Cell Biol.* **168,** 29–33 (2005).

111. Zhou, B. P. *et al.* Dual regulation of Snail by GSK-3beta-mediated phosphorylation in control of epithelial-mesenchymal transition. *Nat. Cell Biol.* **6,** 931–40 (2004).

112. Domínguez, D. Phosphorylation regulates the subcellular location and activity of the snail transcriptional repressor. *… Cell. Biol.* (2003). doi:10.1128/MCB.23.14.5078

113. Thuault, S. *et al.* HMGA2 and Smads co-regulate SNAIL1 expression during induction of epithelial-to-mesenchymal transition. *J. Biol. Chem.* **283,** 33437–46 (2008).

114. Zhang, K. *et al.* Lats2 kinase potentiates Snail1 activity by promoting nuclear retention upon phosphorylation. *EMBO J.* **31,** 29–43 (2012).

115. Viñas-Castells, R. *et al.* Nuclear ubiquitination by FBXL5 modulates Snail1 DNA binding and stability. *Nucleic Acids Res.* **42,** 1079–94 (2014).

116. Yang, Z. *et al.* Pak1 phosphorylation of snail, a master regulator of epithelial-to-mesenchyme transition, modulates snail's subcellular localization and functions. *Cancer Res.* **65,** 3179–84 (2005).

117. Vincent, T. *et al.* A SNAIL1-SMAD3/4 transcriptional repressor complex promotes TGF-beta mediated epithelial-mesenchymal transition. *Nat. Cell Biol.* **11,** 943–50 (2009).

118. Pálmer, H. G. *et al.* The transcription factor SNAIL represses vitamin D receptor expression and responsiveness in human colon cancer. *Nat. Med.* **10,** 917–9 (2004).

119. Peinado, H., Ballestar, E., Esteller, M. & Cano, A. Snail mediates E-cadherin repression by the recruitment of the Sin3A/histone deacetylase 1 (HDAC1)/HDAC2 complex. *Mol. Cell. Biol.* **24,** 306–319 (2004).

120. Herranz, N. *et al.* Polycomb complex 2 is required for E-cadherin repression by the Snail1 transcription factor. *Mol Cell Biol* **28,** 4772–4781 (2008).

121. Lin, Y. *et al.* The SNAG domain of Snail1 functions as a molecular hook for recruiting lysine-specific demethylase 1. *EMBO J.* **29,** 1803–16 (2010).

122. Herranz, N. *et al.* Lysyl oxidase-like 2 deaminates lysine 4 in histone H3. *Mol. Cell* **46,** 369–76 (2012).

123. Hou, Z. *et al.* The LIM protein AJUBA recruits protein arginine methyltransferase 5 to mediate SNAIL-dependent transcriptional repression. *Mol. Cell. Biol.* **28,** 3198–207 (2008).

124. Millanes-Romero, A. *et al.* Regulation of heterochromatin transcription by Snail1/LOXL2 during epithelial-to-mesenchymal transition. *Mol. Cell* **52,** 746–57 (2013).

125. Pham, C. G. *et al.* Upregulation of Twist-1 by NF-kappaB blocks cytotoxicity induced by chemotherapeutic drugs. *Mol. Cell. Biol.* **27,** 3920–35 (2007).

126. Wu, Y. *et al.* Stabilization of snail by NF-kappaB is required for inflammation-induced cell migration and invasion. *Cancer Cell* **15,** 416–28 (2009).

127. Julien, S. *et al.* Activation of NF-kappaB by Akt upregulates Snail expression and induces epithelium mesenchyme transition. *Oncogene* **26,** 7445–56 (2007).

128. Kuphal, S., Poser, I., Jobin, C., Hellerbrand, C. & Bosserhoff, A. K. Loss of E-cadherin leads to upregulation of NFkappaB activity in malignant melanoma. *Oncogene* **23,** 8509–19 (2004).

129. Huber, M. A. *et al.* NF-kappaB is essential for epithelial-mesenchymal transition and metastasis in a model of breast cancer progression. *J. Clin. Invest.* **114,** 569–81 (2004).

130. Hassa, P., Covic, M., Bedford, M. & Hottiger, M. Protein arginine methyltransferase 1 coactivates NF-κB-dependent gene expression synergistically with CARM1 and PARP1. *J. Mol. Biol.* (2008).

131. Hassa, P. O., Covic, M., Hasan, S., Imhof, R. & Hottiger, M. O. The enzymatic and DNA binding activity of PARP-1 are not required for NF-kappa B coactivator function. *J. Biol. Chem.* **276,** 45588–97 (2001).

132. Chiarugi, A. & Moskowitz, M. A. Poly(ADP-ribose) polymerase-1 activity promotes NF-kappaB-driven transcription and microglial activation: implication for neurodegenerative disorders. *J. Neurochem.* **85,** 306–17 (2003).

133. Hassa, P. O. & Hottiger, M. O. A role of poly (ADP-ribose) polymerase in NF-kappaB transcriptional activation. *Biol. Chem.* **380,** 953–9

134. Martín-Oliva, D. *et al.* Crosstalk between PARP-1 and NF-kappaB modulates the promotion of skin neoplasia. *Oncogene* **23,** 5275–83 (2004).

135. Oliver, F. J. *et al.* Resistance to endotoxic shock as a consequence of defective NF-kappaB activation in poly (ADP-ribose) polymerase-1 deficient mice. *EMBO J.* **18,** 4446–54 (1999).

136. Godon, C. & Cordelières, F. PARP inhibition versus PARP-1 silencing: different outcomes in terms of single-strand break repair and radiation susceptibility. *Nucleic acids …* (2008).

137. Hassa, P., Covic, M. & Hasan, S. The enzymatic and DNA binding activity of PARP-1 are not required for NF-κB coactivator function. *J. Biol. …* (2001).

138. Bai, P. *et al.* PARP-1 inhibition increases mitochondrial metabolism through SIRT1 activation. *Cell Metab.* **13,** 461–8 (2011).

139. Hu, B. *et al.* Regulation of myofibroblast differentiation by poly(ADP-ribose) polymerase 1. *Am. J. Pathol.* **182,** 71–83 (2013).

140. McPhee, T. R., McDonald, P. C., Oloumi, A. & Dedhar, S. Integrin-linked kinase regulates E-cadherin expression through PARP-1. *Dev. Dyn.* **237,** 2737–47 (2008).

141. Rodríguez, M. I. *et al.* Poly(ADP-ribose)-dependent regulation of Snail1 protein stability. *Oncogene* **30,** 4365–72 (2011).

142. Barrallo-Gimeno, A. & Nieto, M. The Snail genes as inducers of cell movement and survival: implications in development and cancer. *Development* (2005).

143. Escrivà, M. & Peiró, S. Repression of PTEN phosphatase by Snail1 transcriptional factor during gamma radiation-induced apoptosis. *… Cell. Biol.* (2008).

144. Kajita, M., McClinic, K. N. & Wade, P. A. Aberrant expression of the transcription factors snail and slug alters the response to genotoxic stress. *Mol. Cell. Biol.* **24,** 7559–66 (2004).

145. Vega, S. *et al.* Snail blocks the cell cycle and confers resistance to cell death. *Genes Dev.* **18,** 1131–43 (2004).

146. Franco, D. L. *et al.* Snail1 suppresses TGF-beta-induced apoptosis and is sufficient to trigger EMT in hepatocytes. *J. Cell Sci.* **123,** 3467–77 (2010).

147. Valdes, F. *et al.* The epithelial mesenchymal transition confers resistance to the apoptotic effects of transforming growth factor beta in fetal rat hepatocytes. *Mol. Cancer Res.* **1,** 68–78

148. Jung, A. *et al.* The invasion front of human colorectal adenocarcinomas shows co-localization of nuclear beta-catenin, cyclin D1, and p16INK4A and is a region of low proliferation2. *Am.J.Pathol.* **159,** 1613–1617 (2001).

149. Lyons, J. G. *et al.* Snail up-regulates proinflammatory mediators and inhibits differentiation in oral keratinocytes. *Cancer Res.* **68,** 4525–30 (2008).

150. Batlle, R. *et al.* Snail1 controls TGF-β responsiveness and differentiation of mesenchymal stem cells. *Oncogene* **418,** 3381–3389 (2012).

151. De Frutos, C. A. *et al.* Snail1 controls bone mass by regulating Runx2 and VDR expression during osteoblast differentiation. *EMBO J.* **28,** 686–96 (2009).

152. Hwang, W.-L. *et al.* MicroRNA-146a directs the symmetric division of Snail-dominant colorectal cancer stem cells. *Nat. Cell Biol.* **16,** 268–80 (2014).

153. Mani, S. a S. *et al.* The epithelial-mesenchymal transition generates cells with properties of stem cells. *Cell* **133,** 704–15 (2008).

154. Dontu, G. *et al.* In vitro propagation and transcriptional profiling of human mammary stem/progenitor cells. *Genes Dev.* **17,** 1253–70 (2003).

155. Morel, A.-P. *et al.* Generation of breast cancer stem cells through epithelial-mesenchymal transition. *PLoS One* **3,** e2888 (2008).

156. Rhim, A. D. *et al.* EMT and dissemination precede pancreatic tumor formation. *Cell* **148,** 349–61 (2012).

157. Kretzschmar, K. & Watt, F. M. Lineage tracing. *Cell* **148,** 33–45 (2012).

158. Chen, J. *et al.* A restricted cell population propagates glioblastoma growth after chemotherapy. *Nature* **488,** 522–6 (2012).

159. Driessens, G., Beck, B., Caauwe, A., Simons, B. D. & Blanpain, C. Defining the mode of tumour growth by clonal analysis. *Nature* **488,** 527–30 (2012).

160. Schepers, A. G. *et al.* Lineage tracing reveals Lgr5+ stem cell activity in mouse intestinal adenomas. *Science* **337,** 730–5 (2012).

161. Boutet, A. *et al.* Snail activation disrupts tissue homeostasis and induces fibrosis in the adult kidney. *EMBO J.* **25,** 5603–13 (2006).

162. Francí, C. *et al.* Expression of Snail protein in tumor-stroma interface. *Oncogene* **25,** 5134–44 (2006).

163. Francí, C. *et al.* Snail1 protein in the stroma as a new putative prognosis marker for colon tumours. *PLoS One* **4,** e5595 (2009).

164. Kraus, W. L. & Hottiger, M. O. PARP-1 and gene regulation: Progress and puzzles. *Mol. Aspects Med.* 1–15 (2013). doi:10.1016/j.mam.2013.01.005

165. Batlle, E., Sancho, E. & Francí, C. The transcription factor snail is a repressor of E-cadherin gene expression in epithelial tumour cells. *Nat. cell …* (2000).

166. Schurter, B. T. *et al.* Methylation of histone H3 by coactivator-associated arginine methyltransferase 1. *Biochemistry* **40,** 5747–56 (2001).

167. Strahl, B. D. *et al.* Methylation of histone H4 at arginine 3 occurs in vivo and is mediated by the nuclear receptor coactivator PRMT1. *Curr. Biol.* **11,** 996–1000 (2001).

168. Miettinen, P. J., Ebner, R., Lopez, a R. & Derynck, R. TGF-beta induced transdifferentiation of mammary epithelial cells to mesenchymal cells: involvement of type I receptors. *J. Cell Biol.* **127,** 2021–36 (1994).

169. Amatangelo, M. D., Bassi, D. E., Klein-Szanto, A. J. P. & Cukierman, E. Stroma-derived three-dimensional matrices are necessary and sufficient to promote desmoplastic differentiation of normal fibroblasts. *Am. J. Pathol.* **167,** 475–88 (2005).

170. Beacham, D. Preparation of extracellular matrices produced by cultured and primary fibroblasts. *Curr. Protoc. cell Biol.* 1–21 (2006).

171. Engler, A. J., Sen, S., Sweeney, H. L. & Discher, D. E. Matrix elasticity directs stem cell lineage specification. *Cell* **126,** 677–89 (2006).

172. Basu, S., Dahl, K. & Rohde, G. Localizing and extracting filament distributions from microscopy images. *J. Microsc.* **250,** 57–67 (2013).

173. Stanisavljevic, J., Porta-de-la-Riva, M., Batlle, R., De Herreros, A. G. & Baulida, J. The p65 subunit of NF-κB and PARP1 assist Snail1 in activating fibronectin transcription. *J. Cell Sci.* **124,** 4161–71 (2012).

174. Darby, I., Skalli, O. & Gabbiani, G. Alpha-smooth muscle actin is transiently expressed by myofibroblasts during experimental wound healing. *Lab. Invest.* **63,** 21–9 (1990).

175. Ohashi, T., Kiehart, D. P. & Erickson, H. P. Dual labeling of the fibronectin matrix and actin cytoskeleton with green fluorescent protein variants. *J. Cell Sci.* **115,** 1221–9 (2002).

176. Hatta, K. & Takeichi, M. Expression of N-cadherin adhesion molecules associated with early morphogenetic events in chick development. *Nature* **320,** 447–9 (1986).

177. Wheelock, M. J. & Knudsen, K. A. Cadherins and associated proteins. *In Vivo* **5,** 505–13

178. Nagafuchi, A. Molecular architecture of adherens junctions. *Curr. Opin. Cell Biol.* **13,** 600–603 (2001).

179. Provenzano, P. P. *et al.* Collagen reorganization at the tumor-stromal interface facilitates local invasion. *BMC Med.* **4,** 38 (2006).

180. Conklin, M. W. *et al.* Aligned collagen is a prognostic signature for survival in human breast carcinoma. *Am. J. Pathol.* **178,** 1221–32 (2011).

181. Conklin, M. W. M. & Keely, P. J. P. Why the stroma matters in breast cancer: Insights into breast cancer patient

outcomes through the examination of stromal biomarkers. *Cell Adh. Migr.* **6,** 249–260 (2012).

182. Häyry, V. *et al.* Bmi-1 expression predicts prognosis in squamous cell carcinoma of the tongue. *Br. J. Cancer* **102,** 892–7 (2010).

183. Kroepil, F. *et al.* Snail1 expression in colorectal cancer and its correlation with clinical and pathological parameters. *BMC Cancer* **13,** 145 (2013).

184. Montserrat, N. *et al.* Repression of E-cadherin by SNAIL, ZEB1, and TWIST in invasive ductal carcinomas of the breast: a cooperative effort? *Hum. Pathol.* **42,** 103–10 (2011).

185. Fan, X.-J. *et al.* Snail promotes lymph node metastasis and Twist enhances tumor deposit formation through epithelial-mesenchymal transition in colorectal cancer. *Hum. Pathol.* **44,** 173–80 (2013).

186. Castelló-Cros, R., Khan, D. R., Simons, J., Valianou, M. & Cukierman, E. Staged stromal extracellular 3D matrices differentially regulate breast cancer cell responses through PI3K and beta1-integrins. *BMC Cancer* **9,** 94 (2009).

187. Levental, K. R. *et al.* Matrix Crosslinking Forces Tumor Progression by Enhancing Integrin Signaling. *Cell* **139,** 891–906 (2009).

188. Sahlgren, C., Gustafsson, M. V, Jin, S., Poellinger, L. & Lendahl, U. Notch signaling mediates hypoxia-induced tumor cell migration and invasion. *Proc. Natl. Acad. Sci. U. S. A.* **105,** 6392–7 (2008).

189. Taylor, M. A., Amin, J. D., Kirschmann, D. A. & Schiemann, W. P. Lysyl oxidase contributes to mechanotransduction-mediated regulation of transforming growth factor-β

signaling in breast cancer cells. *Neoplasia* **13,** 406–18 (2011).

190. Leight, J. L., Wozniak, M. a, Chen, S., Lynch, M. L. & Chen, C. S. Matrix rigidity regulates a switch between TGF-β1-induced apoptosis and epithelial-mesenchymal transition. *Mol. Biol. Cell* **23,** 781–91 (2012).

191. Kojima, Y. *et al.* Autocrine TGF-beta and stromal cell-derived factor-1 (SDF-1) signaling drives the evolution of tumor-promoting mammary stromal myofibroblasts. *Proc. Natl. Acad. Sci. U. S. A.* **107,** 20009–14 (2010).

192. Qiu, W. *et al.* No evidence of clonal somatic genetic alterations in cancer-associated fibroblasts from human breast and ovarian carcinomas. *Nat. Genet.* **40,** 650–5 (2008).

193. Walter, K., Omura, N., Hong, S.-M., Griffith, M. & Goggins, M. Pancreatic cancer associated fibroblasts display normal allelotypes. *Cancer Biol. Ther.* **7,** 882–8 (2008).

194. Hosein, A. N. *et al.* Breast carcinoma-associated fibroblasts rarely contain p53 mutations or chromosomal aberrations. *Cancer Res.* **70,** 5770–7 (2010).

195. Swift, J. *et al.* Nuclear lamin-A scales with tissue stiffness and enhances matrix-directed differentiation. *Science* **341,** 1240104 (2013).

196. Kalluri, R. & Zeisberg, M. Fibroblasts in cancer. *Nat. Rev. Cancer* **6,** 392–401 (2006).

197. Shinojima, N. *et al.* TGF-β mediates homing of bone marrow-derived human mesenchymal stem cells to glioma stem cells. *Cancer Res.* **73,** 2333–44 (2013).

198. Sochol, R. D., Higa, A. T., Janairo, R. R. R., Li, S. & Lin, L. Unidirectional mechanical cellular stimuli via micropost array gradients. *Soft Matter* **7,** 4606 (2011).

199. Orlic, D. *et al.* Bone marrow cells regenerate infarcted myocardium. *Nature* **410,** 701–5 (2001).

200. Byrne, C. *et al.* Mammographic features and breast cancer risk: effects with time, age, and menopause status. *J. Natl. Cancer Inst.* **87,** 1622–9 (1995).

201. DeFilippis, R. R. A. *et al.* CD36 repression activates a multicellular stromal program shared by high mammographic density and tumor tissues. *Cancer Discov.* **2,** 826–839 (2012).

202. Rowe, R. G. *et al.* Mesenchymal cells reactivate Snail1 expression to drive three-dimensional invasion programs. *J. Cell Biol.* **184,** 399–408 (2009).

203. Liu, F. *et al.* Increased expression of SDF-1/CXCR4 is associated with lymph node metastasis of invasive micropapillary carcinoma of the breast. *Histopathology* **54,** 741–50 (2009).

204. Yoshitake, N. *et al.* Expression of SDF-1 alpha and nuclear CXCR4 predicts lymph node metastasis in colorectal cancer. *Br. J. Cancer* **98,** 1682–9 (2008).

205. Zhao, B.-C. *et al.* CXCR4/SDF-1 axis is involved in lymph node metastasis of gastric carcinoma. *World J. Gastroenterol.* **17,** 2389–96 (2011).

206. Velling, T., Risteli, J., Wennerberg, K., Mosher, D. F. & Johansson, S. Polymerization of type I and III collagens is dependent on fibronectin and enhanced by integrins alpha 11beta 1 and alpha 2beta 1. *J. Biol. Chem.* **277,** 37377–81 (2002).

207. Sottile, J. & Hocking, D. C. Fibronectin polymerization regulates the composition and stability of extracellular matrix fibrils and cell-matrix adhesions. *Mol. Biol. Cell* **13,** 3546–59 (2002).

208. Haraguchi, M. *et al.* Snail regulates cell-matrix adhesion by regulation of the expression of integrins and basement membrane proteins. *J. Biol. Chem.* **283,** 23514–23 (2008).

209. Henderson, N. C. *et al.* Targeting of αv integrin identifies a core molecular pathway that regulates fibrosis in several organs. *Nat. Med.* **19,** 1617–24 (2013).

210. Czyz, M. & Cierniewski, C. S. Selective Sp1 and Sp3 binding is crucial for activity of the integrin alphaV promoter in cultured endothelial cells. *Eur. J. Biochem.* **265,** 638–44 (1999).

211. Hu, C.-T. *et al.* Snail associates with EGR-1 and SP-1 to upregulate transcriptional activation of p15INK4b. *FEBS J.* **277,** 1202–18 (2010).

212. López-Soto, A. *et al.* Epithelial-mesenchymal transition induces an antitumor immune response mediated by NKG2D receptor. *J. Immunol.* **190,** 4408–19 (2013).

213. Chung, C. & Erickson, H. Glycosaminoglycans modulate fibronectin matrix assembly and are essential for matrix incorporation of tenascin-C. *J. Cell Sci.* **110,** 1413–1419 (1997).

214. Maeda, T., Alexander, C. M. & Friedl, A. Induction of syndecan-1 expression in stromal fibroblasts promotes proliferation of human breast cancer cells. *Cancer Res.* **64,** 612–21 (2004).

215. Stanley, M. J., Stanley, M. W., Sanderson, R. D. & Zera, R. Syndecan-1 expression is induced in the stroma of infiltrating breast carcinoma. *Am. J. Clin. Pathol.* **112,** 377–83 (1999).

216. Yang, N., Mosher, R., Seo, S., Beebe, D. & Friedl, A. Syndecan-1 in breast cancer stroma fibroblasts regulates extracellular matrix fiber organization and carcinoma cell motility. *Am. J. Pathol.* **178,** 325–35 (2011).

217. Provenzano, P. P., Eliceiri, K. W. & Keely, P. J. Shining new light on 3D cell motility and the metastatic process. *Trends Cell Biol.* **19,** 638–48 (2009).

218. Karagiannis, G. S. *et al.* Cancer-Associated Fibroblasts Drive the Progression of Metastasis through both Paracrine and Mechanical Pressure on Cancer Tissue. *Mol. Cancer Res.* **10,** 1403–18 (2012).

219. Tan, A. B.-S., Kress, S., Castro, L., Sheppard, A. & Raghunath, M. Cellular re- and de-programming by microenvironmental memory: why short TGF-β1 pulses can have long effects. *Fibrogenesis Tissue Repair* **6,** 12 (2013).

220. Dave, N. *et al.* Functional cooperation between Snail1 and twist in the regulation of ZEB1 expression during epithelial to mesenchymal transition. *J. Biol. Chem.* **286,** 12024–32 (2011).

221. Gregory, P. A. *et al.* The miR-200 family and miR-205 regulate epithelial to mesenchymal transition by targeting ZEB1 and SIP1. *Nat. Cell Biol.* **10,** 593–601 (2008).

222. Park, S.-M., Gaur, A. B., Lengyel, E. & Peter, M. E. The miR-200 family determines the epithelial phenotype of cancer cells by targeting the E-cadherin repressors ZEB1 and ZEB2. *Genes Dev.* **22,** 894–907 (2008).

223. Wellner, U. *et al.* The EMT-activator ZEB1 promotes tumorigenicity by repressing stemness-inhibiting microRNAs. *Nat. Cell Biol.* **11,** 1487–95 (2009).

224. Hnisz, D. *et al.* Super-enhancers in the control of cell identity and disease. *Cell* **155,** 934–47 (2013).

225. Lovén, J. *et al.* Selective inhibition of tumor oncogenes by disruption of super-enhancers. *Cell* **153,** 320–34 (2013).

226. Whyte, W. A. *et al.* Master transcription factors and mediator establish super-enhancers at key cell identity genes. *Cell* **153,** 307–19 (2013).

227. Lai, F. *et al.* Activating RNAs associate with Mediator to enhance chromatin architecture and transcription. *Nature* **494,** 497–501 (2013).

228. Ørom, U. A. *et al.* Long noncoding RNAs with enhancer-like function in human cells. *Cell* **143,** 46–58 (2010).

229. Goetz, J. G. *et al.* Biomechanical remodeling of the microenvironment by stromal caveolin-1 favors tumor invasion and metastasis. *Cell* **146,** 148–63 (2011).

230. Huang, D. *et al.* Poly(ADP-ribose) polymerase 1 is indispensable for transforming growth factor-β Induced Smad3 activation in vascular smooth muscle cell. *PLoS One* **6,** e27123 (2011).

231. Wang, Z.-Q. *et al.* PARP is important for genomic stability but dispensable in apoptosis. *Genes Dev.* **11,** 2347–2358 (1997).

232. Beg, A. A., Sha, W. C., Bronson, R. T., Ghosh, S. & Baltimore, D. Embryonic lethality and liver degeneration in mice lacking the RelA component of NF-κB. *Nature* **376,** 167–170 (1995).

233. Cheng, D. *et al.* Small molecule regulators of protein arginine methyltransferases. *J. Biol. Chem.* **279,** 23892–9 (2004).

234. Savagner, P. *et al.* Developmental transcription factor slug is required for effective re-epithelialization by adult keratinocytes. *J. Cell. Physiol.* **202,** 858–66 (2005).

235. Hudson, L. G. *et al.* Cutaneous wound reepithelialization is compromised in mice lacking functional Slug (Snai2). *J. Dermatol. Sci.* **56,** 19–26 (2009).

236. Bolos, V. *et al.* The transcription factor Slug represses E-cadherin expression and induces epithelial to mesenchymal transitions: a comparison with Snail and E47 repressors. *J. Cell Sci.* **116,** 499–511

237. Porta-de-la-Riva, M. *et al.* TFCP2c/LSF/LBP-1c is required for Snail1-induced fibronectin gene expression. *Biochem. J.* **435,** 563–568 (2011).

238. Hinz, B. & Pittet, P. Myofibroblast development is characterized by specific cell-cell adherens junctions. *Mol. Biol. …* **15,** 4310–4320 (2004).

239. Tomasek, J. J., Haaksma, C. J., Schwartz, R. J. & Howard, E. W. Whole animal knockout of smooth muscle alpha-actin does not alter excisional wound healing or the fibroblast-to-myofibroblast transition. *Wound Repair Regen.* **21,** 166–76

240. Schäfer, M. & Werner, S. Cancer as an overhealing wound: an old hypothesis revisited. *Nat. Rev. Mol. Cell Biol.* **9,** 628–38 (2008).

241. Bornstein, P., McPherson, J. & Sage, H. Synthesis and secretion of structural macromolecules by endothelial cells in culture. *Pathobiol. Endothel. Cell, P&S …* 415–422 (1982).

242. Bissell, M. J., Hall, H. G. & Parry, G. How does the extracellular matrix direct gene expression? *J. Theor. Biol.* **99,** 31–68 (1982).

243. Chaffer, C. L. & Weinberg, R. a. A perspective on cancer cell metastasis. *Science* **331,** 1559–64 (2011).

244. Herrera, A. *et al.* Protumorigenic effects of Snail-expression fibroblasts on colon cancer cells. *Int. J. Cancer* **134,** 2984–90 (2014).

245. Zhang, K. *et al.* The collagen receptor discoidin domain receptor 2 stabilizes SNAIL1 to facilitate breast cancer metastasis. *Nat. Cell Biol.* **15,** 677–87 (2013).

246. Haage, A. & Schneider, I. C. Cellular contractility and extracellular matrix stiffness regulate matrix metalloproteinase activity in pancreatic cancer cells. *FASEB J.* fj.13–245613– (2014). doi:10.1096/fj.13-245613

247. Gaggioli, C. *et al.* Fibroblast-led collective invasion of carcinoma cells with differing roles for RhoGTPases in leading and following cells. *Nat. Cell Biol.* **9,** 1392–400 (2007).

248. Donà, E. *et al.* Directional tissue migration through a self-generated chemokine gradient. *Nature* **503,** 285–9 (2013).

249. Beacham, D. a & Cukierman, E. Stromagenesis: the changing face of fibroblastic microenvironments during tumor progression. *Semin. Cancer Biol.* **15,** 329–41 (2005).

250. Alcaraz, J. *et al.* Microrheology of human lung epithelial cells measured by atomic force microscopy. *Biophys. J.* **84,** 2071–9 (2003).

251. Marí-Buyé, N., Luque, T., Navajas, D. & Semino, C. E. Development of a three-dimensional bone-like construct in a soft self-assembling peptide matrix. *Tissue Eng. Part A* **19,** 870–81 (2013).

252. Dignam, J., Lebovitz, R. & Roeder, R. Accurate transcription initiation by RNA polymerase II in a soluble extract from isolated mammalian nuclei. *Nucleic Acids Res.* **1,** 1475–1489 (1983).

253. Aoufouchi, S. & Shall, S. Regulation by phosphorylation of Xenopus laevis poly (ADP-ribose) polymerase enzyme

activity during oocyte maturation. *Biochem. J* **551,** 543–551 (1997).

All the vignettes of medieval knights fighting snails are from British Library's digitized manuscripts collection.
http://www.bl.uk/manuscripts/Default.aspx

The main part of this work is included in the following articles:

Stanisavljevic, J., Porta-de-la-Riva, M., Batlle, R., De Herreros, A. G. & Baulida, J. The p65 subunit of NF-κB and PARP1 assist Snail1 in activating fibronectin transcription. *J. Cell Sci.* **124,** 4161–71 (2012).

Stanisavljevic, J. *et al.* Activated fibroblasts promote wound healing and tumor malignance through a Snail1/RhoA control of the extracellular architecture (under submission)

The author collaborated on other projects:

Batlle, R. *et al.* Snail1 controls TGF-β responsiveness and differentiation of mesenchymal stem cells. *Oncogene* **418,** 3381–3389 (2012).

Porta-de-la-Riva, M. *et al.* TFCP2c/LSF/LBP-1c is required for Snail1-induced fibronectin gene expression. *Biochem. J.* **435,** 563–568 (2011).

# Table of Figures

## INTRODUCTION:



## RESULTS:

## Discussion: